Modelling and Experimental Characterization of Photovoltaic/Thermal Systems for Cooling and Heating of Buildings in different climate conditions

Khaled Mohamed Ramadan

UNIVERSITAT ROVIRA i VIRGILI

Modelling and Experimental Characterization of Photovoltaic/Thermal Systems for Cooling and Heating of Buildings in different climate conditions

---

Khaled Mohamed Ramadan

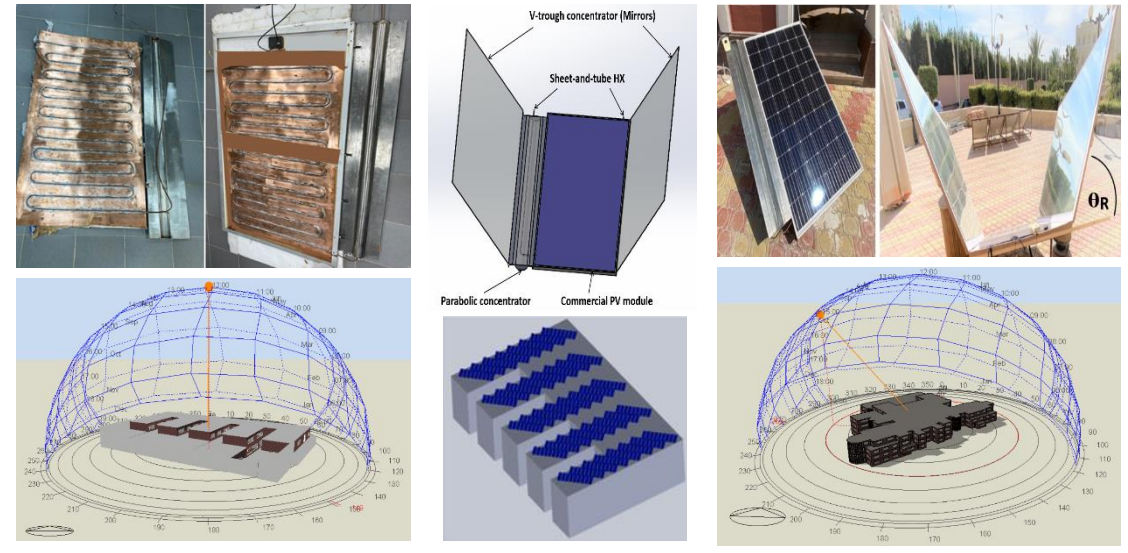

DOCTORAL THESIS

2020

UNIVERSITAT ROVIRA I VIRGILI
Modelling and Experimental Characterization of Photovoltaic/Thermal Systems for Cooling and Heating of Buildings in different climate conditions
Khaled Mohamed Ramadan

Khaled Mohamed Ramadan

Modelling and Experimental Characterization of Photovoltaic/Thermal System for Cooling and Heating of Buildings in different climate conditions

A thesis submitted for the degree of Doctor of Philosophy

Tarragona, November 2020

Supervisor

Prof. Alberto Coronas

CREVER, Mechanical Engineering Department, Rovira i Virgili University

UNIVERSITAT ROVIRA i VIRGILI

UNIVERSITAT
ROVIRA I VIRGILI
DEPARTAMENT D'ENGINYERIA MECÀNICA
Escola Tècnica Superior d'Enginyeria Química (ETSEQ).
Avgda Paisos Catalans, 26 ; 43007 Tarragona (Spain)

Declaration

I STATE that the present thesis, entitled "**Modelling and Experimental Characterization of Photovoltaic/Thermal Systems for Cooling and Heating of Buildings in different climate conditions**", presented by **Khaled Mohamed Ramadan** for the degree of Doctor, has been carried out under my supervision at CREVER Research group in the Department of Mechanical Engineering of Rovira i Virgili University, and that it fulfils all the requirements to be eligible for the International Doctorate Award.

Tarragona, November 23, 2020

Prof. Alberto Coronas

Acknowledgement

First and foremost, I would like to express my thanks and appreciations to my supervisor Prof. Alberto Coronas for his continuous guidance and help. I learned so many valuable things from him.

Many thanks to AGAUR (Generalitat de Catalunya) for the predoctoral fellowship, contract numbers (2017 FI_B_00879), (2018 FI_B1_00160), and (2019 FI_B2 00153).

Many thanks to Prof. Iman El-Mahallawi for her help and guidance during my research stay at the renewable energy laboratory, Mechanical Engineering Department, British University in Egypt for three months.

I would like to acknowledge Prof. Pedro Vicente Quiles, who helped me during my research stay at mechanical engineering and energy department of Miguel Hernandez de Elche university for one month.

I would also like to thank all of the other Rovira i Virgili University, Mechanical Engineering Department, Group of Applied Thermal Engineering-CREVER members.

Many thanks to my colleagues and friends for their support during my thesis.
Special thanks to my family for their care, patience, and love.

Abstract

In recent years, photovoltaic solar cell technology and associated heat extraction techniques have achieved tremendous growth as sustainable sources of energy. This process has enhanced the solar conversion efficiency, technical reliability, and economic viability of the photovoltaic (PV). The PV installations suffer from a drop-in cell efficiency as a result of increasing the PV cell temperature, decreasing the open circuit voltage. Because only photons around the band gap have sufficient energy to produce electricity in photovoltaic cells and the process of electricity generation in these cells is exothermic, the temperature of cells increases.

By coating the PV module by nanoparticles as an optical filter can significantly enhance PV system performance. However, the integration of nanoparticles for cooling and as an optical filter present some critical challenges due to their limited stability time and the high cost of nanoparticles.

By cooling the solar cells with a fluid stream natural or forced circulation can reduce the PV cell temperature. The photovoltaic/thermal (PV/T) system makes it easier to produce thermal energy while generating electricity. By operating the commercial PV/T, it has been observed that the useful hot stream temperature is between 40–60 °C. This temperature range is appropriate for a domestic hot water application and space air heating in winter (cold climate). However, in summer (hot climates) the fluid stream could be wasted because of the limited application based on this temperature range. This application could be the regeneration of dehumidification and adsorption systems (disadvantages: low COP and high capital cost).

By using the solar concentrators in order to increase the input solar radiation to the PV cells, the current output is increased as well as the power output. As the light intensity on the cell is increased by the concentration ratio, the useful hot stream temperature produced from cooling the PV module is increased. For building applications, low concentration photovoltaic/thermal (LCPV/T) systems would be preferable due to their potential for non-tracking, high reliability and low cost. Further, Silicon-based cells fit well into low concentration solutions. The commercial LCPV/T are favorable for building applications with fluid temperature below 75 °C. However, in summer (hot climates) the fluid stream could be wasted. The inconsistency between obtaining high-grade thermal energy and preventing PV module from overheating is the main limitation for PV/T combination. Meanwhile, there are no commercially available spectral splitting concentrated PV/T systems.

Cooling the PV cells improves its efficiency, but the capital cost of the LCPV/T is higher than the cost of PV/T system and the cost of the PV/T is higher than the cost of PV systems. Therefore, the heat produced from cooling the PV cells should be used to reduce the payback period of the PV/T and LCPV/T systems.

A new design of a low-cost PV/T system based on the commercial PV module for improving its electric power and obtaining a sufficient fluid temperature (75-90 °C) is developed and implemented. By heating up the useful fluid leaving the PV/T into the linear parabolic concentrator and insert this combination between V-trough mirrors, this stream could be heated up to 90 °C which makes it useful for operating absorption chillers. Meanwhile, the PV cell temperature is kept below 75 °C.

The experimental energy generation profiles of the selected polycrystalline PV, monocrystalline PV and air-based PV/T modules and the developed LCPV/T system are explored in hot and warm climates. The use of on-site energy production from the validated models of the selected PV and PV/T modules and the developed LCPV/T is investigated along with the integration of efficient cooling and heating systems.

Two proposed bidirectional integration configurations of the LCPV/T system with buildings incorporated into the electricity microgrid and district thermal network are investigated. The integration of the LCPV/T system into the 4th generation heating network (supply temperatures below 70 °C) is dynamically performed using direct heat exchanger for heating and reversible electric water-to-water heat pump (HP) for heating and cooling in the warm climate. The integration of the LCPV/T system into the cooling network (supply temperatures around 7 °C) is dynamically performed using the absorption and electric chillers for mainly cooling in the extremely hot climate. The two proposed configurations along with the traditional configurations of PV driven electric air-to-water HP, PV driven electric chiller and PV/T assisted air-to water HP are modelled. Moreover, the performance of these five solar configurations are compared with the conventional cooling (air-cooled chiller) and heating (gas boiler) systems.

Two case study buildings in hot and warm climate conditions are selected. The two case study buildings are dynamically operated to characterize the thermal demand of the buildings and match the energy demand and on-site energy generation. The first case study building (2,672 m^2) is an existing laboratory building that belongs to the university campus of the URV in Tarragona. The second case study building (16,109 m^2) is an existing university building that belongs to the university campus of the BUE in Cairo.

The design of the grid-tie photovoltaic system has been taken the available roof area, the distance between module rows, the building's orientation and the fulfilment of building's demands into consideration. The cooling and heating systems are sized to meet the building's demands. The solar contribution index, monthly bill saving, CO_2 emissions reduction and the payback of the PV, PV/T and LCPV/T systems coupled with cooling and heating systems in the two case buildings are presented. The proposed method incorporates dynamic modeling simulation environments (DesignBuilder/EnergyPlus engine and TRNSYS dynamic modelling environment) to investigate the match between energy production and consumption hourly, daily, monthly and yearly.

The results of this study reflect that integrating the LCPV/T with compression and absorption chillers in Egypt climate while LCPV/T with water-to-water reversible HP systems in Spain climate into the power grid and cooling/heating district network has a great potential in boosting the recoverable thermal energy utilization. The flexibility of incorporating LCPV/T energy for the bidirectional low temperature network in urban districts provides producer and consumer (prosumer) buildings. In comparison to the typical configuration of PV integrated compression chiller, the proposed configuration of LCPV/T coupled with the compression and absorption chillers reduces the payback period by 10-40% in the case building in Cairo. Substituting the connection to the campus water network with the use of reversible HP reduces the operating cost for cooling and heating in the case building in Spain by 15-30%.

Resumen

En los últimos años, la tecnología de celdas solares fotovoltaicas ha alcanzado un enorme crecimiento como fuentes de energía sostenible. El proceso de extracción de calor ha mejorado considerablemente la eficiencia de conversión solar, la confiabilidad técnica y la viabilidad económica de la energía fotovoltaica. Las instalaciones fotovoltaicas sufren de una caída en la eficiencia de la celda como resultado del aumento de la temperatura de la celda fotovoltaica (PV), disminuyendo la tensión de circuito abierto. Debido a que solo los fotones alrededor de la banda prohibida tienen suficiente energía para producir electricidad en las celdas PV y el proceso de generación de electricidad en estas celdas es exotérmico, la temperatura de las celdas aumenta.

Recubrir el módulo fotovoltaico con nanopartículas como filtro óptico puede mejorar significativamente el rendimiento del sistema fotovoltaico. Sin embargo, la integración de nanopartículas para enfriamiento y como filtro óptico presenta algunos desafíos críticos debido a su tiempo de estabilidad limitado y al alto costo de las nanopartículas.

Al enfriar las celdas solares con una circulación natural o forzada de fluido se puede reducir la temperatura de la celda fotovoltaica. El sistema solar hibrido fotovoltaico/térmico (PV/T) facilita la producción de energía térmica mientras se genera electricidad. Al operar la PV/T comercial, se ha observado que la temperatura útil de la corriente de fluido caliente está entre 40 y 60 °C. Este rango de temperatura es apropiado para una aplicación de agua caliente sanitaria y calefacción de aire en edificios en invierno (clima frío). Sin embargo, en verano (climas cálidos), la energía térmica del fluido podría desperdiciarse debido a la aplicación limitada basada en este rango de temperatura.

Al utilizar los concentradores solares para aumentar la radiación solar de entrada a las celdas fotovoltaicas, la salida de corriente aumenta, así como la salida de potencia. A medida que la intensidad de la luz en la celda aumenta por la relación de concentración, aumenta la temperatura útil de la corriente de fluido caliente producida al enfriar el módulo fotovoltaico. Para aplicaciones en edificios, los sistemas fotovoltaicos/térmicos de baja concentración (LCPV/T) son preferibles debido a su potencial de no seguimiento, alta confiabilidad y bajo costo. Además, las celdas a base de silicio encajan bien en soluciones de baja concentración. Los LCPV/T comerciales son favorables para aplicaciones en edificios con temperatura de fluido por debajo de 75 °C. Sin embargo, en verano (climas cálidos), la energía térmica de la corriente de fluido podría desperdiciarse.

El enfriamiento de las celdas fotovoltaicas mejora su eficiencia, pero el costo de capital del LCPV/T es más alto que el costo del sistema PV/T y el costo de la PV/T es más alto que el costo de los sistemas PV. Por lo tanto, el calor producido a partir del enfriamiento de las celdas fotovoltaicas debe utilizarse para reducir el período de recuperación de los sistemas PV/T y LCPV/T.

En esta tesis, se desarrolla e implementa un nuevo diseño de un sistema LCPV/T de bajo costo basado en el módulo PV comercial para aumentar su potencia eléctrica y obtener una adecuada temperatura de fluido (75-90 °C). Mediante el calentamiento del fluido que sale del PV/T en el concentrador parabólico lineal y adjuntar el PV/T con el parabólico lineal entre espejos de canal en V, el fluido podría calentarse hasta 90 °C, temperatura útil para activar enfriadores por absorción. Mientras tanto, la temperatura de la celda fotovoltaica se mantiene por debajo de 75 °C.

Los perfiles experimentales de generación de energía de los módulos fotovoltaicos policristalinos y monocristalinos PV, PV/T basados en aire y el sistema LCPV/T desarrollado se investigan. También, se investiga el uso de la producción de energía in situ a partir de los modelos validados de los módulos PV y PV/T seleccionados y el LCPV/T desarrollado junto con la integración de sistemas de calefacción y refrigeración eficientes.

Se analizan dos configuraciones de integración bidireccional del sistema LCPV/T en edificios incorporados a la microrred eléctrica y la red térmica del distrito. La integración del sistema LCPV/T en la red de calefacción de cuarta generación (temperaturas de suministro inferiores a 70 °C) se realiza dinámicamente utilizando un intercambiador de calor directo y una bomba de calor agua-agua eléctrica reversible para calefacción y refrigeración en climas cálidos. La integración del sistema LCPV/T en la red de agua fría (temperaturas de suministro alrededor de 7 °C) se realiza dinámicamente utilizando enfriadores térmicos y eléctricos para enfriar principalmente en climas extremadamente cálidos. Se modelan las dos configuraciones propuestas junto con las configuraciones tradicionales de bomba de calor (HP) aire-agua eléctrico activado por PV, enfriador eléctrico activado por PV y HP aire-agua asistido por PV/T. Además, el rendimiento de estas cinco configuraciones solares se compara con los sistemas convencionales de refrigeración (enfriador de aire) y calefacción (caldera de gas).

Dos edificios de casos de estudio se operan dinámicamente para caracterizar la demanda de energía de los mismos y hacer coincidir la demanda y la generación de energía en el sitio. El primer edificio de caso de estudio (2.672 m^2) es un edificio de laboratorio que pertenece al campus universitario de la URV en Tarragona. El segundo edificio de caso de estudio (16.109 m^2) es un edificio universitario que pertenece al campus universitario de la BUE en El Cairo. El diseño del sistema fotovoltaico conectado a la red considera el área disponible del techo, la distancia entre las filas de módulos, la orientación del edificio y la demanda de energía de los edificios. Mientras tanto, los sistemas de refrigeración y calefacción están dimensionados para satisfacer las demandas de energía de los edificios. Se presentan el índice de contribución solar, el ahorro en la factura mensual, la reducción de emisiones de CO_2 y la recuperación de la inversión de los sistemas PV, PV/T y LCPV/T junto con los sistemas de refrigeración y calefacción en los dos edificios utilizados como casos de estudio.

Los resultados de este estudio reflejan el gran potencial para la revalorización de energía térmica que se desprende de la integración del LCPV/T con un enfriador por absorción y también para la utilización de electricidad que produce el LCPV/T con enfriadores de compresión en el clima de Egipto. Mientras que, para el clima de España, los resultados demuestran que es más favorable la integración del LCPV/T con sistemas HP reversibles agua-agua en la red eléctrica y la red de distrito de refrigeración/calefacción. En comparación con la configuración típica del enfriador por compresión integrado con un sistema PV, la configuración propuesta de LCPV/T junto con los enfriadores por compresión y absorción reduce el período de recuperación en un 10-40% en el edificio en El Cairo. Sustituir la conexión a la red de agua caliente del campus por el uso de una bomba de calor reversible reduce el coste operativo de refrigeración y calefacción en el edificio en Tarragona en un 15-30%.

Author's contribution

Publications

- **K. Ramadan**, E. El-Shazly I. El-Mahallawi, A. Coronas. Dynamic simulation, experimental characterization of photovoltaic/thermal for cooling and heating of buildings in the Mediterranean climate. Energy and buildings (in preparation).
- **K. Ramadan**, J. C. Bruno, A. Coronas. State-of-the-art of Solar Photovoltaic/Thermal Systems for Building Integration and Air Conditioning. Renewable & Sustainable Energy Reviews (in preparation).

Conferences

- **K. Ramadan** and A. Coronas. Energy management in existing office building incorporated in a university campus microgrid using photovoltaics and heat pumps. The International Conference on Renewable Energy 2019. Hail (Saudi Arabia), March 5-7.
- **K. Ramadan**, J. Bruno, A. Coronas. Integration of hybrid Photovoltaic/Thermal and Heat Pump heating/cooling system using a split heat flow configuration. EuroSun 2018. International Conference on Solar Energy for Buildings and Industry. Rapperswil (Switzerland), September 10-13.
- **K. Ramadan**, J. Prieto, A. Coronas. Energetic and Economic Optimization of Photovoltaic System for Handling Power, Heating and Cooling Demands in Existing Office Building in the Mediterranean Climate. I-PVTC 2018. Integrated Photovoltaic Technical Conference. Cassis (France), September 10-12.
- **K. Ramadan**, J. Prieto, A. Coronas. Modelling and dynamic simulation of an off-grid PV cooling system for an office building in different climate locations. CYTEF 2016. VIII Congreso Ibérico/VI Congreso Iberoamericano de las Ciencias y Técnicas del Frío. Coimbra (Portugal), May 3-6.

Fellowships, grants and awards

- Catalan government fellowship. AGAUR – FI. (2017 – 2020).
  NUM. (2017FI_B_00879), (2018FI_B1_00160), (2019FI_B2 00153).
- Best poster award. (CYTEF, 2016).
  VIII Congreso Ibérico/VI Congreso Iberoamericano de las Ciencias y Técnicas del Frío.
- Spanish scientific research grant. UMH – EPSO. (2015 – 2016).
  Management of Energy and Water Resources.
- Young researcher award. (URV, 2015).

Internships and research visits

- Renewable Energy Laboratory, the British University in Egypt (BUE), three-month stay, from December 2019 to March 2020.
- Mechanical Engineering and Energy Department, Universidad Miguel Hernández de Elche (UMH), one month stay (22nd of January - 21st of February 2019).

Other Publications

- K. Salhi, K. Ramadan, M. Hadjiat, A. Hamidat. Energetic and Exergetic Performance of Solar-Assisted Direct Expansion Air-Conditioning System with Low-GWP Refrigerants in Different Climate Locations. Arabian Journal for Science and Engineering (2020).
- K. Salhi, M. Korichi, K. Ramadan. Thermodynamic and thermo-economic analysis of compression–absorption cascade refrigeration system using low-GWP HFO refrigerant powered by geothermal energy. International Journal of Refrigeration, 2018, 94, pp.214-229.
- K. Ramadan, M. J. Oates, J.M. Martínez, A. Ruiz-Canales. Design and Implementation of a low-cost photovoltaic soil moisture monitoring station for irrigation scheduling with different frequency

domain analysis probe structures. Computers and Electronics in Agriculture, 2018, 148, pp.148-159.

- M. Oates, K. Ramadan, A. Ruiz-Canales, A. Vazquez de Leon. Automatic fault detection in a low-cost frequency domain Soil Moisture Sensor. Agricultural Water Management, 2017, 183, pp. 41-48.

List of contents

List of figures

List of tables

Nomenclature

Nomenclature		Greek letters	
T	Temperature [°C]	τ	Collector transmittance [-]
IRR	Irradiance [kW/m^2]	α	Collector absorptance [-]
A	Area [m^2]	ρ	Density [kg/m^3]
Q	Energy [kWh]	η_{el}	Collector electric efficiency [%]
m	Mass flow rate [kg/hr]	α_{Isc}	Temperature coefficient [A/K]
t	Time (s)	ε_g	Semiconductor bandgap [eV]
k	Boltzmann constant [J/K]	β_{Voc}	Temperature coefficient [V/K]
n	Refractive index [-]	γ_{damper}	Damper control [-]
C	Concentration ratio [-]	ω_{air}	Air humidity ratio [kgH_2O/kgAir]
G	Total solar radiation [kW/m^2]	ε_p	Plate emissivity [-]
R	Resistance [Ω]	ρ_p	Plate reflectivity [-]
F	Efficiency factor [-]	η_{th}	Collector thermal efficiency [%]
N	Number of collectors [-]	ρ_g	Ground reflectivity [-]
L	Length [m]	θ	Angle of incidence radiation [°]
d	Distance [m]	η_{op}	Operation efficiency
I	Current [A]	γ_s	Azimuth angle [°]
V	Voltage [V]	θ_R	Reflector inclination angle [°]
De	Degradation factor [-]	α_s	Sun altitude angle [°]
H	Relative humidity [%]	β	Module tilt angle [°]
Cp	Specific heat capacity [kJ/kg.K]	θ_i	Effective solar angular [°]
D	Diameter [m]	$\triangle T$	Temperature difference [°C]
W	Width [m]	**Subscripts**	
M	Mass [kg]	p	Parallel
p	Pressure [kPa]	s	Series
h	Enthalpy [kJ/kg]	sh	Shunt
P	Power [kW]	m	Mean
v	Wind speed [m/s]	av	Average
s	Distance between fins [m]	a	Aperture
Nu	Nusselt number [-]	comp	Electric compressor
Re	Reynolds number [-]	abs	Absorption chiller
DNI	Direct radiation [kW/m^2]	in	Inlet fluid
CO_2	Carbon dioxide	out	Outlet fluid
Al_2O_3	Aluminum oxide	t	Thermal

Abbreviations

PV	Photovoltaic panel
PV/T	Photovoltaic/Thermal collector
CPV/T	Concentrated PV/T
LCPV/T	Low-Concentrated PV/T
DHC	District Heating and Cooling
DH	District Heating
FC	Fan Coil
COMP	Compressor chiller
ABS	Absorption chiller
HP	Heat pump
HX	Heat exchanger
EC	Electric chiller
ASHP	Air source heat pump
WSHP	Water Source Heat Pump
COP	Coefficient of Performance

Chapter 1. Introduction, overview of photovoltaic/thermal assisted cooling and heating systems, justification, and thesis objectives

This chapter presents an introduction to renewable energy technologies for buildings and general view about the most common strategies used to achieve near zero energy consumption in buildings. Also, it presents an introduction to solar PV, PV/T and LCPV/T systems and presents an overview of recent investigations on the use of both electric and thermal energy from the PV, PV/T and LCPV/T systems for cooling and heating in buildings. Also, it illustrates the justifications, objectives and methodological approach of this thesis.

1.1 Introduction

1.1.1 Our carbon footprint

While human civilization continues to grow and thrive, our progress sometimes yields unfortunate side-effects. In the 20th century alone, humanity has advanced more technologically than we have in our entire recorded history. One unfortunate result of our progress, however, has been our carbon footprint. The carbon footprint is defined as the amount of greenhouse gas emissions (GHG) released into the atmosphere as a direct or indirect result of human activity. Carbon dioxide, primarily, is the most emitted greenhouse gas produced as a result of human activity and contributes to approximately 63.5% to the overall global emissions [1]. Since the effects of CO_2 and other GHGs, such as nitrous oxide, methane or HFC refrigerants, result in more than just rising temperatures, a more precise term is "climate change," which helps convey that other changes such as ocean acidification from increased absorption of CO_2 and sea-level rise from thermal expansion are taking place as well [2]. Burning fossil fuels to generate electricity for its various uses, to produce heat and to power transportation are direct and major sources of GHG emissions. Globally, two thirds of electricity (about 67%) is generated from fossil fuels, mainly 40.8 % from coal, 21.6% from natural gas and 4.3% from oil. The International Energy Agency (IEA) assessed the impact of fossil fuel use on global temperature increases. It found that CO_2 emitted from coal combustion was responsible for over 0.3 °C of the 1 °C increase in global average annual surface temperatures [3]. In the 23-year span from 1990 to 2013, global CO_2 emissions directly related to the production of electricity increased significantly from 6,282 to 11,749 $MtCO_2$, while electricity production itself increased from 11,627 to 22,592 TWh [4]. In 2018, the energy consumption worldwide grew by nearly twice the average rate of growth since 2010 associated with the vigorous global economy as well as higher heating and cooling needs in some parts of the world. As a result of the high energy demand in 2018, global energy-related CO_2 emissions increased to 33.1 Gt CO_2 [5]. The demand for energy over the next decades is predicted to show rising levels [6]. According to the IEA scenarios, the demand for electricity is expected to increase over 70% to reach an expected 34,500 TWh in 2040. This projected increase represents an average annual growth rate of 2.0% [7] as illustrated in (Figure 1-1).

An increase in energy demand is even more likely when considering the growth in energy consumption associated with the growth in world population. In the 1950's, the world population

was 2.5 billion, and today, the estimated world population resides at 7.7 billion. By 2050, the world population is expected to rise to 9 billion, with growth largely focused in developing nations [8].

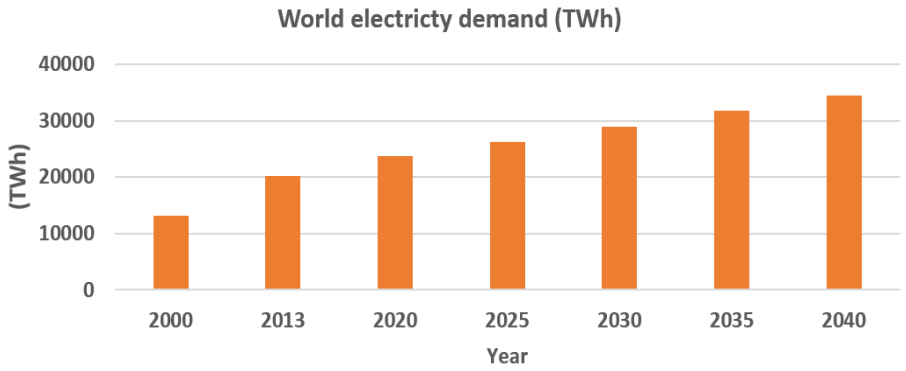

Figure 1-1.World electricity demand, 2000-2040 (TWh) [7].

Mediterranean countries consume around 8% of the world's primary energy demand while, the main source of CO_2 emissions in the Mediterranean region is the combustion of fossil fuels that are used to generate electricity [9]. In the south, electricity consumption had an annual growth rate of approximately 6% between 1990 and 2010, a rate three times greater than the northern Mediterranean countries whose consumption grew at an annual growth rate of 1.8% [10].

The Covid-19 pandemic has caused an unprecedented global economic crisis. The pandemic has a significant impact across all fields of the economy, including the energy sector. For the first time in history, oil price went subzero; this was due to the failing fundamentals even demand shock as a supply shock. Global demand has fallen to 33% as a result of travel disruptions. Meanwhile, the price war between Saudi Arabia and Russia caused an oversupply of discounted oil [11]. The COVID-19 emergency is a global challenge for the entire power sector so as for the renewable energy industry. China plays an important role in the technological implementation of green solutions, so delivery difficulties caused by the coronavirus results in significant delays in new renewable energy projects worldwide. Nevertheless, renewable energy will be the only industry that could increase its demand in 2020. Renewable energy sources should be given priority because of the flexibility of solar, hydro and wind energy to the unprecedented decline in energy demand [12].

1.1.2 Buildings energy consumption

The building sector has been considered one of the major fields for energy consumption. It accounts for approximately 36% of global energy demands and nearly 40% of total direct and indirect CO_2 emissions. Energy demand from buildings and buildings construction continues to rise, driven by improved access to energy in developing countries, greater ownership and use of energy-consuming devices, and rapid growth in global buildings floor area, at nearly 3% per year [13]. The rapid growth of the electricity demand growth in buildings has been documented over the last 25 years, accounting for nearly 60% of the total increase in global electricity demand. In some rapidly developing economies, including China and India, electricity consumption in buildings grew on average by more than 8% per year over the last decade [14].

Currently, the vast majority of energy used in buildings is from non-renewable, fossil fuel resources.

On the other hand, the building sector also has the highest potential for energy efficiency. The building final energy consumption by fuel types in the U.S., China and the E.U. in 2010 is illustrated in Figure 1-2. It can be observed that electricity and natural gas are the primary fuels sources for building energy use in the U.S., with shares of nearly 50% and 40% of final energy usage, respectively. Electricity is the largest final energy source in the U.S. building sector and is primarily used for heating, cooling, lighting and appliances. When considering source-to-site losses, electricity accounts for 72.9% of the total primary energy used in the building sector in 2010. However, conventional heating and cooling equipment fueled by natural gas and oil are still widespread in the U.S., and natural gas is also the primary fuel source for water heating. Coal and renewable energy only account for 3.2% of the total building final energy usage in the U.S. Conversely, biomass and waste are the dominant energy sources in the residential sector in China due to their use for heating and cooking. Conversely, biomass and waste are the dominant energy sources in the residential sector in China due to their use for heating and cooking. The residential sector in China consumes more than five times the energy consumed by the services sector. Therefore, switching fuel sources from traditional biomass to modern fuel choices is crucial for reducing the energy used in rural areas. In addition, coal accounts for 14.3% of Chinese building energy use a much higher level than that in the U.S. and E.U. However, the use of electricity for commercial heat sharply increased during the last decade. In 2013, electricity accounted for 57% of total building energy consumption in China. In the E.U., final energy usage is dominated by electricity and natural gas, similar to trends in the U.S. Biomass and other renewables account for 9% of building energy use, mostly for heating purposes [15].

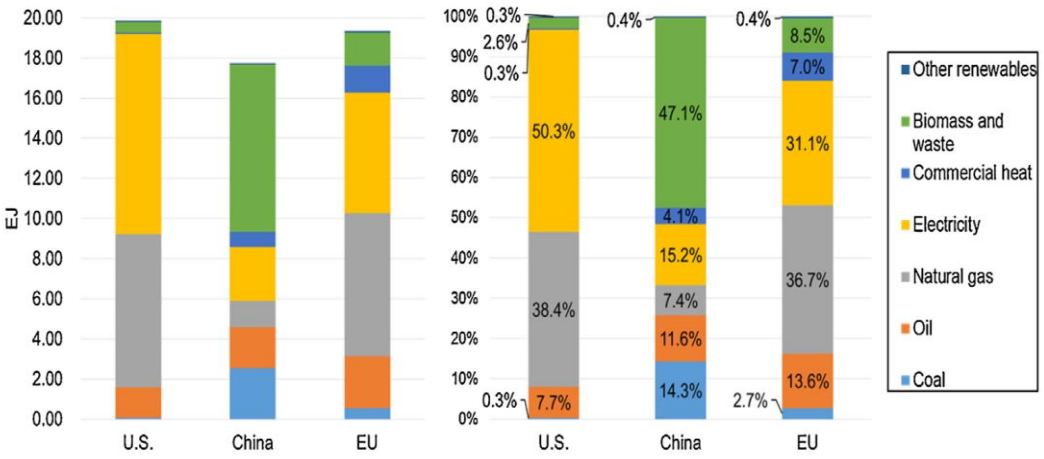

Figure 1-2. Building final energy consumption by fuel types in the U.S., China and the E.U. [15].

The breakdown of primary energy use in commercial and residential buildings demonstrates that space conditioning (heating and cooling) energy consumption in U.S. is nearly 43% for residential buildings and 30% for commercial buildings [16]. In the E.U., the main use of energy by households is for space conditioning and water heating. It represents 78.9 % of the final energy consumed by households [17]. Both Australia and Turkey's households consume around 40% of the total energy used for space heating and cooling, while residential air conditioning in Kuwait consumes 58.4% of the total electric energy delivered by power plants at peak usage time on hot summer days [18].

In broad terms, heating or cooling of enclosed spaces to maintain thermal comfort reaches 40 – 60% of building energy consumption. Meanwhile, the market of air conditioning systems is growing rapidly; it increased by 70% between 2010 and 2015 [19]. The consumption of electricity for household air conditioning is growing very rapidly in half of the G20 countries: by more than 12%/year over 2000-2018 in China, India, Indonesia and Turkey, and in a range of 6 to 10%/year in Australia, Brazil, Canada, the E.U., Saudi Arabia and South Korea [20]. In the long run, considering climate change, worldwide heating demand is projected to decrease by 34% by the year 2100. Moreover, cooling demand is estimated to increase by 72% over the same period [21]. In some buildings, a large fraction of cooling load is due to solar input, while many other buildings have cooling requirements that are not directly related to solar input such as heat loads from working computers and office equipment [22]. In many Middle East and North Africa countries, the ambient temperature during summer approaches 40–45 °C or sometimes higher. During these predominant conditions, the air conditioning system continuously works and consumes more electricity [23].

1.1.3 Near zero energy buildings

As a result, a special focus is directed to tackle the issues on energy consumption and carbon footprint in new and renovated buildings. For instance, the recast of European Directive on the energy performance of buildings is making nearly zero-energy buildings (nZEBs) a standard for new buildings by 2020. These buildings are self-sufficient in meeting their energy needs by reducing the energy demand and by using on-site renewable energy sources to meet the remaining needs [24].
Several ways have been proposed to reduce load, increase efficiency, and utilize renewable energy resources in all types of facilities. During a building's design and development, the reuse, renovation or repair of existing buildings as well, apply a comprehensive integrated approach to: i) reduce heating, cooling, and lighting demand through passive strategies such as climate-responsive design, daylighting, and conservation practices; ii) specify efficient HVAC and lighting systems that consider part-load conditions and utility interface requirements; iii) employ renewable energy sources such as solar heating for hot water, photovoltaics, geothermal space heating, and groundwater cooling, sized for the reduced building loads; iv) optimize building performance by employing energy modeling programs during design; v) optimize system control strategies by using occupancy sensors, CO_2 sensors, and other air quality alarms during operation; vi) Monitor project performance through a policy of commissioning, metering, annual reporting, and periodic re-commissioning; vii) Consider Retro-Commissioning of buildings which were never commissioned initially; and Integrate water-saving technologies to reduce the energy burden of providing potable water [25].
The accelerated deployment of renewables, combined with deep electrification and increased energy efficiency, can achieve over 90% of the energy-related CO_2 emissions reductions needed by 2050 to reach the well-below 2 °C aim of the Paris Agreement (see Figure 1-3).

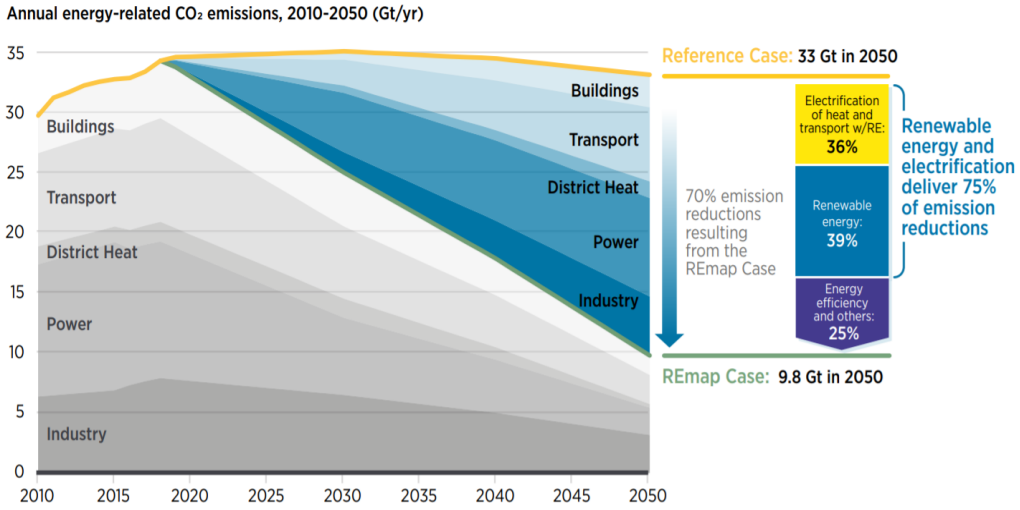

Figure 1-3. Annual energy-related CO_2 emissions in the reference case and reductions in the REmap case, with the contribution by sector, 2010-2050 (Gt/yr) [26].

Electrification with renewable power is key, together making up 60% of the mitigation potential; if the additional reductions from direct use of renewables are considered, the share increases to 75%. When adding energy efficiency, that share increases to over 90%.

1.1.4 Heat pumps and chillers for cooling and heating

One of the leading consumers of building energy is the process of cooling and heating to sustain thermal comfort. In 2019, the direct and indirect emissions from energy used in buildings rose to 10 $GtCO_2$ as a result of increasing energy demand for heating and cooling with growing air-conditioning installations and extreme climate conditions. Cooling is the most rapidly growing end use in buildings, as its energy demand went higher than triple between 1990 and 2018 to around 2,000 terawatt-hour (TWh) of the global electricity consumption [27].

Cooling strategies can be classified into passive and active. The passive cooling techniques enable lowering the indoor temperatures of the buildings using natural energy sources including the dissipation of surplus heat to the low-temperature natural sinks, the control of solar and heat gains and the use of thermal insulations. Active cooling can be implemented in building by using air-conditioning systems (i.e. air handling unit and packing air conditioner) [28, 29].

Most active cooling systems are electric vapor compression systems and thermally driven absorption chillers [30]. Electric compression chillers have higher energy efficiency and have less heat rejection systems than thermally driven sorption cooling systems. Vapor compression chillers are powered by electricity to compress the refrigerant, and then the refrigerant is allowed to expand and evaporate to remove heat from the system. The refrigerant is then compressed again to continue the cooling cycle. Centrifugal, screw, scroll and reciprocating compressors are used in vapor compression chillers depending on the application [31]. The use of the cooling tower gives water-cooled systems an efficiency advantage over air-cooled. In many large-size buildings, water-cooled chillers can offer a more effective cooling option compared to the air-cooled chillers and packaged rooftop units. This because they circulate water, which is more energy dense than air.

Various advanced cycles have been proposed and the performance of these cycles can be improved compared to the vapor compression cycle. The combined compression-absorption system keeps the advantages of both vapor compression and absorption refrigeration systems and simultaneously minimizes the limitations of both. An experiment was carried out on the absorption/compression chiller or heat pump with working pair water/LiBr and mechanical vapor compressor [32]. It was noted that the minimum driving temperature of 80 °C was required to operate the absorption chiller without operating the compressor. The concept of the compression–absorption cascaded refrigeration systems has been visualized in references [33-35]. It was noted that the electric power consumption in cascaded vapor compression-absorption system is reduced by 61% and COP of compression section is improved by 155%. The minimum generator temperature for compression–absorption cascaded refrigeration system was 67 °C. The hybrid evaporative cooling-based vapor compression system reduces the compressor power consumption by 10-18% [36-38]. It was noted that the evaporative cooling-based vapor compression maximized the life duration of the vapor compression system and reduced its electricity consumption. The desiccant regeneration temperature systems have been reported to operate at temperatures greater than 50 °C for satisfactory performance [39, 40]. However, the desiccant cooling system is suitable for high humidity climates and countries with high energy prices. The average regeneration temperature for the adsorption chiller (COP of 0.59) is 62–65 °C [41].

1.1.4.1 Thermal absorption chillers

The utilization of absorption chiller systems as the part of poly-generation systems has led to the promotion of a number of worldwide projects in the last years. While the advantages of this cycle include very little electric input requirements and the ability to utilize various heat sources, disadvantages include a low coefficient of performance (COP) in comparison to electric chillers, a higher capital cost and their requirement for larger cooling towers. There are several possible working pairs (absorbent–refrigerant) that can be used in absorption refrigeration systems. However, the conventional absorption chillers use H_2o/LiBr for air-conditioning [42, 43]and NH_3/H_2O mainly for refrigeration [44]. The water lithium bromide pair uses water as refrigerant and lithium bromide as absorbent, while the ammonia water system uses water as absorbent and ammonia as refrigerant.

A recent review of the new developed water/LiBr chillers and heat pumps was presented in [45]. It was found that the new water/LiBr absorption chillers include the air-cooled chiller with small capacity of 2.5 kW, compact chillers with asymmetric plate heat exchangers and nominal capacity of 15, 30, and 65 kW, compact absorption heat pump systems for cooling and heating with nominal cooling capacities of 50, 160 and 500 kW, single-effect double lift chiller with a heat source temperature glide of 40 K and solar gas-fired absorption chillers which are the future of robust solar space cooling solutions. Moreover, the R718 turbo compressor boosted water/LiBr chillers showed the desired operation flexibility with a heat rejection temperature above 35 °C.

The traditional single-stage absorption chiller is driven by a hot water temperature of 70-95 °C and release it at 60-85 °C [46, 47]. Table 1-1 summarizes the main characteristics of a commercial single

stage hot water driven absorption, single stage double-lift absorption and low generator temperature single stage absorption chillers.

Table 1-1. Characteristics the traditional single-stage hot water driven absorption chillers [48]

Hot water driven absorption chiller	Traditional single effect	Single effect double-lift	Low-generator temperature
Nominal cooling capacity (kW)	264	264	264
Chilled water supply temperature (°C)	8	7	13
Chilled water return temperature (°C)	13	12	18
Chilled water flow rate (m^3/h)	45.4	45.4	45.4
Cooling water inlet temperature (°C)	31	31	31
Cooling water outlet temperature (°C)	36.5	36.5	36
Cooling water flow rate (m^3/h)	99.1	107	156
Hot water inlet temperature (°C)	95	95	70
Hot water outlet temperature (°C)	80	55	60
Hot water flow rate (m^3/h)	21	9.0	56.3
Electric power consumption (kW)	2.5	3.1	3.8
COP (-)	0.72	0.72	0.72

Table 1-2 summarizes the main characteristic of new absorption chillers. the water-cooled absorption heat pump water/LiBr (MODEL-BEE-50) is driven by a hot water at a temperature ≥ 55 °C with a cooling capacity of 50 kW [49]. While the new air-cooled absorption chillers feature small size without cooling towers (directly and indirectly air-cooled) and high efficiency with the use of dual heat sources. The air-cooled absorption chiller (PURIX ApS-type A25s) has a cooling capacity of 2.5 kW with a COP of 0.76. This chiller is driven by the hot water at temperature greater than 75 °C produced from 2 flat-plate collectors with a total aperture area of 4.8 m^2 and/or backup heating systems of 3.1 kW as a heat supply capacity [50].

Table 1-2. Main characteristics of new air-cooled and water-cooled absorption chillers

Hot water fired absorption chiller	BEE-50 [49]	PURIX-A25s [50]
Cooling tower	water-cooled	air-cooled
Nominal cooling capacity (kW)	50	2.5
COP (-)	0.80	0.76
Chilled water supply temperature (°C)	9	13
Chilled water return temperature (°C)	14	18
Cooling water flow rate (m^3/h)	14.4	-
Outdoor temperature (°C)	35	35
Minimum heating capacity(kW)	65	-
Hot water driven temperature (°C)	≥ 55	≥ 75

The condenser and absorber of the absorption chiller can be cooled by either water or air. The water-

cooled absorption chiller is most widely used, but the difficulty of configuring the cooling tower for the water-cooled absorption makes the air-cooled absorption chillers favorable as a single unit (saves water and space) in residential buildings [51].

1.1.4.2 Electric heat pumps

The initial cost of a compression chiller is equal to that of purchasing a reversible heat pump, whereas the heat pumps can provide thermal needs throughout the year. Heat pumps (HP) have a great potential for heating and cooling, especially in climates where the winter is not very cold, as is the case of areas with a Mediterranean climate. The HP is one of the environmentally friendly technologies using renewable energy. In the Directive 2010/31/E.U. [52], Article 2 point 18, heat pump means a machine, a device or installation that transfers heat from natural surroundings such as air, water or ground to buildings or industrial applications by reversing the natural flow of heat such that it flows from a lower to a higher temperature.

The global market of HP systems is expected to achieve $102.5 billion by 2025. The Most popular type of heat pump in residential sector is the air-source HP that transfers energy between the building and ambient air [53]. The scroll compressor HP system was experimentally investigated in four modes: air to air, air to water, water to water and water to air. The COP was 3.94 for water-to air HP, 3.73 for water-to water HP, 3.54 for air-to-air HP and 3.40 for air to water HP [54]. Water source heat pumps (WSHPs) are popular because they can efficiently supply simultaneous heating and cooling. This leads to comfortable conditions in zones that have different requirements. Air source heat pumps (ASHPs) have been extensively employed to maintain indoor thermal comfort due to their convenience and energy saving potential. ASHPs are a potential solution, due to the low cost, the convenience of installation, and flexibility of load adjustment to meet personalized requirements for heating and cooling. However, the outdoor temperature has great impact on the performance of ASHP and a frost layer can be accumulated on the surface of the evaporator under the environmental condition of low temperature and high humidity [55]. The WSHPs makes it possible to obtain better performance with less required space compared to air source heat pumps. The water supply may be a recirculating closed loop or a once-thru system using water from a well, a pond, or a stream. The high initial and long-term cost of cooling towers (large water coil and the centrifugal fan) are considered as a main limitation for closed-loop water source HP systems [56].

The main characteristics of the reversible HP to provide buildings with cooling and heating using radiant floor and fan coil are shown in Table 1-3. In cooling mode, the supply and return chilled water temperatures are 18 °C and 23 °C for the radiant floor system and 7 °C and 12 °C for the fan coil system. In heating mode, the supply and return hot water temperatures are 35 °C and 30 °C for the radiant floor system and 45 °C and 40 °C for the fan coil system.

Table 1-3. Characteristics of two commercial water-to-water electric HP systems [57]

water-to-water HP (VXT-16-Scroll- R410A)	Radiant Floor	Fan Coil
Cooling mode		
Cooling capacity (kW)	20.3	15.26
Electricity consumption (kW)	3.5	3.52
Chilled water supply temperature (°C)	18	7
Chilled water return temperature (°C)	23	12
Evaporator flow rate (l/h)	3500	2620
Hot water supply temperature (°C)	35	35
Hot water return temperature (°C)	30	30
Condenser flow rate (l/h)	4080	3200
Heating mode		
Heating capacity (kW)	18.6	17.79
Electricity consumption (kW)	3.6	4.5
Hot water supply temperature (°C)	35	45
Hot water return temperature (°C)	30	40
Condenser flow rate (l/h)	3200	3,060
Chilled water supply temperature (°C)	5	5
Chilled water return temperature (°C)	10	10
Evaporator flow rate (l/h)	2610	2320
COP (-)	5.17	3.95
EER (-)	5.80	4.34

1.1.5 Renewable energy resources

As a viable solution, renewable energy sources can provide energy free of air pollutants and greenhouse gases by emitting zero or nearly zero percent of these gases [58]. Renewable sources can be used to produce energy again and again, i.e. solar energy, wind energy, geothermal energy, biomass energy, etc. and are also often called alternative sources of energy. According to the Energy Outlook 2019, the share of renewable energy continues to show rising levels of energy demand over the next three decades. In Figure 1-4, worldwide renewable energy consumption increases by 3% per year between 2018 and 2050 driven by electricity demand growth and economic and policy scenarios [59].

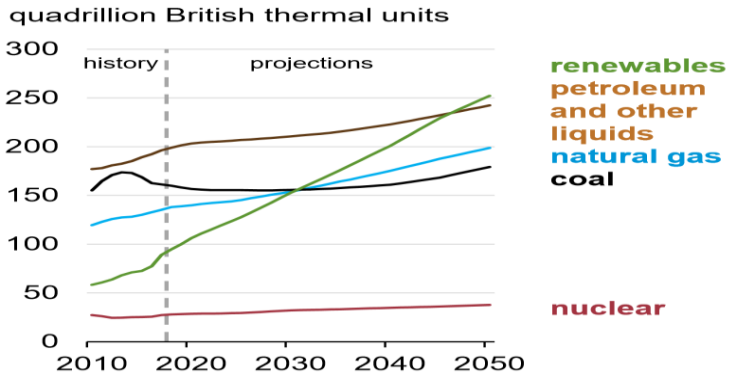

Figure 1-4. Primary energy consumption by energy source [59].

The Sun is the most abundant energy source for the earth. Solar energy is the most promising resource as it plays a vital role in the economic growth, improvement in the quality of life and the achievement of a sustainable future of a nation [60]. Nowadays, generating solar power costs significantly less than new nuclear and coal plants, however, also it costs less than gas, and in the range of wind, depending on the region, even less. The latest levelized cost of energy analysis, released in November 2018 by U.S. investment bank Lazard, shows utility-scale solar cost improving over the previous version by 14%. Utility-scale solar is again cheaper than new conventional power generation sources nuclear and coal, as well as combined cycle gas turbines (CCGT) (see Figure 1-5).

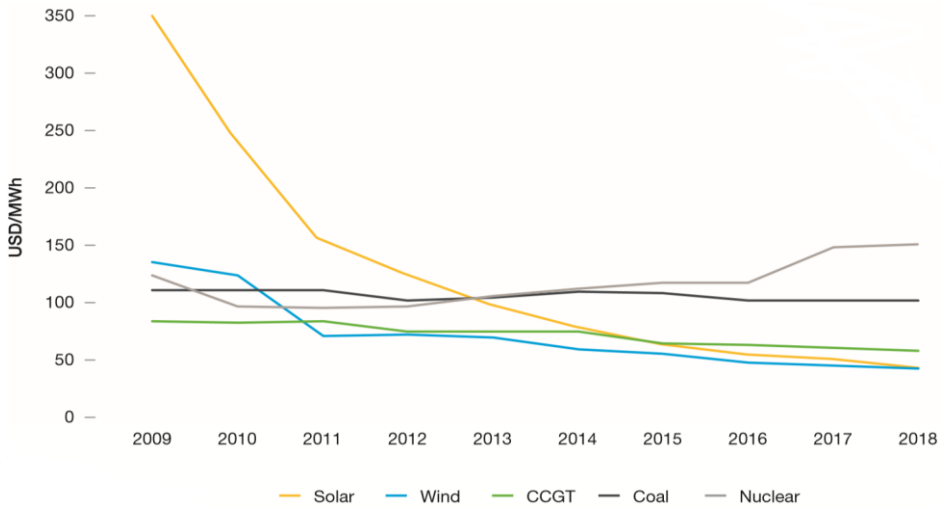

Figure 1-5. Solar electricity generation cost in comparison with other power sources from 2009 to 2018 [61].

Solar energy technologies can be classified as both a passive and an active technology. Passive solar energy technology merely collects the energy without converting its heat or light into other forms (i.e. maximizing the use of daylight or heat through building design) [62] whilst active solar energy technology stores and converts the solar energy to be used for other applications. This can be broadly classified into photovoltaic (PV) technology, solar thermal technology and hybrid photovoltaic/thermal (PV/T) technology [63]. The most significant difference between solar thermal and photovoltaic systems is that solar thermal systems produce heat and photovoltaic systems

produce electricity. The PV panel or module consists of cells made of semi-conducting materials. These cells directly convert solar energy to electricity, which demonstrates the photovoltaic effect.

Solar PV is set to increase the fastest of all renewable energy sources in 2020. However, the material uncertainty affecting the small-scale solar sector, with installations having stopped or slowed as a result of the lockdown restrictions [64]. The Mediterranean region presents favorable conditions for the solar energy implementations. Moreover, countries in the region have committed to collaborate throughout the energy transition path, in this way hoping to achieve their ambitious national and regional objectives.

1.1.6 Photovoltaic technologies

Solar PV systems have advanced markedly resulting in increased PV conversion efficiency and the expanded utilization awareness of solar energy. According to the International Energy Outlook 2018, solar capacity will rise by 9% per year in the residential sector and 6% per year in the commercial sector, from 2017 through 2050 owing to the cost and value trade-offs between fixed-tilt and tracking solar technologies [65]. Solar PV modules have been utilized at an exponential rate; the total global installed capacity grew from 6 GW in 2006 to 219 GW by the end of 2015 [66]. Solar PV experienced another year of record growth in 2015, with the annual market for new capacity up 25% over 2014. More than 50 GW was added – equivalent to an estimated 185 million solar panels – bringing total PV global capacity to about 227 GW [67]. In addition, PV system price reduction of around 75% in less than 10 years has brought solar power close to cost competitiveness in several countries. The lowest reported in-house module production cost in China was $0.37/W in 2016, whilst the Canadian solar market saw module costs as low as $0.29/W for 2017 [68]. In 2018, tenders and power purchase agreements showed several instances of bids, awards and contracts with solar power prices in the 2 U.S. cents/kWh range. Such price levels were reached in various geographies around the world. The lowest solar power price bid in 2018 was recorded at 1.86 U.S. cents per kWh in India and at 2.8 U.S. cents per kWh in Egypt [69].

The PV performance can be enhanced by using two main approaches: firstly, enhancing the PV thermal performance by different cooling techniques to reduce the PV cells temperature which leads to an increase in the voltage output as well as the power output. Secondly, enhancing the PV power performance by using different solar concentrators to increase the input solar radiation to the PV cells, which leads to increase the current output as well as the power output.

The hybrid photovoltaic/thermal (PV/T) collector allows to serve various purposes. A main purpose is cooling the solar cells with a fluid stream either by natural or forced circulation can reduce the PV cell temperature and the PV performance increases. Additional purposes include the extracted heat from PV panels used as a source for heat pumps, domestic hot water, pool heating, ventilation and desiccant cooling systems. Also, the area required to install PV/T collector is about 40% less than the area required for each one installed separately with the same capacity [68].

In comparison to a simple flat plate PV system, a low concentration photovoltaic system (LCPV) can reduce the costs of production by up to 40% [70], due to their attributes of non-tracking, high reliability and low cost (the cost of reflector material is lower than the cell cost). Furthermore,

Silicon-based cells fit LCPV solutions. At concentration gains G<10x, the angular acceptance of the optics increases and may become compatible with a stationary installation [71]. With the potential to be fabricated from a single aluminum sheet, the V-trough concentrator is one of the easiest of all low-concentrating systems to be constructed [72]. Consisting of two flat reflectors fixed on the PV module placed as a V letter, the V-trough concentrator is designed to increase the intake of solar radiation to the PV device. Simple fabrication, uniform reflection on the PV with low PV cell heating, use without sun-tracking, and relatively lower production costs are some of the key advantages of the V-trough concentrator [73]. The PV/T systems in comparison to the PV, has the potential to achieve a reduction that reaches about 50% in the cost payback time, providing that the extracted heat from PV module is used [74]. Various researchers verify the prospect of generating electricity and heat energy from PV/T solar collector with either a forced or a natural flow. The PV/T system efficiency depends on various factors like cooling fluid type, the system design, the PV panel used, in addition to operational parameters such as the climate conditions, fluid flow rate and the application used.

To make PV technologies more accessible, different forms of financing have been made available within the last decade. In the United States, for example, tax credits, net metering, and renewable portfolio standard (RPS) policies have been used as incentives to drive the development of the PV industry. In Europe, PV systems are primarily supported by feed-in-tariff (FiT) and net metering [75]. FiT remains the most popular support scheme for all sizes of grid-connected PV systems in Europe, ranging from small household rooftop applications to large-scale PV plants. Ground-mounted PV plants, however, are generally less profitable than rooftop PV systems. More specifically, in France, the FiT range (€/kWh) is about 0.0755 to 0.2969, while in Greece the range is between 0.095 and 0.125 €/kWh (where the FiT payments are guaranteed for the duration of the eligibility period of 20 years for PV plants) [76].

The E.U. Climate and Energy Commission imposes cutting at least 40% of the greenhouse emissions, setting at least 32% for renewable energy and improving energy efficiency at least at a 32.5% by 2030 [77]. PV in buildings also has the ability to turn into small-distribution net electricity producers. It can be mounted on buildings, mounted on special support structures, or be made an integrated part of the building. Today, PV in buildings appear as the most promising in the market offering a connection between PV from scattered small-scale and major power generating technologies for the twenty-first century. PV systems can be incorporated into buildings by either superimposition, where the system is attached over the existing building envelope, or integration, where the system is formed as a part of the building envelope. One of the restrictions of PV systems in buildings is the limited available area on the roof. Building with limited roof area requires efficient PV systems to maximize the production per available area and efficient air-conditioning system to maximize the use of on-site PV energy.

1.1.7 Solar power configurations

There are three standard configurations for solar power: Stand-Alone or off-grid, Grid-tie or on-grid, and Grid-tie with power backup or grid-interactive.

Stand-alone PV system to provide power at a location where there is no other source available. Stand-alone systems fundamentally all work in the same way: the solar panel generates power; the electricity is stored in a battery and then used as required. Grid-tie is gaining popularity in Europe and the united states. This is due to the availability of grants to reduce the installation costs and the ability to earn money by selling electricity back into the electricity companies through a feed-in tariff. In a grid-tie system, solar power system runs during the day and any surplus energy produced is then fed into the grid. In the evening and at night, when solar energy system is not producing electricity, the power is supplied from the grid. The benefit of grid-tie solar installations is that they reduce the reliance on the electricity companies and ensure that more of electricity is produced in an environmentally efficient way. Grid-tie with power backup also known as a grid interactive system that combines a grid-tie installation with a bank of batteries. It is also possible to a system incorporate other power generators into a grid interactive system such as a generator, this would allow a grid interactive system to work as a highly efficient uninterruptable power supply for extended periods of time. The cost of grid-tie system with power backup is higher than a standard grid-tie system, because of the additional cost for batteries and battery controllers.

1.1.8 Micro-Grid and district heating and cooling networks

Recently interests in the micro-grid have been growing as a new eco-friendly energy system a flexible architecture for deploying distributed energy resources. Because it can be designed to accommodate renewable resources, improve energy efficiency and provide ancillary services for the bulk electric power system. It is anticipated that many micro-grids will penetrate into power grids, especially electrical distribution systems. The micro-grid consists of the power conditioning system, energy storage, the loads and energy management and control system. This smart power systems are designed to provide a reliable electricity supply and better quality for a small number of consumers such as households, small islands. However, the amount of energy generated by the PV varies with time and does not usually match the consumption profiles. In on-grid systems, demand response is often used to reduce operating costs. Demand response involves a change in consumption pattern in response to a change in electricity price over time or to cost incentives aimed at reducing consumption or shifting it to another time during hours when the market price of electricity is high.

The most common type of district energy system is the district heating (DH) system, however, depending on the climate condition and location, the hot water might be used in absorption chiller or heat pumps to generate cooling during summertime. On the other hand, if the primary purpose of the district energy system were to provide cooling energy to the building, the system would be referred to as district cooling (DC) system. There is often a combination of heating and cooling energy provided by the district energy plants; such plants would be called district heating and cooling (DHC) system. If the energy input for the plant is coming from various sources and the output is not limited to heating and cooling, the configuration would be named as district energy network (DEN). DEN could provide heating, cooling and electricity to the supporting district [77].

There are five different generations of district heating networks. The first generation (technology period: 1880–1930) was a steam-based system fueled by coal. Nowadays, this generation is

technologically outdated. The second generation (technology period: 1930–1980) burned coal and oil to supply temperatures above 100 °C, the energy was transmitted through pressurized hot water. The third Generation (technology period: 1980–2020) usually used coal, biomass and waste heat as energy sources to supply hot water temperatures around 55-70 °C. In some systems, geothermal and solar energy were also used. High-temperature district heating networks suffer from significant heat losses especially in summer and high installation costs. As a viable solution, current investigations focus on the fourth and fifth generation district networks to achieve higher operating efficiency at low temperatures. The fourth generation (technology period: 2020–2050) district network requires a very large capacity centralized thermal storage and a separate system to supply chilled water without the ability to exchange heat with buildings The fourth generation used heat recovery from renewable energy sources to supply temperatures of 70 °C and lower [78]. The fifth generation is the latest stage in the development of district heating and cooling systems while the individual reversible HP is essential for all buildings on the network. The fifth generation district network is a bidirectional and decentralized network with the ability to recover waste heat, integrate renewable energy sources, supply heat at ultra-low temperature below 45 °C and having low transmission losses for cooling and heating [79, 80]. District cooling and heating network is the most cost-effective way to integrate renewable energy into buildings.

1.2 Overview of photovoltaic/thermal assisted cooling and heating systems

The use of solar energy to provide the energy source for cooling and heating is a promising concept. This can be done by using PV electricity and an electricity-driven vapor compression chiller/heat pump or by using solar thermal energy with thermally driven chillers. Currently, the photovoltaic powered air conditioning systems have been found to yield higher energy efficiency, technical reliability, and economic viability in comparison to other solar thermal options. In this configuration, the photovoltaic input to the air conditioner can occur either as a direct current or as an alternating, and batteries can also be used to enhance performance. Systems connected to the grid are simpler in design and consist of photovoltaic panels and inverters. While some of these systems will only import energy, some of the systems connected to the grid will even export excess energy back to the grid.

In the recent technical and economic comparison of different solar cooling approaches, photovoltaic air conditioning options were predicted to be more economically and efficient than thermal cooling alternatives [81, 82]. The study also found that the PV modules required a lower installation area than solar thermal collectors, and that the CO_2 emissions per thermal kWh of production for the photovoltaic systems were significantly lower than that of the thermal systems. The study attributed the lower CO_2 emissions to the higher COP values associated with solar electric cooling. Another study conducted a TRNSYS dynamic simulation on a typical office building in Milan and Trapani, Italy that comparatively assessed energy and economic efficiency of both thermal and photovoltaic solar cooling systems [83]. The simulation concluded that photovoltaic solar cooling options maintained a higher performance and were more economically than thermal cooling systems. Moreover, electric compression chillers have higher energy efficient and have less heat rejection systems than sorption

cooling systems [84]. This means that PV air conditioning systems will consume less water and need a lower auxiliary energy.

A simulation study looked at the use of two different energy storage systems for a photovoltaic heat pump assisted system [85]. Results of the study indicated a self-consumption rate of 89% for battery reliant systems and 88% for systems reliant on a hot water tank for energy storage. Worth noting, however, is that the levelized cost of electricity for the system that used batteries was twice as high as the cost associated with the system that used a hot water tank. The study highlighted the limitations of battery use in that lead acid batteries have a very short lifespan (of about seven years).

Solar based heating and cooling systems may assume various configurations depending upon the manner in which the individual system components are inter-connected and the adopted control scheme. Figure 1-6 shows the different integration configurations of different solar electric systems, including PV modules, PV/T collectors and LCPV/T systems. The solar systems are integrated into the micro grid utilizing the bidirectional integration method (Export and import electricity) and they are coupled with air conditioning systems including compression chiller, absorption chiller, heat pump and liquid desiccant wheel with the possibility of the bidirectional integration mode of exporting to and importing from the chilled/hot water network for maximizing the solar energy conversion.

Figure 1-6.a shows the base integration method of a PV cooling system: the electric chiller is powered by the PV system via the inverter and controller for space cooling. An experiment was carried out on an inverter air conditioning unit connected simultaneously to the grid and to 3 PV panels [86]. The unit was working in an office of 35 m^2 located in Alicante (Spain) during six summer months that required cooling, with a working timetable from 8:00 to 20:00. It was shown that the ratio between the energy produced from the solar panels and the total energy consumed by the equipment in cooling mode from May to October was 64.5% and the ratio between the power supplied by the PV panels connected directly to the system and the PV panels connected to the grid, was 65.1%.

Figure 1-6.b shows the base integration method of a PV heating system: the heat pump is powered by the PV system via the inverter and controller for space heating and DHW applications. An economic and energy assessment study analyzed the performance of photovoltaic systems using three different heating mechanisms: district heating, direct electric heating, and a heat pump [87]. The study analyzed a community of 10 single-family homes in Finland. During operation, once the system had fulfilled the appliance demand for energy, the surplus photovoltaic power was used to charge a thermal storage, storing the energy as heat so that the excess power would not be returned to the grid. The study found that the zero-energy level (ZEL) indicator, (defined as the ratio of the primary energy generation to demand), reached 0.96 for the heat pump, 0.84 for the district heating system, and 0.50 for the direct electric heating system at 10 kW PV capacity. As a result, the study concluded that the heat pump was the closest to a near zero energy building grade and that the thermal storage had nearly no effect on the ZEL. Another experimental work was carried out on a heat pump used for DHW production, which was powered from photovoltaic panels and the grid simultaneously [88]. It was concluded that the annual average efficiency of the heat pump could be

close to 3.5 and the annual average efficiency of the whole system including PV was near 9, while the solar contribution was higher than 60%.

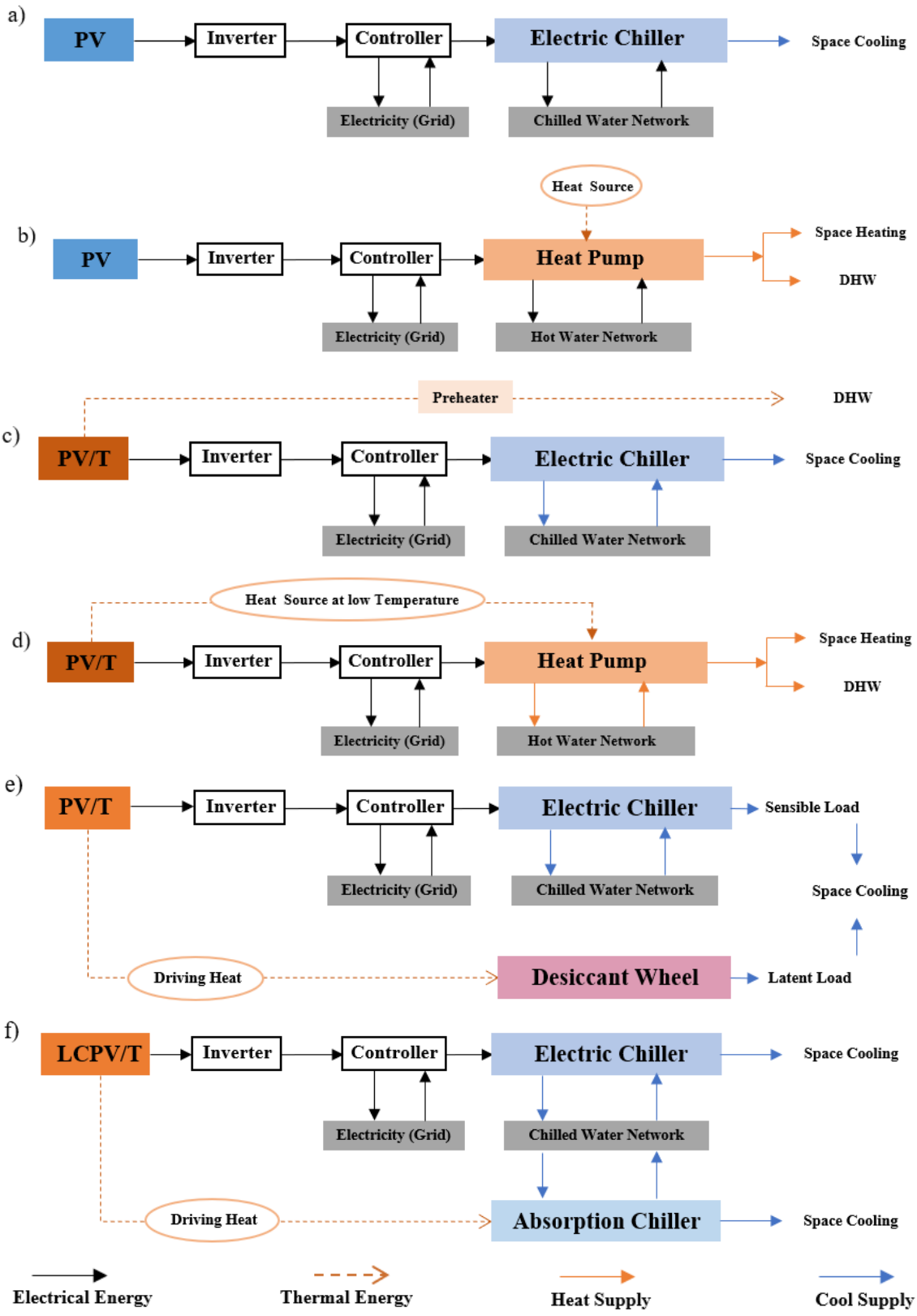

Figure 1-6. Study systems and their bidirectional configurations with electricity microgrid and chilled/hot water network for cooling and heating of buildings in different climate conditions.

The reversible heat pumps have the greatest potential in areas similar to that of the Mediterranean climate, where it is not exposed to severe winter conditions [89, 90].

Hybrid PV/T systems can be used efficiently to meet heating demands for space heating and DHW applications and/or cooling demands in enclosed spaces using various configurations. This may be achieved by: i) using the PV/T system to provide both the electric power and heat-source temperature input to a heat pump which maximizes the system's performance; ii) coupling the PV/T system to an electricity-driven air conditioning system; iii) coupling the PV/T system to a thermally-driven cooling and heating systems. Heat pumps and hybrid photovoltaic/thermal systems are environmentally friendly technologies and their integration into buildings allows provision of cooling, heating and electricity.

Figure 1-6.c shows the integration of the PV/T and chiller systems where the electric power generated is used to power the electric chiller. Meanwhile, the produced thermal energy is used for DHW applications. An experiment was carried out on the preheated water produced from the absorbed heat from the photovoltaic conducted to a water heater to meet the DHW demand [91]. The study found that the average efficiency of the PV without the cooling system was 10.9%, while, equipping the PV with the heat exchanger improved the electrical efficiency to 12.3%. In this case, the average thermal efficiency of the PV/T was 49.4%. A techno-economic analysis was carried out to assess PV/T systems for distributed electricity and hot-water provision in a typical house in London, UK [92]. The water based PV/T system demonstrated an annual electricity generation of 2.3 MWh, or a 51% coverage of the household's electrical demand (compared to an equivalent PV-only value of 49%), plus a significant annual water heating potential of 1.0 MWh, or a 36% coverage of the hot-water demand. The PV/T system comprised an array of 9 modules, each with a nominal electrical power rating of 250 W and a total surface area of 1.62 m^2.

Figure 1-6.d shows the typical integration method of PV/T where the generated electric power is used to power the heat pump. Meanwhile, the produced thermal energy is used to assist the heat pump in the evaporator for space heating and DHW applications. Solar assisted heat pumps are categorized into 2 groups based on the integration scheme between the solar system and the heat pump. These are termed Direct Expansion Solar Assisted Heat Pump (DX-SAHP) and Indirect Expansion Solar Assisted Heat Pump (IDX-SAHP). The DX-SAHP allows for the refrigerant to flow through the solar collector while the IDX-SAHP requires a heat exchanger between the refrigerant and the fluid that goes through the solar collector. The integrated PV/T system with a heat pump, which provides both thermal energy and electrical power, is the PV-evaporator type [93]. In DX-SAHP configuration, the PV/T is coupled to heat pump systems through the heat exchanger beneath the PV modules as an evaporator. Depending on the climate conditions, sometimes the PV/T collectors are cooling the water stream instead of heating it. Therefore, the control is required to ensure switching off the system when the evaporator temperature is below a certain value. IDX-SAHP systems are divided into three types: series systems; parallel systems; and dual systems. The heat transfer medium is typically antifreeze solution, water or air. For series and dual systems, the heat pump performance is boosted by the utilization of solar energy.

An experiment was performed on a solar driven direct-expansion heat pump system employing PV/micro-channels-evaporator modules under the real-time operational conditions of Lvliang, China [94]. It was found that the average thermal, electrical and overall efficiency were 56.6%, 15.4% and 69.7% respectively, while the average COP of the system reached 4.7. An experimental study on a novel PV/T air dual-heat-source composite heat pump hot water system was conducted in two operation modes, namely, dual-heat-source operating mode and single-heat-source operating mode [95]. It was shown that the temperature and solar irradiance were in the range of 25°C to 27°C and 820 W to 872 W, respectively. The electrical gain and electrical efficiency were in the range of 268 W to 283 W and 13.7% to 14.9%, with mean values of 278 W and 14.5%, respectively. The COP value was in the range of 2.74 to 5.98, with an average value of 4.08. The exergy efficiency was in the range of 0.12 to 0.45, with a mean value of 0.33. It was concluded that the PV/T air dual-heat-source composite heat pump hot water system had excellent performance.

The potential of a PV/T system to heat and cool office buildings using a reversible air-to-water heat pump in three different climates (Moscow, Stuttgart, Dubai) was investigated [96]. The PV/T system was used as a heat source and heat sink for a reversible HP. In the heating mode, during the day, the thermal energy produced from the PV/T system is used as the heat source for the HP. In the cooling mode, during the night, heat is removed from the PV/T system by long-wave radiation between the collector surface and the night sky along with the convective heat transfer caused by the temperature difference between the PV/T surface and the ambient. Based on the deployed dynamic simulation, the seasonal performance factor was between 3.6 and 4.8 for heating and between 5.7 and 6.5 for cooling.

The COP values of the PV/T water-source heat pump and PV/T air-source heat pump based heating mode were 3.18 and 2.53 respectively which was significantly higher than the COP of a conventional air-source heat pump- heating mode which had a value of 2.23 [97].

The performance of the solar-assisted heat pump and an adsorption chiller, both driven by PV/T collectors was investigated [98]. The total energy efficiency of the PVT was 49%, a heat pump yearly coefficient of performance for heating mode above 4 and a coefficient of performance of the adsorption chiller of 0.55. PVT thermal energy is fluctuating due to the external radiation and temperature. Thus, an auxiliary system is always mandatory in order to satisfy the DHW and space cooling demand.

Figure 1-6.e shows the integration of the CPV/T and the electric Chiller – dehumidification system where the electric power generated by the CPV/T system is used to power the compression chiller (sensible cooling) while the heat produced from the CPV/T is used to assist/drive the liquid desiccant wheel (latent cooling). The performance of the integrated two-stage liquid desiccant cycle driven by the heat from a PV/T collector for trigeneration application was performed [99]. It was found that the PV/T liquid desiccant system was adopted to treat the latent heat load of an office building in Beijing and thus improve the electric chiller performance. Compared to conventional air-conditioning systems, electricity could be saved by producing the same amount of cooling energy for 50% at the design point. In another investigation contributed by the same group of authors [100], It

was shown that the liquid desiccant system integrated with a concentrated PV/T had a superior power saving ability of 56% comparing with the conventional air conditioning system.

Figure 1-6.f shows the integration of the CPV/T with compression and absorption chillers where the electric power generated from the CPV/T is used to power the electric chiller. Meanwhile, the heat produced is used to assist/drive the absorption chiller. Recently, a LCPV/T triple-generation system for heating, cooling and electricity in Beijing, China was proposed in [101]. This system involved the low-concentrating PV/T system, high-temperature water source heat pump, lithium bromide absorption chiller and capillary net radiant ceiling. The LCPV/T module consists of monocrystalline PV cells, Compound Parabolic Concentrator and aluminum cooling channels where the coolant water flows through. It was found that under the low concentration condition, the system produces hot water of 45 °C–90 °C. Meanwhile, the lithium bromide absorption chiller operates stably, with the COP above 0.5. The electric efficiency of the LCPV/T was about 10% and the thermal efficiency was around 60%–69%.

1.3 Justification

The 2030 Framework for Climate and Energy established that E.U. countries need to increase the share of renewable energy and save energy to reduce their greenhouse gas emissions. The incorporation of photovoltaic technologies into buildings has a great potential in reducing the CO_2 emissions for climate change mitigation. Buildings with limited roof area require efficient solar systems to maximize the production per available area and efficient air-conditioning system to maximize the use of on-site PV energy. District cooling and heating network is the effective solution to use and share renewable energy sources in buildings.

Most of photovoltaic installations suffer from a drop-in cell efficiency as a result of increasing the PV cell temperature, decreasing the open circuit voltage. By cooling the solar cells with a fluid stream either by natural or forced circulation can reduce this PV cell temperature. The flexibility of integrating hybrid photovoltaic/thermal systems into building for solar heating and electricity generation, makes it possible to attain higher performance with less space needed. However, photovoltaic/thermal systems are efficient only when its heat was used for a useful purpose. The useful heat stream from the PV/T is appropriate for a domestic hot water application and space air heating in winter (cold climate). Nevertheless, in summer (hot climates) the fluid stream could be wasted because of the limited application based on this temperature range.

The PV power performance can be enhanced by using different solar concentrators in order to increase the input solar radiation to the PV cells which leads to increase the current output as well as the power output. As the light intensity on the cell is increased by the concentration ratio, the useful hot stream temperature produced from cooling the PV module is increased. For building applications, LCPV/T systems would be preferable due to their potential for non-tracking, high reliability and low cost. Further, Silicon-based cells fit well into low concentration solutions.

The available literature features a broad number of studies that have explored solar PV, PV/T and LCPV/T systems, but none of them presenting a comprehensive enough assessment of i) the effect of modifying the selected PV module to water-based LCPV/T ; ii) the dynamic performance of

on-site energy generation from PV, PV/T and LCPV/T and iii) the dynamic matching between energy generation and production in buildings with limited available area.

A solar PV, PV/T and LCPV/T coupled with efficient space cooling and heating systems can provide buildings with electricity, heating and cooling in a very flexible way throughout the year. The energy efficiency in buildings requires cost and efficient optimal solutions to reduce the investment cost and to increase the energy production as much as possible. The leading challenges faced upon accepting the PV systems for cooling and heating approach is that the hours of the day that experience the greatest production of solar power may occur when the consumption is at its lowest rate or vice versa, as well as the required high capital investment of storage batteries and water tanks. Balancing supply and demand with a connection to the electricity grid and the district cooling and heating network minimizes the effect of these problems reported.

The available literature features a broad number of studies that have explored solar cooling and heating systems and district coming and heating network, but none of them presenting a comprehensive enough assessment of i) the PV, PV/T and LCPV/T systems energy flow with cooling and heating systems in buildings incorporated into electricity microgrid and district thermal network under different climate conditions; and ii) the grid-tie photovoltaic technologies coupled with cooling and heating systems using different configuration methods and control mechanisms based on the solar contribution index, monthly bill saving, CO_2 emissions reduction and the payback Most research and development of solar PV/T assisted heat pump systems are based on the use of the heat recovery from cooling the PV module in the evaporator of the heat pump to improve the system performance for heating purposes. In extremely hot climates in summer, boosting the cost-effectiveness of LCPV/T could be achieved by assisting the thermal chiller along with powering the electric chiller when DHW applications are not demanded. In cold climates, boosting the cost-effectiveness of LCPV/T could be achieved by assisting the HP along with powering the compressor.

1.4 Thesis objectives

The core objective is to evaluate the effectiveness of integrating grid-tie photovoltaic systems (PV, PV/T and LCPV/T) coupled with space cooling and heating systems (air-cooled electric chillers, air-to-water electric heat pumps, water-to-water electric HPs and absorption chillers) into different existing buildings under different climate conditions.

The specific objectives required to achieve the core objective are:

i) Presenting the state of the art of photovoltaic technologies (PV, PV/T, LCPV/T) and overviewing their integration methods with air-conditioning systems for buildings.
ii) Investigating the experimental generation profiles of the PV technologies with displaying the modelling validation and simulation of PV, PV/T and LCPV/T in different climate conditions.
iii) Modelling of different configurations of integrating PV technologies with chiller and heat pump systems for cooling and heating.
iv) Illustrating the characterization of existing buildings to investigate their energy performance with displaying the sizing and design of PV, PV/T and LCPV/T.

v) Assessing the on-site energy production from grid-tie photovoltaic technologies coupled with efficient cooling and heating systems in buildings based on the solar contribution index, monthly bill saving, CO_2 emissions reduction and system payback.

1.5 Structure and methodological approach

This thesis adheres to the following structure. **Chapter 1** presents an introduction to renewable energy technologies for buildings and general view about the most common strategies used to achieve near zero energy consumption in buildings. Also, it presents an introduction to solar PV, PV/T and LCPV/T systems. Moreover, it presents an overview of recent investigations on the use of both electric and thermal energy from the PV, PV/T and LCPV/T systems for cooling and heating in buildings. Also, it illustrates the justifications, objectives and structure and methodological approach of this thesis. **Chapter 2** will take a close look at the current state-of-the-art of PV cells with a particular focus on developments in the PV/T and LCPV/T systems for building applications. It presents the integration methods for PV modules and thermal absorbers including the recent efforts on the conventional and novel PV/T systems i.e. air, water, air-water, bi-fluid, heat pipe, nanofluid, phase change materials based PV/T, PV/T evaporator and thermoelectric integrated PV/T. Also, it explores the development of low, medium and high concentration PV systems. It presents an overview of building integration photovoltaic (BIPV/T) systems including air based BIPV/T, water based BIPV/T, semi-transparent PV/T window and multifunctional bifacial BIPV modules. Also, it explores the available market products of PV, PV/T and LCPV/T systems. **Chapter 3** will investigate the experimental performance of the selected PV systems (PV, PV/T and the developed LCPV/T) and explore the development of a low-cost LCPV/T and its experimental implementation. It presents the model validation of the PV systems (PV, PV/T and LCPV/T) and investigates the dynamic performance of the PV, PV/T and water based LCPV/T systems in nine climates conditions. **Chapter 4** will investigate dynamically the energy impact of the selected PV, PV/T and the developed LCPV/T coupled with space cooling and heating systems in existing case buildings incorporated into the electricity micro-grid and thermal district network. It illustrates the working conditions of cooling and heating systems involving air-cooled electric chiller, air-cooled absorption chiller, air-to-water heat pump and reversible water-to-water HP. Furthermore, it investigates the energy performance of the selected case buildings with the sized cooling and heating systems based on the building loads. It illustrates the design and the sizing of the commercial PV, PV/T and LCPV/T systems based on the available rood area. It investigates the solar contribution index, monthly bill saving, CO_2 emissions reduction and the payback of the PV, PV/T and LCPV/T systems coupled with different cooling and heating systems. The proposed method incorporates dynamic modeling simulation environments (DesignBuilder/EnergyPlus engine and TRNSYS dynamic modelling environment) to investigate the match between energy production and consumption hourly, daily, monthly and yearly. Finally, **Chapter 5**, will present the "Conclusion and recommendations" of the study. It presents the summing up of the reasoned arguments and recommendations (see Figure 1-7).

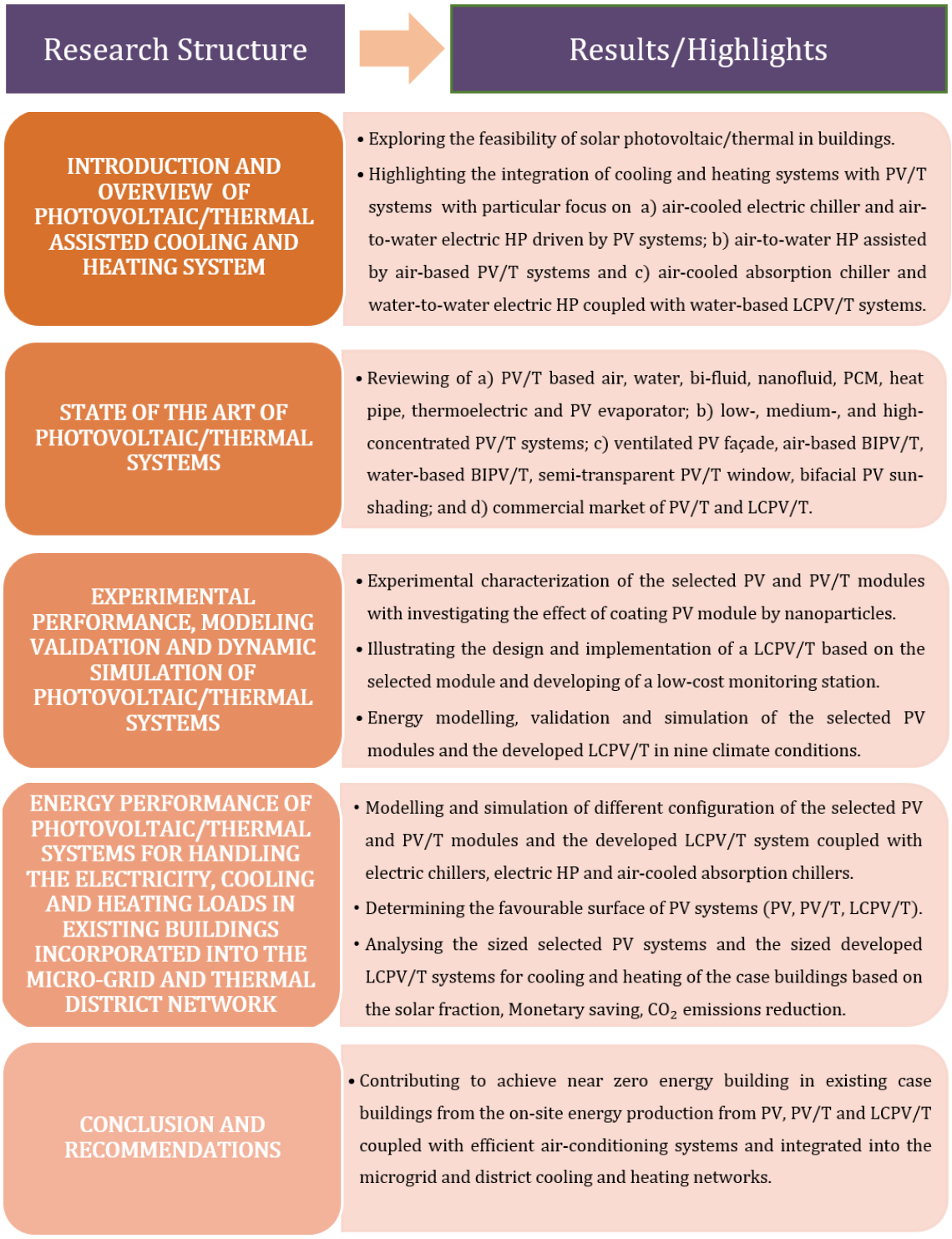

Figure 1-7. Thesis outline and structure.

References

[1]- Zeng S, Liu Y, Liu C, Nan X. A review of renewable energy investment in the BRICS countries: History, models, problems and solutions. Renewable and sustainable energy reviews 2017; 74: 860-872.

[2]- The Cost of Energy - Environmental Impact, (http://needtoknow.nas.edu/energy/energy-costs/environmental/); 2019 [Accessed 2019.09.19].
[3]- International Energy Agency - Global Energy and CO2 Status Report 2018, (https://www.eenews.net/assets/2019/03/26/document_cw_01.pdf); 2018 [Accessed 2019.07.19].
[4]- Ang BW, Su, B. Carbon emission intensity in electricity production: A global analysis. Energy Policy 2016; 94: 56-63.
[5]- IEA. Global Energy & CO2 Status Report - The latest trends in energy and emissions in 2018, (https://www.iea.org/geco/emissions/); 2019 [Accessed 2019.07.19].
[6]- eia - U.S. Energy Information Administration. International Energy Outlook 2016, (https://www.eia.gov/outlooks/ieo/); 2016 [Accessed 2017.01.12].
[7]- IEA. International Energy Agency - World Energy Outlook 2015, (http://www.iea.org/publications/); 2015 [Accessed 2017.01.10].
[8]- Population Matters, (https://www.populationmatters.org/); 2019 [Accessed 2019.02.10].
[9]- Allal HBJ, El Agrebi H and Campana D. Mediterranean energy transition: 2040 scenario, Executive Summary, Horizons. ISBN: 979-10-297-0489-5.
[10]- Tagliapietra S. The Future of Renewable Energy in the Mediterranean. Translating Potential into Reality. (https://papers.ssrn.com/sol3/papers.cfm?abstract_id=2596601). FEEM Working Paper No. 030.2015.
[11]- Desjardins J. How oil prices went subzero: explaining the COVID-19 oil crash. Visual capitalist news explainer, (https://www.visualcapitalist.com/subzero-oil-price-crash-covid-19/); 2020 [Accessed 2020.05.13].
[12]- Mylenka T and Novyk B. Impact of Covid-19 on the global energy sector. PV magazine, (https://www.pv-magazine.com/2020/04/24/impact-of-covid-19-on-the-global-energy-sector/); 2020 [Accessed 2020.05.14].
[13]- IEA. Energy Efficiency: Buildings, (https://www.iea.org/topics/energyefficiency/buildings/); 2019 [Accessed 2019.09.15].
[14]- IEA. Digitalisation and Energy, (https://www.iea.org/reports/digitalisation-and-energy); 2017 [Accessed 2019.08.15].
[15]- Cao X., Dai X, Liu J. Building energy-consumption status worldwide and the state-of-the-art technologies for zero-energy buildings during the past decade. Energy and Buildings 2015; 128: 198-213.
[16]- Urge-Vorsatz D. Energy End-Use: Buildings, (http://www.iiasa.ac.at/web/home/research/Flagship-Projects/Global-Energy-Assessment/GEA_CHapter10_buildings_lowres.pdf); 2011 [Accessed 2019.01.18].
[17]-EUROSTAT. Energy consumption in households, (https://ec.europa.eu/eurostat/statistics-explained/index.php/Energy_consumption_in_households); 2017 [Accessed 2019.05.20].
[18]- eia. International Energy Outlook 2016. U.S. Energy information Administration, (https://www.eia.gov/outlooks/ieo/); 2016 [Accessed 2017.01.18].
[19]- Chiesa G, Huberman N, Pearlmutterb D. Geo-climatic potential of direct evaporative cooling in the Mediterranean Region: A comparison of key performance indicators. Building and Environment 2019; 151: 318-337.
[20]- Enerdata. Global Energy Trends, 2019 Edition: Historically High Energy Consumption & CO2 Emissions in 2018, (https://www.enerdata.net/publications/executive-briefing/the-future-air-conditioning-global-demand); 2019 [Accessed 2019.09.5].
[21]- Isaac M, Vuuren DPV. Modeling global residential sector energy demand for heating and air conditioning in the context of climate change. Energy policy 2009; 37: 507-521.
[22]- Gunay B, Shen W, Newsham G. Inverse blackbox modelling of the heating and cooling load in buildings. Energy and Buildings 2017; 142: 200-210.
[23]- Lelieveld J, Proestos Y, Hadjinicolaou P, Tanarhte M, Tyrlis E, Zittis G. Strongly increasing heat extremes in the Middle East and North Africa (MENA) in the 21st century. Climatic Change 2016; 137: 245-260.

[24]- Good C, Andresen I, Hestnes AG. Solar energy for net zero energy buildings – A comparison between solar thermal, PV and photovoltaic-thermal (PV/T) systems. Solar Energy 2015; 122: 986-996.
[25]- WBDG. Whole building design guide – a program of the national institute of building sciences, (https://www.wbdg.org/design-objectives/sustainable/optimize-energy-use); 2018 [Accessed 2019.09.10].
[26]- IRENA. Global energy transformation - A road map to 2050, (https://www.irena.org/DigitalArticles/2019/); 2019 [Accessed 2019.09.25].
[27]- IEA. Tracking Buildings, (https://www.iea.org/reports/tracking-buildings); 2019 [Accessed 2020.02.18].
[28]- Figueiredo A, Figueira J, Vicente R, Maio R. Thermal comfort and energy performance: Sensitivity analysis to apply the passive house concept to Portuguese climate. Building and environment 2016; 103: 276-288.
[29]- Geetha NB, Velraj R. Passive cooling for energy efficient buildings with and without thermal energy storage - A review. Energy education science and technology part A: Energy science and research 2012; 29: 913-946.
[30]- Birol F. Towards a zero-emission, efficient, and resilient buildings and construction sector, Global status report 2017, (https://www.worldgbc.org); 2017 [Accessed 2018.04.05].
[31]- Tredinnick S, Phetteplace G. District cooling, current status and future trends; Chapter 6. In Advanced District Heating and Cooling (DHC) Systems. 2016: 167-188.
[32]- Schweigler C, Helm M, Eckert T. Flexible heat pump or chiller with hybrid water/LiBr absorption/compression cycle. International Journal of Refrigeration 2019; 105: 178-187.
[33]- Jain V, Kachhwaha SS, Sachdeva G. Thermodynamic performance analysis of a vapor compression–absorption cascaded refrigeration system. Energy Conversion and Management 2013; 75: 685-700.
[34]- Cimsit C, Ozturk IT. Analysis of compression–absorption cascade refrigeration cycles. Applied Thermal Engineering 2012; 40: 311-317.
[35]- Colorado D, Rivera W. Performance comparison between a conventional vapor compression and compression-absorption single-stage and double-stage systems used for refrigeration. Applied Thermal Engineering 2015; 87: 273-285.
[36]- Islam MR, Jahangeer KA, Chua KJ. Experimental and numerical study of an evaporatively-cooled condenser of air-conditioning systems. Energy 2015; 87: 390-399.
[37]- Wang T, Sheng C, Nnanna AGA. Experimental investigation of air conditioning system using evaporative cooling condenser. Energy and Buildings 2014; 81: 435-443.
[38]- Dakkama HJ, Elsayed A, AL-Dadah RK, Mahmoud SM, Youssef P. Integrated evaporator–condenser cascaded adsorption system for low temperature cooling using different working pairs. Applied Energy 2017; 185: 2117-2126.
[39]- Goldsworthly MJ, White S. Design and performance of an internal heat exchange desiccant wheel. International Journal of Refrigeration 2014; 39: 152-159.
[40]- La D, Dai YJ, Li Y, Ge TS, Wang RZ. Use of regenerative evaporative cooling to improve the performance of a novel one-rotor two-stage solar desiccant dehumidification unit. Applied Thermal Engineering 2011; 42: 11-17.
[41]- Sapienza A, Glaznev IS, Santamaria S, Freni A, Aristov YI. Adsorption chilling driven by low temperature heat: New adsorbent and cycle optimization. Applied Thermal Engineering 2012; 32: 141-146.
[42]- Somers C, Mortazavi A, Hwang Y, Radermacher R, Rodgers P, Al-Hashimi S. Modeling water/lithium bromide absorption chillers in ASPEN Plus. Applied Energy 2011; 88: 4197-4205.
[43]- Balghouthi M, Chahbani MH, Guizani A. Feasibility of solar absorption air conditioning in Tunisia. Building and Environment 2008; 43: 1459-1470.
[44]- Darwish NA, Al-Hashimi SH, Al-Mansoori AS. Performance analysis and evaluation of a commercial absorption–refrigeration water–ammonia (ARWA) system. International Journal of Refrigeration 2008; 31: 1214-1223.

[45]- Ayou DS, Coronas A. New Developments and Progress in Absorption Chillers for Solar Cooling Applications. Appl. Sci. 2020; 10: 4073. doi:10.3390/app10124073.
[46]- LG. LG HVAC solution- Absorption chiller HVAC SOLUTION ABSORPTION CHILLER, (https://www.lg.com/global/business/download/resources/sac/Catalogue_Absorption%20Chillers_ENG_F.pdf); 2015 [Accessed 2020.06.01].
[47]- York. YHAU-CL/CH Single Effect Hot Water Absorption Chiller, (https://www.york.com/Commercial-Equipment/Chilled-Water-Systems/Absorption-Chillers/YHAU_CL_CH_CH); 2016 [Accessed 2020.07.16].
[48]- World Energy. Absorption Chiller Heat Pump, (http://www.eco-cooline.ch/docs/kalt_world%20energy%20absorbtions%20chiller.pdf); 2011 [Accessed 2020.09.02].
[49]- Baelz automatic. MODEL "BEE" 50 KW, (https://www.baelz.de/en/theme-vorlagenseiten/bee/); 2017 [Accessed 2020.05.02].
[50]- PURIX. Solar Cooling System: Product Catalogue A25s, (http://www.purix.com/wp-content/uploads/2017/10/PURIX-Catalogue-A25s-EN.pdf); 2015 [Accessed 2020.06.06].
[51]- Chen JF, Dai YJ, Wang RZ. Experimental and analytical study on an air-cooled single effect LiBr-H2O absorption chiller driven by evacuated glass tube solar collector for cooling application in residential buildings. Solar Energy 2017; 151: 110-118.
[52]- European Union. Directive 2010/31/EU of the European Parliament and of the Council of 19 May 2010 on the energy performance of buildings (recast), (http://eur-lex.europa.eu/LexUriServ/LexUriServ.do?uri=OJ:L:2010:153:0013:0035:EN:PDF); 2010 [Accessed 2018.02.15].
[53]- kbvresearch. Global Heat Pump Market By Technology (Air Source, Water Source and Ground Source) By Application (Residential, Industrial and Commercial), (https://www.kbvresearch.com/heat-pump-market/); 2019. [Accessed 2020.09.08].
[54]- Çakır U, Çomaklı K, Çomaklı O, Karslı S. An experimental exergetic comparison of four different heat pump systems working at same conditions: As air to air, air to water, water to water and water to air. Energy 2013; 58: 210-219.
[55]- Mengjie S, Shiming D, Chaobin D, Ning M, Zhihua W. Review on improvement for air source heat pump units during frosting and defrosting. Applied Energy 2018; 211: 1150-1170.
[56]- Hepbasli A, Biyik E, Ekren O, Gunerhan H, Araz M. A key review of wastewater source heat pump (WWSHP) systems. Energy Conversion and Management 2014; 88: 700-722.
[57]- VXT. Technical manual installation manual-R410A-Water/water or geothermic heat pumps, (https://planetaklimata.com.ua/instr/Aermec/Aermec_VXT_Installation_manual_Eng.pdf); 2008 [Accessed 2020.10.08].
[58]- Panwar NL, Kaushik SC, Kothari S. Role of renewable energy sources in environmental protection: A review. Renewable and sustainable energy reviews 2011; 15: 1513-1524.
[59]- International Energy Outlook 2019 with projections to 2050, (https://www.eia.gov/outlooks/ieo/); 2019 [Accessed 2019.09.18].
[60]- Sindhu S, Nehra V, Luthra S. Solar energy deployment for sustainable future of India: Hybrid SWOC-AHP analysis. Renewable and sustainable energy reviews 2017; 72: 1138-1151.
[61]- GET - Global Market Outlook For Solar Power / 2019 – 2023, (http://www.solarpowereurope.org/global-market-outlook-2019-2023/); 2019 [Accessed 2019.07.10].
[62]- Pacheco R, Ordóñez J, Martínez G. Energy efficient design of building: A review. Renewable and sustainable energy reviews 2012; 16: 3559-3573.
[63]- Mussard M. Solar energy under cold climate conditions: A review. Renewable and sustainable energy reviews 2017; 74: 733-745.
[64]- Hall M. Solar, wind and hydro resilient during Covid-19 crisis. PV magazine, (https://www.pv-magazine.com/2020/04/30/solar-wind-and-hydro-resilient-during-covid-19-crisis/); 2020 [Accessed 2020.05.13].

[65]- AEO - Annual Energy Outlook 2018 with projections to 2050. U.S. Energy information administration, (https://www.eia.gov/outlooks/aeo/); 2018 [Accessed 2018.02.10].
[66]- IRENA - Abu Dhabi. Renewable Capacity Statistics 2016, (http://www.irena.org/menu/); 2016 [Accessed 2017.01.10].
[67]- REN21 - Renewable energy policy network for the 21st century. Renewables 2016 - Global status report, (http://www.ren21.net/status-of-renewables/global-status-report/); 2016 [Accessed 2017.01.13].
[68]- Global Market outlook for solar power, (https://resources.solarbusinesshub.com/solar-industry-reports/item/global-market-outlook-for-solar-power-2016-2020); 2017 [Accessed 2017.05.12].
[69]- Ibrahim A, Othman MY, Ruslan MH, Mat S, Sopian K. Recent advances in flat plate photovoltaic/thermal (PV/T) solar collectors. Renewable and sustainable energy reviews 2011; 15: 352-365.
[70]- Sarmah, N., Richards, B., Mallick T., 2014. Design, development and indoor performance analysis of a low concentrating dielectric photovoltaic module. Solar Energy, 103, pp. 390-401.
[71]-Varieras, R., Wang, J., King, D., 2012. System performance considerations for low concentration linear-focus silicon-based photovoltaic modules. 38th IEEE Photovoltaic Specialists Conference, USA. doi: 10.1109/PVSC-Vol 2.2013.6656791.
[72]- Al-Shohani, W., Al-Dadah, R., Mahmoud, S., Algareu, A., 2016. Optimum design of V-trough concentrator for photovoltaic applications. Solar Energy, 140, pp. 241-254.
[73]- Kunnemeyer, R., Anderson, T., Duke, M., Carson, J., 2014. Performance of a V-trough photovoltaic/thermal concentrator. Solar Energy, 101, pp. 19-27.
[74]- Al-Waeli, A., Sopian, K., Kazem, H. and Chaichan, M., 2017. Photovoltaic/Thermal (PV/T) systems: Status and future prospects. Renewable and Sustainable Energy Reviews, 2017, pp. 109-130.
[75]- Sarasa-Maestro CJ, Dufo-Lopez R, Bernal-Agustin JL. Photovoltaic remuneration policies in the European Union. Energy Policy 2013; 55: 317-328.
[76]- Dusonchet L, Telaretti E. Comparative economic analysis of support policies for solar PV in the most representative EU countries. Renewable and Sustainable Energy Reviews 2015; 42: 986-998.
[77]- European Commission. 2030 climate & energy framework, (https://ec.europa.eu/clima/policies/strategies/2030_en); 2020 [Accessed 2020.09.12].
[78]- Lund H, Werner S, Wiltshire R, Svendsen S, Thorsen JE, Hvelplund F, Mathiesen VB. 4th Generation District Heating (4GDH) Integrating smart thermal grids into future sustainable energy systems. Energy 2014; 68: 1-11.
[79]- Rismanchi B. District energy network (DEN), current global status and future development. Renewable and Sustainable Energy Reviews 2017; 75: 571-579.
[80]- Revesz A, Jones P, Dunham C, Davies G, Marques C, Matabuena R, Scott J, Maidment G. Developing novel 5th generation district energy networks. Energy 2020; 201: 117389.
[81]- Lazzarin RM, Noro M. Past, present, future of solar cooling: Technical and economical considerations. Solar Energy 2018; 172: 2-13.
[82]- Todd O, Taylor RA, Phelan PE, Prospects for solar cooling – An economic and environmental assessment. Solar Energy 2012; 86: 1287-1299.
[83]- Noro M, Lazzarin RM, Solar cooling between thermal and photovoltaic: An energy and economic comparative study in the Mediterranean conditions. Energy 2014; 73: 453-464.
[84]- Eicker U, Pietruschka D, Schmitt A, Haag M, Comparison of photovoltaic and solar thermal cooling systems for office buildings in different climates. Solar Energy 2015; 118: 243-255.
[85]- Thygesen R, Karlsson B. Simulation and analysis of a solar assisted heat pump system with two different storage types for high levels of PV electricity self-consumption. Solar Energy 2014; 103: 19-27.
[86]- Aguilar FJ, Aledo S, Quiles PV, 2017. Experimental analysis of an air conditioner powered by photovoltaic energy and supported by the grid. Applied Thermal Engineering, 123, pp. 486-497.

[87]- Hirvonen J, Kayo G, Hasan A, Sirén K. Zero energy level and economic potential of small-scale building-integrated PV with different heating systems in Nordic conditions. Applied Energy 2016; 167: 255-269.
[88]- Aguilar FJ, Aledo S, Quiles PV. Experimental study of the solar photovoltaic contribution for the domestic hot water production with heat pumps in dwellings. Applied Thermal Engineering 2016; 101: 379-389.
[89]- Stabat P, Marchio D. Opportunities for reversible chillers in office buildings in Europe, BUILD SIMUL. 2009; 2: 95-108.
[90]- Sayegh MA, Jadwiszczak P, Axcell BP, Niemierka E, Jouhara H. Heat pump placement, connection and operational modes in European district heating. Energy and Buildings 2018; 166: 122-144.
[91]- Fakouriyan S, Saboohi Y, Fathi A. Experimental analysis of a cooling system effect on photovoltaic panels' efficiency and its preheating water production. Renewable Energy 2019; 134: 1362-1368.
[92]- Herrando M, Markides CN. Hybrid PV and solar-thermal systems for domestic heat and power provision in the UK: Techno-economic considerations. Applied Energy 2016; 161: 512-532.
[93]- Kamel RS, Fung AS, Dash PRH. Solar systems and their integration with heat pumps: A review. Energy and Buildings 2015; 87: 395-412.
[94]- Zhou J, Zhao X, Ma X, Qiu Z, Ji J, Du Z, Yu M. Experimental investigation of a solar driven direct-expansion heat pump system employing the novel PV/micro-channels-evaporator modules. Applied Energy 2016; 178: 484-495.
[95]- Wang G, Quan Z, Zhao Y, Sun C, Deng Y, Tong J. Experimental study on a novel PV/T air dual-heat-source composite heat pump hot water system. Energy and Buildings 2015; 108: 175-184.
[96] Braun R, Haag M, Stave J, Abdelnour N, Eicker U. System design and feasibility of trigeneration systems with hybridphotovoltaic-thermal (PVT) collectors for zero energy office buildings indifferent climates. Solar Energy 2020; 196: 39-48.
[97]- Wang G, Zhao Y, Quan Z, Tong J. Application of a multi-function solar-heat pump system in residential buildings. Applied thermal engineering 2018; 130: 922-937.
[98]- Calise F, d'Accadia MD, Figaj RD, Vanoli L. A novel solar-assisted heat pump driven by photovoltaic/thermal collectors: Dynamic simulation and thermoeconomic optimization. Energy 2016; 95: 346-366.
[99]- Su B, Han W, Qu W, Liu C, Jin H. A new hybrid photovoltaic/thermal and liquid desiccant system for trigeneration application. Applied Energy 2018; 226: 808-818.
[100]- Su B, Qu W, Han W, Jin H. Feasibility of a hybrid photovoltaic/thermal and liquid desiccant system for deep dehumidification. Energy Conversion and Management 2018; 163:457-467.
[101]- Yang L, Heng Z, Haiping C, Han Y, Fei Y. Simulating and experimental research on a low-concentrating PV/T triple-generation system. Energy Conversion and Management 2019;199: 111942.

Chapter 2. State of the art of photovoltaic and photovoltaic/thermal systems

This chapter presents a state-of-the-art review on the latest progress of bifacial and monofacial photovoltaic solar cells, commercial and novel hybrid photovoltaic/thermal collectors and also presents an overview of commercial and novel concentration photovoltaic/thermal systems and building integration photovoltaic/thermal (BIPV/T) approach. It presents the integration methods for PV modules and thermal absorbers including the recent efforts on the conventional and novel PV/T systems i.e. air, water, air-water, bi-fluid, heat pipe, nanofluid, phase change materials based PV/T, PV/T evaporator and thermoelectric integrated PV/T. Also, it explores the development of low, medium and high concentration PV systems. It presents an overview of building integration photovoltaic (BIPV/T) systems including air based BIPV/T, water based BIPV/T, semi-transparent PV/T window and multifunctional bifacial BIPV modules. Also, it explores the available market products of PV, PV/T and LCPV/T systems.

2.1 Introducing to solar power photovoltaic cells

Often referred to as photovoltaic (PV) solar energy, solar electricity is generated within PV cells as a result of the photovoltaic effect. The photovoltaic effect was first discovered when scientists observed that two layers of a semi-conducting material were generating an electric charge while it was exposed to sunlight. The layers of material were observed to absorb photons from the solar radiation thereby charging the depleted electrons in one layer causing some of them to jump from one layer to the other producing an electric current. The efficiencies of different standard PV cell types have been reported in Table 2-1.

Solar cells generate most of their electricity from direct sunlight and the more powerful the sun's energy, the more power generated. Accordingly, the amount of electricity generated reflects the intensity of sunlight exposure. However, so successful is this process, that solar electricity (in proportionally smaller amounts) can even be produced on cloudy days and on bright moonlit nights. As individual solar cells typically generate minuscule amounts of electric energy alone, these cells are connected to form a solar module or panel, also known as a photovoltaic module. Most solar panels are rated as 12 V solar panels, although higher voltage panels are also available. A typical solar cell only produce half a volt, so by connecting them together in a series inside the panel, a higher and therefore more useful voltage is achieved. A PV module based on crystalline silicon typically consists of strings PV solar cells, back sheet tedlar of polyvinyl fluoride (PVF) film, Ethylene vinyl acetate (EVA-encapsulate), aluminum cover and Anti-reflective glass cover.

Solar cells are typically named by the semiconducting material they are made of. These materials must have certain characteristics to absorb sunlight. Solar cells can either be made of a single layer of light-absorbing material (single-junction) or can be created by using multiple physical configurations (multi-junctions) so that various absorption and charge separation mechanisms can be benefited. Progress in PV research and development is moving rapidly, and the most promising

near-term PV cells will consist of thin films. Although high-efficiency multi-junction PV cells are under development, the large majority of current PV installations use mono-junction modules.

Table 2-1. Summary of standard PV cells efficiencies measured under the global AM1.5 spectrum (1000 W/m^2) at a cell temperature of 25°C [1]

Solar cell type	Efficiency (%)	Area (cm^2)	J_{sc} (mA/cm^2)	V_{oc} (V)
Crystalline: single junction				
Mono-C-Si	26.7	79 (da)	42.65	0.738
Poly-C-Si	21.9	4.003 (t)	40.76	0.6726
Thin-Si	21.2	239.7 (ap)	38.50	0.687
Amorphous-Si	11.9	1.044 (da)	28.72	0.550
GaAs	18.4	4.001 (t)	23.20	0.994
InP	24.2	1.008 (ap)	31.15	0.939
Thin-film: single junction				
CZTS	10	1.113 (da)	21.77	0.7083
CdTe	21	1.0623 (ap)	30.25	0.8759
GaAs	28.8	0.99927 (da)	29.68	1.122
Crystalline: multijunction				
GaInP/GaAs/Si	31.3	3.981 (ap)	11.7	3.046
III-V: multijunction				
InGAP/GaAs/InGaAs	37.9	1.047 (ap)	14.27	3.065
Thin-film: multijunction				
a-Si/nc-Si/nc-Si	14.0	1.045 (da)	9.94	1.922
Photoelectrochemical				
Dye-sensitised	11.9	1.005 (da)	22.47	0.744
Organic	11.2	0.992 (da)	19.30	0.780

Abbreviations: (da), designated illumination area; (t), total area; (ap), aperture area; J_{sc}, current intensity; V_{oc}, open circuit voltage.

PV cells can be grouped into three main categories called generations: first, second and third generation cells. Crystalline cells are generally considered to be the first generation of PV cells, and thin films are considered to be the second generation.

Made of crystalline silicon and possessing a bandgap of 1.1 eV, first-generation (or conventional/traditional) cells are identified as wafer-based silicon solar cells. First generation cells are also classified according to their crystalline levels and are divided into two types: (i) single or mono-crystalline (sc-Si) and (ii) multi-crystalline (mc-Si). Multi-crystalline and polycrystalline are often synonyms, but multi-crystalline is often meant to refer to thick-film silicon with crystallites larger than 1 mm, whereas the silicon is deposited in a continuous process onto a base material giving

a fine grained and sparkling appearance. In practices, the efficiencies of mono-crystalline and multi-crystalline are 18-21% and 13-14%, respectively. Mono-crystalline silicon has been noted as the most efficient technology available in terms of wattage output in relation to the panel's size. This efficiency, however, can be costly. Multi-crystalline technology, on the other hand, has been noted to offer the best value on efficiency levels close to monocrystalline panels, but at half the costs in some cases. As such, the multi-crystalline cell has the largest market share amounting to approximately 55% [2].

Second generation cells are single junction devices that aim to use less materials and maximize efficiency. Thin film technique uses only 1-10 μm of the active material and they are commercially significant in utility-scale photovoltaic stations, building integrated photovoltaics, and/or in small stand-alone power systems. Second generation solar cells involve amorphous silicon (a-Si) or micromorph silicon (μc-Si), cadmium telluride (CdTe), copper indium selenide (CIS) or ($CuInSe_2$) and copper indium gallium diselenide (CIGS) or ($CuInGaSe_2$) cells. The micromorph silicon cell is the combination of amorphous and microcrystalline Si. Advantages of lower cost per watt, ease of manufacturing, and lower material consumption among others continue to interest installers and developers in thin films. Moreover, several II-VI chalcopyrite compounds and their mixed compounds were found to be very suitable for photovoltaic applications. The most important of them are CIS, CGS and CIGS. The CIGS, specifically, is an excellent absorber compared with silicon, due to its direct bandgap.

Considered emerging technologies, third-generation solar cells are still relatively new, under both experimentation and observation, and there for have a limited market presence. They primarily comprise of several technologies that encompass copper zinc tin sulfide (CZTS), dye-sensitized, organic, hybrid, tandem, nanostructured including hot-carrier cells and optical up- and down-conversion, concentrating PV, in addition to thermophotovoltaic approach.

2.2 Bifacial solar cells

A promising high-efficiency structure for enhancing the power output over standard (monofacial) photovoltaic modules is the bifacial solar cell, since this cell type can produce more electric power by harvesting sunlight from both front and rear sides. Bifacial modules can produce more electric power compared with standard modules (up to 30% under sunny conditions and 70% under cloudy conditions); depending on the albedo of the underlying surface, module elevation and tilt angle [3]. In addition, bifacial solar cells operate at lower temperature compared to monofacial panels owing to the reduced infrared absorption in the absence of the aluminum back metallization. In contrast with a monofacial solar cell, bifacial solar cells simultaneously collect photons from incident and albedo radiation reaching both front and back surfaces when the nearby ground or other artificial surfaces are extremely reflective. The albedo is determined by the ratio of sunlight reflected from these various surfaces compared to incoming irradiance and is dimensionless scaled from zero to one. whilst zero refers to no reflected light, and one represents a perfect reflector. Albedo reflectance of 0.5 or more is observed naturally for snow-covered ground or can be achieved artificially for example by white concrete.

Bifacial modules can be mounted either vertically facing (east-west) or tilted at latitude towards the equator as with conventional monofacial PV modules. Vertically Mounted Bifacial Modules (VMBM) permit unique commercial applications. They have been installed as noise barriers along roadways, fencing, and building components. In this orientation, VMBM generates more electric power in the morning and afternoon than conventionally mounted monofacial modules. It has been shown that a vertical bifacial farm will yield 10–20% more energy than a traditional monofacial farm for a practical row-spacing of 2m (corresponding to 1.2m high panels) [4]. On the other hand, bifacial PV panels installed with an optimal tilt angle facing south will perform better than the bifacial PV panels installed vertically and facing east-west under the same environmental conditions. Bifacial photovoltaic panels installed with an optimal tilt angle facing south can supply up to 32% more energy compared with vertical bifacial panels facing east-west [5].

The most commonly used substrate in conventional bifacial cells is based crystalline silicon. Additionally, the transparent TCO (Transparent Conductive Oxides) coated glass is typically considered as a substrate for flexible thin films (CdTe), CIGS, perovskite, and dye-sensitized devices. However, bifacial cells based on silicon substrates considerably surpass the other alternative substrates. The majority of today's bifacial cells are the p^+-p-n^+ for a p-type or p^+-n-n^+ for an n-type structure. For n-type cells, the p^+ diffused layer serves as an emitter, whilst the n^+ Layer serves as a back-surface field, and vice versa for the p-type structure. Compared with the p-type structure, n-type structure based heterojunction (HJT) and back-contacts cell concepts deliver high efficiency. Further, recent extensive attention has been paid to n-type c-Si owing to several advantages including negligible light induced degradation, insensitivity to common metal impurities, and higher bulk lifetime [6]. However, there is about $0.10/W price difference between products that are formed on p-type polycrystalline technology versus those that employ more expensive n-type monocrystalline wafers.

Bifacial solar cells can be encapsulated in modules with either a glass/glass or a glass/backsheet structure. A glass/backsheet structure offers additional module current under standard test conditions (STC), due to the backsheet scattering effects, whilst a glass/glass structure has the potential to produce additional energy under outdoor conditions by using Albedo from surroundings [7]. Further, glass-glass modules offer greater than 30 years lifespan. It is also possible to reflect the solar radiation inside a glass-to-glass bifacial module and increase radiation concentration. This interlamination reflector is called a "holographic planer concentrator". In the meantime, glass-glass bifacial modules tend to command a $0.05-$0.15/W premium over traditional bifacial cells that contain a back-sheet [8]. In general, Bifacial module based glass-to-glass structures have great potential when applied to BIPV systems.

To date, there are not many bifacial module manufacturers available commercially due to a lack in standardized testing and modeling procedures that can accurately predict the performance of bifacial systems. In the absence of a standard definition of rear irradiance given 1000W/m^2 on the front, a different approach has been required to find out the influence of front and rear side. Bifacial modules deployed at 1m height over 0.21 albedo (soil) ground with existing 1-sun irradiance at 37° tilt angle, lead to a bifacial condition of 1000W/m^2 for front and 130–140W/m^2 for rear side [9].

Commercially available bifacial solar modules have front and rear efficiencies of 16.6% and 12.8%, respectively [10]. As HJT cells have a symmetrical structure and are bifacial without the need for additional process steps, the cost of bifacial panels is almost the same as that of monofacial monocrystalline PV panels. Based on the fact that these panels produce an additional yield of 15% in comparison with the monofacial panels, manufacturing companies estimate a 13% reduction in the lower levelized cost of energy (LCOE) using bifacial construction. Meanwhile, one-year outdoor testing in China shows that the average daily electricity output of commercial bifacial PV modules installed at 0.5m over soil ground and facing south with a tilt angle of 45°, is about 4.03% higher than that of the standard ones for a micro inverter PV system [11].

2.3 Hybrid photovoltaic/thermal systems

Because only photons around the band gap have sufficient energy to produce electricity in photovoltaic cells and the process of electricity generation in these cells is exothermic, the temperature of cells increases. Increasing the cell temperature decreases the open circuit voltage and thus reduces the electric efficiency of the PV module. There can be two undesirable consequences: i) a drop-in cell efficiency (typically 0.45% per °C rise for standard crystalline-silicon cells, 0.25%/°C for standard amorphous-silicon, and 0.22%/°C for bifacial cells), and ii) permanent structural damage of the module if the thermal stress remains for prolonged period [12]. Cooling the solar cells with a fluid stream either by natural or forced circulation can reduce the PV cell temperature. This leads to an increase in the voltage output as well as the electricity yield.

There are various types of hybrid PV/T collectors. They can be classified based on: i) the type of the integrated PV panel; ii) thermal absorber design; iii) type of heat transfer fluid; iv) the configuration of heat transfer fluid; v) glazed or unglazed; and vi) on the use of lens/reflectors (concentrating) or flat plate.

The main classification of PV/T systems based on various heat transfer techniques is illustrated in Figure 2-1.

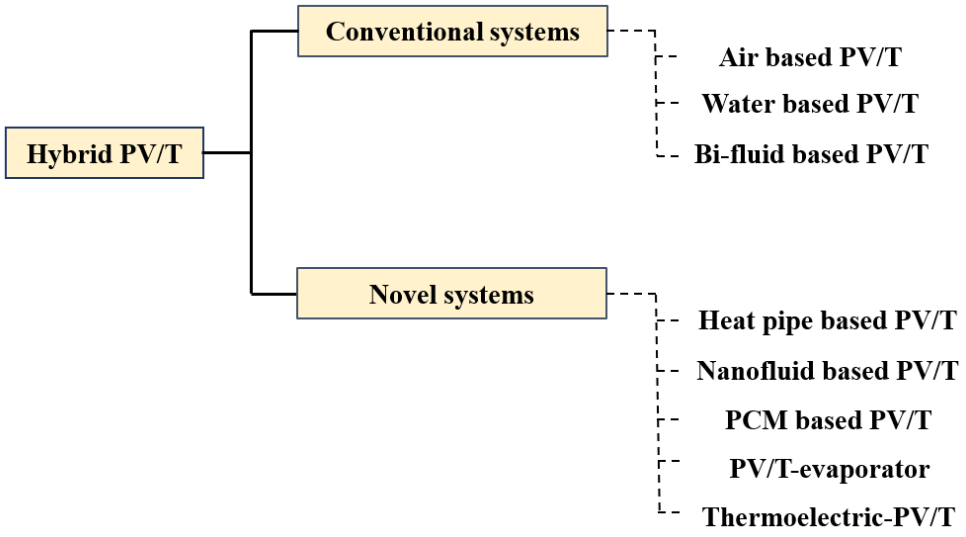

Figure 2-1.Classification of PV/T system based on heat transfer techniques.

Air and water are used as a conventional thermal fluid and extensive research work has been carried out on optimization of conventional fluid based PV/T systems. In recent years, many new thermal techniques have evolved other than air and water with some desirable system outputs. These novel systems are: i) heat-pipe based PV/T; ii) nanofluid based PV/T; iii) phase change materials (PCM) based PV/T; iv) PV/T-evaporator; and v) thermoelectric integrated PV/T.

Both air PV/T and ventilated PV façade systems have been widely applied to cool PV cells and to produce low grade thermal energy for space heating in residential applications. The hybrid PV/T based air collectors have some advantages over water collectors such as the reduced corrosion and leakage, no freezing, no need for high pressure protection, lighter weight and easiness of installation. However, the thermal output is inferior to the water collectors because of poor heat transfer between the absorber plate and the flowing air, and lower density per unit mass.

Heat pipe-based PV/T is a relatively new technology and its operation is often in conjunction with a heat pump or heat cycle. However, there arise some disadvantages that require further resolution (i.e. high cost and effective control). The system transfers heat very fast and works without using any external power, but the heat pipe is difficult to fabricate and integrate with the PV/T systems for high power systems.

The use of nanofluids as coolants could be an effective technique to enhance the efficiency of PV/T systems without changing their design. Because the suspension of the nanoparticles in the base fluid improves the energy transmission in the fluid leading to better thermal conductivity properties and improved heat transfer characteristics. However, nanofluids present some critical challenges due to their limited stability time, the high cost of nanoparticles, and the increased pressure drop in the system.

The merits of PCM thermal management are considered to be: higher heat transfer rates compared to both forced air circulation and forced water circulation; higher heat absorption due to latent heating; isothermal heat removal; no electricity consumption; passive heat exchange; no noise; no maintenance cost; and heat delivery on demand. On the other hand, the drawbacks are considered to be: higher PCM cost compared to natural and forced air circulation; some PCMs are toxic; some PCMs have fire safety issues; some PCMs are strongly corrosive; and PCMs may have disposal problem after their life cycle is complete.

The PV/T-evaporator system usually operates in conjunction with a heat pump in which the evaporation coil is incorporated under the PV module for its cooling. PV/T-evaporator could significantly progress the solar utilization rate over air- and water- based systems. This system represents a step forward in building integration PV technology but in practice faces several challenges namely, potential refrigerant leakage and difficulty in pressure maintenance over the operation duration.

The commercial flat pate PV/T collector typically consists of a PV module on the back of which a thermal absorber plate (a heat extraction device) is attached using adhesive often comprising EVA-encapsulation (ethylene vinyl acetate film) and back sheet tedlar of polyvinyl fluoride (PVF) film, an insulation cover and optional glass cover.

2.3.1 Air based PV/T

In air-based PV/T systems, air is allowed to pass through the PV surface in either an active or passive mode, using a single or double pass and through different absorber configurations.

A performance analysis of single pass and double pass air based PV/T confirmed 24-28% thermal efficiency and 25-30% combined efficiency for single pass, while, 32-34% thermal efficiency and 40-45% combined efficiency in a double pass air based PV/T system [13]. A performance comparison of four heat exchanger models of single pass air based PV/T has been carried out in reference [14]. The four heat exchangers were honeycomb, V-groove, ∇-grooved and rectangular tunnel model (see Figure 2-2). It was disclosed that a PV/T with honeycomb heat exchanger (Fig. 2-2.a) was capable of increasing electric efficiency by 0.2% with thermal efficiency of ~50%. PV/T with V-groove (Fig. 2-2.c) was capable of achieving thermal efficiency of ~40% but with no significant improvement for electric efficiency. PV/T with ∇-grooved heat exchanger (Fig. 2-2.b) showed an increased value of 2.0% for electric energy with thermal efficiency of ~35 %. Finally, a PV/T with triangular tunnel heat exchanger (Fig. 2-2.d.) showed an increased value of 0.2% for electric efficiency with thermal efficiency of ~35%.

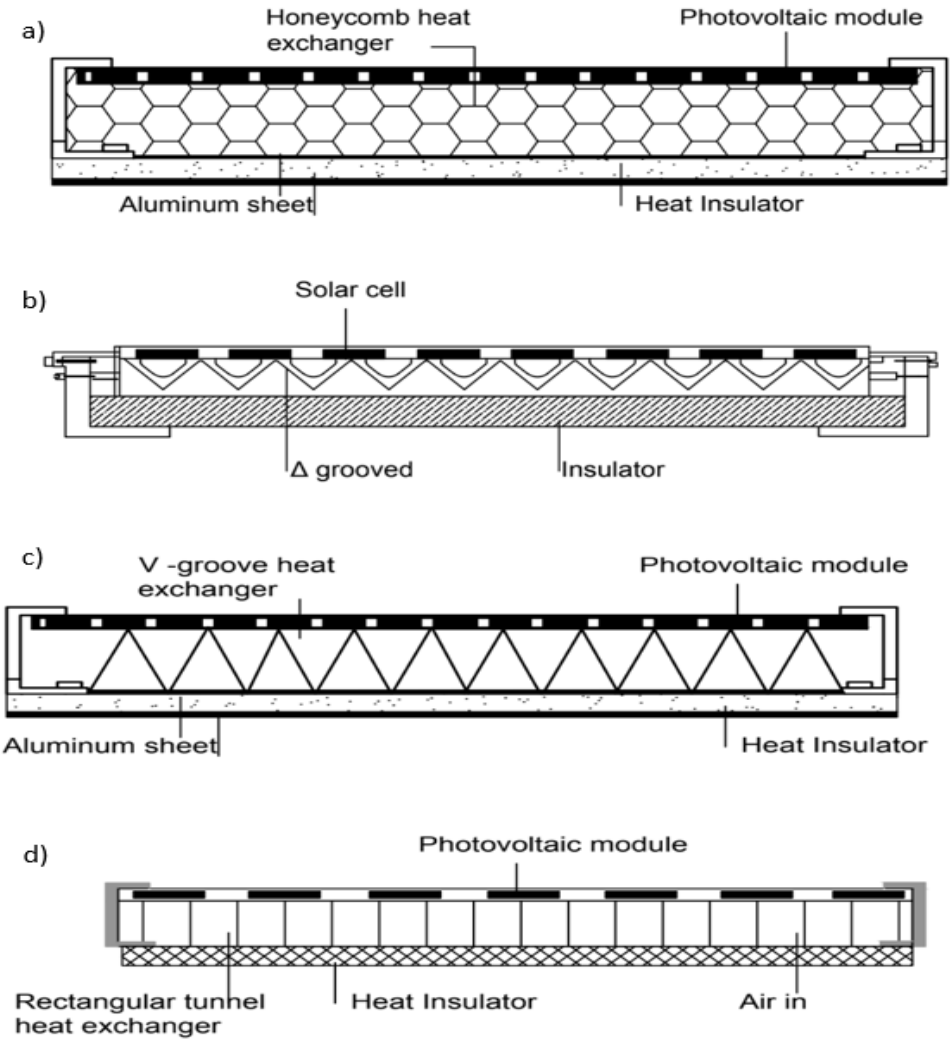

Figure 2-2. Cross section of various heat exchanger models for air based PV/T system: a) honeycomb; b) ∇-groove; c) V-grooved; and d) rectangular tunnel [14].

An experimental study dealing with performance evaluation of a hybrid PV/T based air collector system with two types of PV modules (namely PV module with glass-to-tedlar and glass-to-glass) concluded that a hybrid air collector with PV module glass-to-glass gives better performance in terms of overall thermal efficiency because the back-surface temperature is higher in glass-to-glass PV/T air collector than in glass to tedlar PV/T air collector [15]. Overall thermal efficiency decreases with increase in length of the duct in both cases, and overall thermal efficiency initially - increases with the increase in the velocity of duct air until it saturates.

The performance of a double pass PV/T solar air collector with fins and compound parabolic concentrator (CPC) was analyzed to study the performance over a range of operating conditions [16]. Fins were attached beneath the PV cells to help removed the heat from PV cells (see Figure 2-3). It was noted that annual thermal gain was 1% higher for flat-PV/T with fins compared to flat-PV/T without fins. On the other hand, the annual electric gain for flat-PV/T with fins was 3% higher than flat-PV/T without fins. The CPC-PV/T with fins was estimated to have more than 3% thermal and 8% electric gain compared to CPC-PV/T without fins. It was concluded that, among the four configurations, the CPC-PV/T with fins system had the best performance.

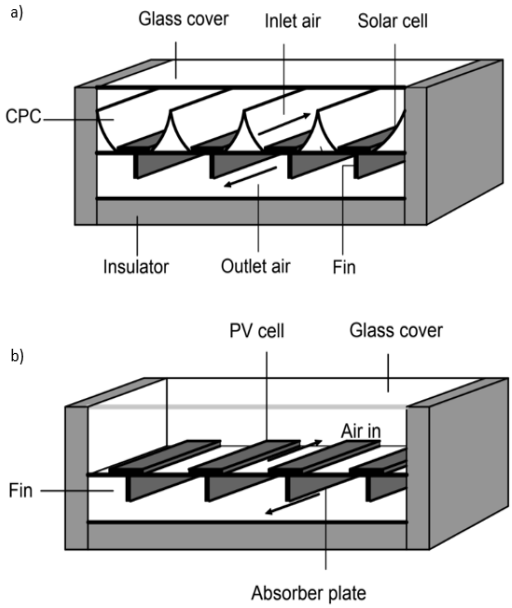

Figure 2-3. Cross-section of double pass PV/T solar collector with fins: a) with CPC; and b) without CPC [16].

2.3.2 Water based PV/T

Water-based PV/T is also a very popular technology. However, the scope of improvement is limited due to some inherent technical difficulties, namely rising water temperature during the operation and complex system layout. The most commonly adopted flat plates are sheet and tube, roll bond and box channel (see Figure 2-4).

The sheet-and-tube design (Fig. 2-4.a) comprises a flat plate to which are generally welded, soldered or glued circular cross section channels. The roll bond (Fig. 2-4.b) manufacturing technique a sandwich of two aluminum sheets is formed by means of a special hot or cold rolling process. The

box channel (Fig. 2-4.c) is made of parallel ducts with a rectangular cross section which forms the plate. It can be made from an extruded or pultruded profile, in which almost the entire surface is in contact with the fluid in order to significantly increase the convective exchange [17].

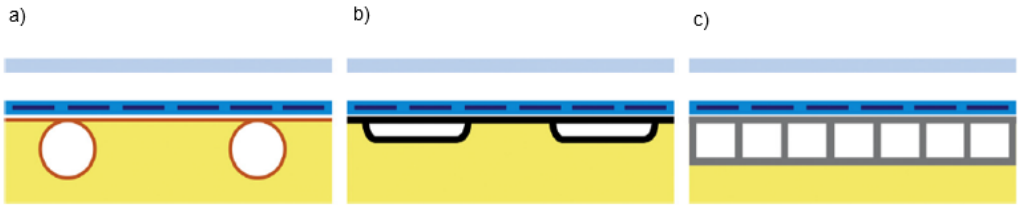

Figure 2-4. Water based PV/T system with the most commonly used thermal absorbers for: a) sheet and tube; b) roll bond; and c) box channel [17].

The main features of different thermal absorber types are described in Table 2-2. Seven different types of thermal absorbers are discussed in terms of their advantages/disadvantages and their applications. In comparison with traditional thermal absorbers, such as sheet-and-tube structure, rectangular tunnel and flat-plate tube, the four types such as micro-channel heat pipe, extruded heat exchanger, roll-bond heat exchanger and cotton wick structure, are promising due to the significant enhancement in terms of efficiency, structure and weight.

Table 2-2. Main features of different thermal absorber types

Thermal absorber	Material [18]	Advantages [19]	Disadvantages [19]
Sheet and tube	Copper or Aluminum	Low manufacturing cost and good heat transfer efficiency	Complex structure, heavy weight, require precise welding and leakage risks
Rectangular tunnel	Aluminum or polymer or metal	Simple structure, low weight and low cost	Relatively low efficiency
Flat plate tube	Stainless steel or copper	Provide a good contact between PV panel and stream fluid	High flow resistance, choking risk and leakage risk
Extruded heat exchanger	Metal sheets	Simple structure and low cost	Special hydrologic design and high volume of working fluid
Roll-bond heat exchanger	Aluminum	High efficiency, low weight and cost-effective	Problem of long-term reliability and corrosion risk
Micro-channel heat pipe	Aluminum	High reliability, high heat transfer efficiency, low cost and small thermal contact resistance	Additional thermal resistance between the condenser manifold
Cotton wick structure	Aluminum spikes	Simple structure and very low cost	Limited cooling efficiency

The thermal and electric efficiencies for the most common thermal absorbers in water-based PV/T collectors are illustrated in Table 2-3. The electric and thermal efficiencies of commercial

water-based PV/T with different thermal absorber designs are: 9-14% and 50-66% for sheet-and-tube; 10-14% and 45-60% for box-channels; 9-11% and 50-79% for roll bond respectively.
While the performance with fluid temperature of different PV/T based water systems is summarized in Table 2-4. It can be seen that the usable fluid temperature is in the range 30-65°C.

Table 2-3. Thermal and electric efficiency for the conventional water-based PVT collectors

Plate type	Glazed (G) or Unglazed (UG)	Flow rate (kg/s) [Ref.]	Thermal efficiency (%)	Electric efficiency (%)	Analysis type
Sheet and tube	UG	0.02 [20]	66	14	Experimental
	UG	0.02 [21]	52	9.7	Numerical
Box channels	UG	0.02 [22]	48.6	12.3	Experimental
	G	0.02 [23]	57	12	Numerical
	G	0.02 [24]	45	10.15	Experimental
Roll bond	G	0.01 [25]	49.3	10.3	Numerical
	G	0.02 [26]	79	8.7	Experimental

Table 2-4. Performance of flat plate PV/T based water demonstrations the fluid temperature

Plate type	Glazed (G) or Unglazed (UG)	I ($kWh/m^2.day$) [Ref.]	T (ambient) °C	T (inlet Water) °C	T (tank) °C	η_{th} (%)	η_{EL} (%)
Sheet and tube	UG	1.8-4.4 [27]	25-34	25-40	33-50	12-44	9
	G	2.8-5.8 [28]	14-37	17-34	34-60	16-43	10-14
Box channels	UG	4.0-6.5 [29]	14-23	N/A	44	28	7
	G	2.6-5.9 [30]	20-37	14-39	35-62	29-57	4-10

A numerical analysis of water based PV/T was carried out to obtain the thermal efficiency for different collector designs (see Figure 2-4 and Figure 2-5). It was shown that for zero reduced temperature the thermal efficiency of the uncovered sheet-and-tube collector design was 51% and the thermal efficiency of the single cover sheet-and-tube design was 58%, while the thermal efficiency for the channel above PV design was 65%, the channel below transparent PV design was 63% and the channel below opaque PV design was 59%. On the other hand, the electric efficiency of the uncovered sheet-and-tube collector design was 9.8% and the electric efficiency of the single cover sheet-and-tube design was 8.8%. While, the electric efficiency for the channel above PV design was 8.4% and the channel below PV design was 9%. Also, it was concluded that the channel-below-PV (transparent) configuration appears to be the best option from the efficiency point of view, while the more economical was the single-cover sheet-and-tube design since its efficiency was only 2% less [31].

The performance of PV/T collector under real operating conditions in Italy showed that Water-cooled PV modules' electric performance increases by as much as 33% [32]. It was also found that switching from a no-cooling condition to 0.5 l/min circulation results in a 2% electric efficiency increase. In another investigation [33], It was shown that the average power of the PV/T collector was 6% higher than average power of conventional PV module in Oman climate conditions.

A laboratory test of water based PV/T demonstrated that the PV/T panel could achieve an electric efficiency of the PV cells of around 16.8% (about 5% increase), and produce an extra amount of heat at thermal efficiency of nearly 65% under standard testing conditions. The nominal mass flow rate of the working fluid was at the recommended rate of 0.01 kg/s [34].

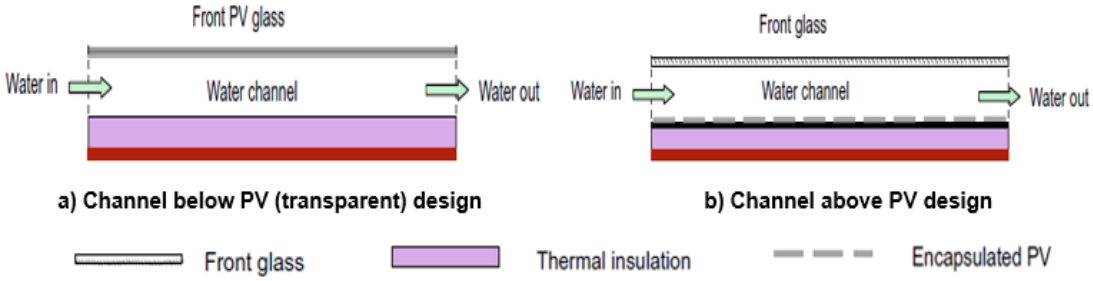

Figure 2-5. Cross-sections of channel water based PV/T collector designs: a) channel below the transparent PV; and b) channel above the PV panel [31].

An extensive monitoring of a PV/T water based solar system was carried out in Forlì (Italy) [35]. The PV/T solar plant consisted of four solar modules and a 800 L storage tank. The cooling fluid of the primary circuit was a 30% vol. mixture of propylenic glycol and water with a mass flow rate of 0.224 kg/s. The main characteristics of each PV/T module are gross area of 1.65 m^2, peak electric power of 230 W, and recommended flow rate of 1.2 l/min. It was concluded that PV cooling produces a negligible increase in the electric yield (1-3%), the PV/T solar system was able to reach a simultaneous generation of electricity (835 kWh/m^2) and heat (1600 kWh/m^2) at a mean outlet temperature over 40°C. The installed PV/T solar system can produce about 1362 kWh/year of electricity for 1 kW_{power} system installed, while yearly heat generation may vary between 443 and 267 kWh/m^2 depending on mean inlet temperature of the cooling fluid. The investment cost was about 3700-4700 €/kW_{power}.

2.3.3 Bi-fluid based PV/T

Some researchers have worked on the use of two fluids in single PV/T system. The use of two fluids (bifluid) also creates a greater range of thermal applications and offers options in which hot and/or cold air and/or water can be utilized depending on the energy needs and applications.
An indoor experimental performance and a numerical analysis was conducted on a bi-fluid PV/T (see Figure 2-6) [36]. The test included all three modes of fluid operation under the same PV/T system, namely: the air mode, the water mode, and the simultaneous mode of water and air. It was observed that with both fluids operating simultaneously, the primary energy saving was 12% higher than the independent mode of fluid operation. In comparison to the water mode operation, the air mass flow rate was fixed at 0.0262 kg/s, the water was set to vary between 0.0017 kg/s to 0.0265 kg/s for which

the total thermal efficiency and primary energy saving efficiency increased from 51.88% to 65.70% and 64.02% to 77.90% respectively. In comparison to the air mode operation, the water mass flow rate was fixed at 0.0066 kg/s, the air was set to vary between 0.0074 kg/s and 0.090 kg/s, for which the total thermal efficiency and primary energy saving efficiency increased from 51.87% to 66.12% and 64.01% to 78.98%, respectively. It was concluded that the Bi-fluid PV/T system was capable of achieving high efficiency and temperature rise even at a very low flow rate of fluid operation with a reduction in pumping power even though the system used two pumps.

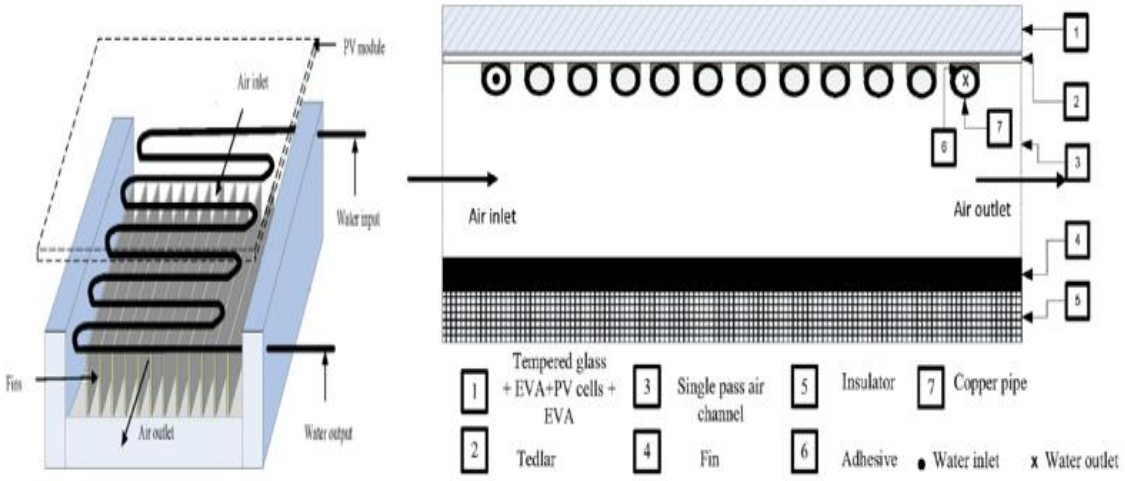

Figure 2-6. Bi-fluid based hybrid PV/T collector [36].

A transparent PV panel was used and mounted on top of a custom designed hybrid PV/T system with air and water as a heat removal [37]. Hottel-Whillier-Bliss equation were used for evaluating system performance. Air flow rate was varied from 0.01 to 0.07 kg/s, water flow rate was varied from 0.02–0.10 kg/s and solar irradiance were varied from 350 W/m^2 to 800 W/m^2. It was noted that, electric efficiency and total thermal efficiency were 17% and 76% respectively at 800 W/m^2 of solar irradiations with 0.05 kg/s and 0.02 kg/s optimum flow rate of air and water respectively. The overall evaluation indicated that when both fluid mass flow rate and solar radiation were set to their maximum settings, the calculated electric and thermal efficiency achieved the highest value for both media. It was also concluded that; the combined air and water PV/T system offers less payback time period and less construction cost.

The packing factor of a PV/T system causes significant changes in the electric and thermal outputs. The packing factor of the BIPV/T system decreases from 0.83 to 0.42, which deliver an increase in efficiency of 0.2–0.6% by reducing the module temperature by 10% [38].

2.3.4 Heat pipe-based PV/T

The flat heat pipe allows a working fluid to change phase inside the collector. The bottom section of the heat pipe represents an evaporator, and the top section represents a condenser. Once a high temperature is produced at the evaporator portion that is facing the solar radiation, the heat transfer fluid in liquid phase evaporates and flows up to the condenser portion and gives up its heat. Then, with the influence of gravity, the liquid fluid returns to the evaporator section to boil it again.

A heat pipe based PV/T was used as an energy-active building envelope material to cover the whole roof of a building in Cardiff, UK [39]. It was concluded that, from thermal point of view, the solar/thermal energy conversion efficiency was observed to be around 64% for the heat mat with no PV while this value was observed to be around 50% for the PV/T mat. The effect of cooling on the solar/electric energy conversion of the PV/T heat mats was shown to increase the PV/T's electric output by about 15% when compared to uncooled PV heat mats.

In another investigation [40], It was shown that the conversion efficiency of solar to thermal energy for the solar flat heat pipe collector was between 45.4 and 64.2%, the conversion efficiency of solar to thermal energy for the integrated heat pipe solar collector with PV panels was between 35 and 52%, and the temperature of the cooled PV panels was lower in comparison with the uncooled PV panels by 18-48%. During the tests the temperature of the hybrid flat heat pipe solar PV/T panel did not exceed 35°C, and the temperature of the uncooled PV panels reached up to 60°C. It was concluded that the hybrid PV/T collector was capable of providing 58% of the required energy for Domestic Hot Water (DHW) need at low solar radiation levels of up to 2.5 kWh/m^2 per day and covering 100% of DHW demands for a family house at solar radiation levels higher than 5.0 kWh/m^2 per day.

2.3.5 Nanofluid based PV/T

In last two decades, applications of nanofluid can be found in almost all sectors. Nanofluid generally contains nanoparticles of size less than 100 nm in conventional base fluids like water, glycol and oil. Nanofluids are principally heat transfer fluids and thus can be used efficiently in various solar energy conversion systems. Several researchers are working on the applicability of nanofluids in solar systems either as a heat transfer fluid or as an optical filter. It was observed that the properties of nanofluids can be improved for particular applications depending on many parameters including: nanoparticle type; volume fraction of nanoparticles and base fluid; particle size; base fluid type etc. [41, 42] The nanofluid based PV/T system shows promise, but very limited experimental work is available. A heat transfer system must be optimized to enhance heat transfer from nanofluid to base fluid. Nanofluid also has its applications as an optical filter, thus integrating nanofluid for cooling and as an optical filter in a single system can meaningfully enhance PV/T system performance [43].

An experimental evaluation of SiC (Silicon carbide) nanofluid as a base-fluid for a photovoltaic thermal PV/T system was performed [44]. This indicated that adding 3% by weight of nanoparticles to water increases the fluid density by up to 0.0082% and the viscosity by up to 1.8%. Moreover, the thermal conductivity was enhanced by up to 8.2% for the tested temperature range of 25-60°C. It indicated that the use of PV/T cooled by a SiC nanofluid system caused an enhancement in the electric efficiency of up to 24% as the PV panel generated voltage was increased, though the generated current showed a only negligible improvement. The high thermal conductivity enhanced the heat transfer for the PV/T nanofluid-cooled system compared to the PV/T water-cooled system by about 100.19%.

A nanofluid-based PV/T configuration was tested in two designs, one with separate channels and one with a double-pass design [45]. The first channel enhanced heat removal from the PV cells while

the other controlled the optical properties. These designs were simulated for both Si- and GaAs-based PV cells at various concentration ratios. The tests indicated that the separate channel system outperformed the double-pass design by 8.6%, in terms of the electric efficiency of GaAs (at C = 45) and Si (at C = 30). The overall efficiency of the separate channel system with GaAs (at C = 160) and Si (at C = 100) had been improved by 5.8% and 4.6%, respectively, by increasing the volume fraction of the thermal nanofluid from 0.001 to 1.5%.

A review on the performance of nanofluid-based photovoltaic/thermal systems [46] concluded that to improve the performance of the system, adding nanoparticles was more efficient in a laminar regime than in a turbulent one. Also, it was indicated that using nanoparticles of larger diameter lead to greater total energy and exergy efficiency in the turbulent regime, while contrary behavior was observed in laminar flow. Moreover, it was observed that employing aluminum oxide in nanofluids improved the system performance more than titanium oxide, where water based nanofluids displayed higher energy and exergy efficiency compared to ethylene glycol-water based nanofluids. A comparative study using nanoparticles (Al_2O_3, CuO, and SiC) with water to enhance photovoltaic thermal PV/T collectors was performed in an indoor laboratory [47]. The studied volume fractions were 0.5, 1, 2, 3, and 4%. It was indicated that nanofluid gave higher thermal conductivity with very little increase in the fluid density and viscosity compared with the base fluid. The improvement in thermal conductivity was 1.96, 3.42, and 4.8% for Al_2O_3, CuO, and SiC nanofluids with 4% volume fractions, respectively. It was noted that, silicon carbide nanoparticles had the best stability and the highest thermal conductivity and was shown to improve the performance of the PV/T system more than the other two nanofluids when compared to the other two nanoparticles. Copper oxide nanofluid was shown to have higher thermal conductivity than aluminum oxide but lower stability.

2.3.6 PCM based PV/T

Phase change materials (PCMs) absorb the waste heat during the sunlight hours by melting and maintain the PV module at a favorable operating temperature level. On the other hand, during the nighttime, PCMs release their absorbed thermal energy and return to solid phase material. Phase change materials can be used efficiently for the thermal management of PV systems, but it was observed that the PCM was efficient only when its heat was used for a useful purpose i.e. it was fully integrated with the PV/T system. Thus, PV to PCM combined with PCM to a thermal system. PCMs have been used quite extensively in solar water systems [48]. A PCM layer wrapped around the pipes and bonded to the thermal absorber plate of the PV/T module was found to reduce the PV cell temperature and improve its heat loss to ambient. Thermal conductivity, transition temperature, chemical interaction, and fusion heat are important parameters to select the appropriate PCM layer for PV/T applications. Also, a low melting temperature of PCM layer is recommended for PV/T modules [49].

An experiment was performed to compare the overall energy efficiencies of PV/T-PCM and PV/T systems. A glazed water based PV/T module with a copper sheet-and-tube heat exchanger was used [50]. In the PV/T-PCM systems, the absorbing pipes were wrapped in a PCM material layer (capric acid) and bonded to the copper sheet beneath the PV module. It was noted that the total solar energy

conversion efficiency was 76.87% with PV/T-PCM and 63.93% with PV/T module alone, while the primary energy saving efficiency was 87.5% with PV/T-PCM and around 73% with PV/T module. An experimental study investigated the effects of simultaneous use of a ZnO/water nanofluid with 0.2% by weight as the coolant as well as paraffin wax as the PCM, on the electric and thermal efficiency of a PV/T system [51]. It was noted that the PCM integrated with nanofluid based PV/T system enhanced its specific thermal and electric efficiencies by 11.8% and 0.61%, respectively.

2.3.7 PV/T-evaporator

Most research and development of solar assisted heat pump systems consist of a solar thermal collector, which produces only thermal energy, linked with the evaporator of a heat pump, i.e., thermal energy is extracted from the solar thermal system for heating purposes only. The integrated PV/T system with a heat pump, which provides both thermal energy and electric power, is the PV-evaporator type [52].

Solar assisted heat pumps are categorized into 2 groups based on the integration scheme between the solar system and the heat pump. These are termed direct expansion solar assisted heat pump (DX-SAHP) [53] and indirect expansion solar assisted heat pump (IDX-SAHP) [54]. The DX-SAHP allows for the refrigerant to flow through the solar collector while the IDX-SAHP requires a heat exchanger between the refrigerant and the fluid that goes through the solar collector.

As a method of low-temperature solar thermal conversion, the DX-SAHP was introduced in 1955 [55]. In this configuration, the PV/T is coupled to heat pump systems through the heat exchanger beneath the PV modules as an evaporator. Depending on the climate conditions, sometimes the PV/T collectors are cooling the water stream instead of heating it. Therefore, the control is required to ensure switching off the system when the evaporator temperature is below a certain value.

IDX-SAHP systems are divided into three types: series systems; parallel systems; and dual systems. The heat transfer medium is typically antifreeze solution, water or air. For series and dual systems, the heat pump performance is boosted by the utilization of solar energy.

2.3.8 Thermoelectric integrated PV/T

Thermoelectric (TE) coolers operate based on the Peltier effect. TE devices are composed of two different types of materials: n-type and p-type. The materials are attached thermally in parallel, but electrically in series. When a temperature gradient exists, the majority carriers diffuse from the hot side to the cold side setting up a voltage and a resultant current. In the reverse case, an applied voltage forces current through the materials causing an effective HP that cools one side and warms up the other.

Experimental study and performance analysis of a thermoelectric cooling and heating system driven by a photovoltaic/thermal system was carried out in summer and winter operation modes [56, 57]. It was indicated that: i) in summer condition, the COP of the TE device was greater than 0.45, the thermal efficiency of the whole system was 12.06%, the PV electric efficiency was 10.27%, and the water temperature had risen about 9 °C; and ii) in winter condition, the COP of the TE device was about 1.7, the maximum reached electric efficiency of the PV/T module was 16.7%, and the whole system thermal efficiency was 23.5%.

2.4 Concentrated photovoltaic/thermal systems

The general idea of concentration photovoltaics (CPV) is to use optics to focus sunlight on a small receiving solar cell, thus the cell area in the focus of the concentrator can be reduced by the concentration ratio. At the same time, the light intensity on the cell is increased by the same ratio. The concentrating optics are composed of either lenses or mirrors or a combination of both types. CPV systems can be categorized based on the nature of sun-tracking methods: on-axis tracking design and off-axis tracking design. Medium concentration photovoltaic (MCPV) and high concentration photovoltaic (HCPV) systems require accurate tracking to maintain the focus of the light on the solar cells as the sun moves throughout the day. This adds extra costs and complexity to the system and also increases the maintenance burden during operation. Although the concept of using light concentration with PV module is simple, it is difficult to implement, especially for high concentration ratios. The high concentration ratio puts stringent constraints on the solar PV cell, heat dissipation and sun tracking.

In a standard flat-plate PV panel, the area of the solar cell stores and converts the sunlight in a single unit, while in CPV storing and converting the sunlight are done by two separate units. The sunlight is first collected on an optical element. This optical element is used to guide and concentrate the sunlight onto a smaller area. Two elements are used to describe the concentration factor. One is based on the ratio between lens area (A_{lens}) and cell area (A_{cell}) referred to as 'geometrical concentration' ($C_{geometrical}$) as represented by Equation 2-1. The other is based on the power concentration (C_{power}) that describes the ratio between the power input (P_{in}) to the lens and to the solar cell ($p_{in,cell}$), (see Equation 2-2). Both of these are connected to the optical efficiency ($\eta_{Optical}$) [58].

$$C_{geometrical} = A_{lens}/A_{cell} \qquad (2\text{-}1)$$

$$C_{power} = P_{in,lens}/p_{in,cell} = \eta_{Optical} \cdot C_{geometrical} \qquad (2\text{-}2)$$

Notably, the optical efficiency depends on the concentration level. Within a given optical element, higher concentration factors reduce optical efficiency Optical efficiency accounts for loss in the optical element due to reflection, refraction, chromatic aberration, or other optical losses. Practical optical efficiencies range between 78% and 90% [59, 60]. In CPV systems available in the market today, preferred optical elements are either Fresnel lenses or mirrors.

Under normal circumstances, the maximum concentration (C_{max}) achievable on Earth (as a result of the divergence of light from the sun) is about 46,000x for a full-tracking 3D system, and only 216x for a single-axis tracking 2D system as calculated from the sun's diameter [61]. Equations (2-3) and (2-4) maintain that the concentrator is immersed in a refractive index, n, (for air this becomes 1), and θ_i as the input angle (i.e. effective solar angular radius: 4.7 mrad or 0.267°). For a linear concentrator, the maximum concentration equation is shown as:

$$C_{max} = n/\sin\theta_i \qquad (2\text{-}3)$$

While the maximum concentration for a point focus concentrator is described as:

$$C_{max} = (n/\sin\theta_i)^2 \qquad (2\text{-}4)$$

Because a CPV panel is more sensitive to the distribution of focused sunlight than a heat receiver, a properly designed optical concentrator is required that can spread the focused sunlight evenly over the receiver surface.

Although a wide variety of concentration technologies are available, the majority of them can be categorized into five main groups based on their method of focus. Those categories are: linear focusing lens; two-dimensional focusing lens; linear focusing reflectors; two-dimensional focusing reflectors; and central receiver systems. Moreover, the concentration systems are divided into low (1-10 suns), medium (10-100 suns), high (100-2000 suns), and very high (greater than 2000 suns) concentration systems based on their concentration ratio (1 sun = 1000 W/m^2).

2.4.1 Low concentration photovoltaic system

In comparison to a simple flat plate PV system, a low concentration photovoltaic system (LCPV) can reduce the costs of production by up to 40%, due to their attributes of non-tracking, high reliability and low cost (the cost of reflector material is lower than the cell cost). Furthermore, Silicon-based cells fit LCPV solutions. At concentration gains G<10x, the angular acceptance of the optics increases and may become compatible with a stationary installation [62].

A considerable amount of research has been done into the development of various types of LCPV applications. Low-aspect ratio compound parabolic concentrators, planar diffusive or luminescent concentrators, and holographic planar concentrators have all been suggested as viable ways to enhance stationary LCPV modules. A simple compound parabolic concentrator (CPC) can achieve a concentration ratio in the range of 2-7 without a tracker by providing the system with a seasonal tilt adjustment. In order to maximize the annual collectible radiation, a mathematical model was created to identify the yearly optimal tilt-angle of aperture [63].

A comparative performance analysis was performed between a conventional photovoltaic system and a low-concentration photovoltaic system [64]. Two typical photovoltaic modules and two compound parabolic concentrating photovoltaic systems were examined in Egypt. A cooling system was employed to lower the temperature of the solar cells in each of the two configurations. Experimental and numerical investigations of the performance of the two arrangements with and without cooling were presented. The concentration ratio of the concentrated photovoltaic system was considered to be 2.4x. It was indicated that, by employing cooling, the temperatures of the conventional photovoltaic system and the concentrated photovoltaic system were effectively lowered by approximately 25% and 30%, respectively, resulting in a significant enhancement in the electric power output of the photovoltaic system by 11% and that of the concentrated photovoltaic system by 15%. Furthermore, the concentrated photovoltaic system outperformed the non-concentrated photovoltaic system, for both non-cooling and cooling cases, by 33% and 52%, respectively.

A 3-D ray trace model has been developed to determine the theoretical optical efficiency and the optical flux distribution at the photovoltaic cell [65]. It was found that the 3-D crossed compound parabolic concentrator with a concentration ratio of 3.6x represented an improved geometry compared to a 3-D compound parabolic concentrator (CPC) for the use as a static solar concentrator. A 3-D static concentrator of 4x has been designed and coined the symmetric elliptical hyperboloid (SEH) to be integrated in glazing windows or facades [66]. It was found to have a constant optical efficiency of 40% for an acceptance angle equal to 120° (-60°, +60°) which enabled capture of both direct beam and diffuse sun rays all day long. With a geometric concentration of 6x, it typically consists of a dielectric based SEH concentrating element attached to a silicon solar cell and when evaluated, showed a maximum power ratio of 3.7 under a constant solar cell temperature [67]. A low-concentration reflector for a vertical bifacial panel has been developed with the objective to optimize the energy harvest for the winter [68]. It was noted that the retro reflector increased the energy output on a winter day by 30-70% relative to the reference setup and this significantly increases with latitude.

With the potential to be fabricated from a single aluminum sheet, the V-trough concentrator is one of the easiest of all low-concentrating systems to be constructed [69]. Consisting of two flat reflectors fixed on the PV module placed as a V letter, the V-trough concentrator is designed to increase the intake of solar radiation to the PV device. Simple fabrication, uniform reflection on the PV with low PV cell heating, use without sun-tracking, and relatively lower production costs are some of the key advantages of the V-trough concentrator [70].

The design of a modified PV module fitted with V-trough concentrator and cooled using water was investigated [71]. It was observed that the maximum temperature difference between the top PV glass layer and bottom tedlar sheet was 4.95 °C. The maximum temperature of the top layer for the modified PV module with V-trough mirrors (1.91×) was recorded as follow: i) 58.37 °C (0.25 kg/s, with glazing); ii) 58.03 (0.25 kg/s, without glazing); iii) 98.16 °C (without cooling, with glazing); and iv) 82.65 °C (without cooling, without glazing). On the other hand, the maximum temperature of the top layer for the reference PV module was 66.79 °C. A performance evaluation of an implemented concentrator V-trough using 0.5 mm thick aluminum sheet for housing mono-crystalline Si PV module was performed [72]. It was noted that the low-concentrated photovoltaic system outperformed the non-concentrated photovoltaic system, for both non-cooling and cooling cases, by 33% and 52%, respectively [73]. A simulation study of a V-trough concentrator used with photovoltaic module investigated the effects of V-trough geometric parameters [74]. Results show that the optimum vertex angles of the V-trough concentrator for 1.5×, 2×, 2.5×, and 3× are 30°, 30°, 22°, and 19°, respectively.

A performance evaluation of an implemented concentrator V-trough using 0.5 mm thick aluminum sheet for housing mono-crystalline Si PV module was performed [75]. It was noted that the module temperature rose about 20°C under the V-trough concentration when no cooling arrangement was made under outside conditions of irradiation of 750 W/m^2 at 34.3°C ambient temperature. On the other hand, due to the use of continuous Al sheet as a heat sink, the temperature of the concentrator V-trough module rose only by about 2.7°C as compared to the flat plate PV

module. The electric efficiency of module with the concentrator V-trough was increased about 7.6% as compared the flat plate PV module.

2.4.2 Medium concentration photovoltaic system

The medium concentration photovoltaic system, possessing a concentration ratio between 10 and 100, only needs one-axis tracking and has symmetrical concentrators. This system is based on parabolic trough reflectors [76].

The point-focus parabolic dish and the line-focus parabolic trough can be either concave or convex (inverse). Where the active side (used to redirect the light) faces the source, the parabolic dish is a paraboloid of revolution, providing a surface obtained by revolving part of the parabolic about its axis of symmetry. Figure 2-7 shows a parabola that can be represented in Cartesian coordinates as [77]:

$$D_r^2 = 8 \cdot F_r \cdot t_r \quad (2\text{-}5)$$

$$4 \tan (A_r/2) = 2x/F_r \quad (2\text{-}6)$$

$$x_1/f_1 = x_2/f_2 \quad (2\text{-}7)$$

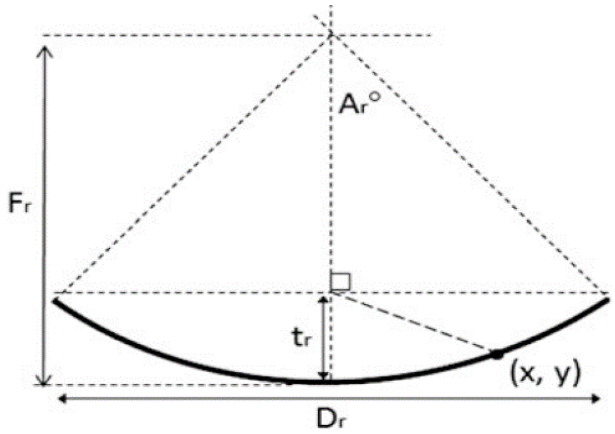

Figure 2-7. Dimensions and geometry of a parabolic curve reflector in two dimensions [77].

Usually designed for low to medium concentration ratios, parabolic troughs feature a half-acceptance angle 2-3 times the apparent angular width of the sun's disk. The maximum concentration ratio of a parabolic trough concentrator is limited to ~70x without the assistance of a secondary optic [78].

2.4.3 High concentration photovoltaic system

MCPV and HCPV systems generally make use of Multijunction (MJ) solar cells. The majority of HCPV concentrators will be point focus and require two-axis tracking. They are well suited for large field installations in the 10-100 MW range. The most developed refractive concentrator is the Fresnel lens, which is made up of a chain of prisms where each prism contributes a section of the slope of the lens surface but without the material of the full body of a conventional single lens. In general, high-concentration Fresnel lenses are actually avoided commercially because in large structures mainly

formed from glass, such lenses are still considered unwieldy, heavy and expensive. This gives more reason for modular designs with Fresnel lenses focusing toward very small solar cells or focusing to one PV receiver.

The 3D parabolic dish is the most efficient high-concentration optic with the fewest documented limitations. Unfortunately, however, reaching the device's fullest potential is extremely expensive; especially as compared to the point-focus Fresnel lens [79]. Parabolic dishes possess a greater level of optical efficiency than the linear Fresnel reflector or central receivers where cosine losses occur. A research effort compared the optical and thermal performance for both parabolic trough and linear Fresnel concentrators under summer and winter months throughout the day [80]. It was found that the end loss factor of the parabolic trough is always less than that of the linear Fresnel with maximum difference from 0.1 to 0.01 in January and June, respectively. Likewise, the optical efficiency of the linear Fresnel is lower by about 0.32 and 0.17 than the parabolic trough in December and June, respectively. Solar cells and optical devices are not the only components to be considered in the design of an HCPV module. Mechanisms for thermal management and heat dissipation must be analyzed. Objectives include cooling in HCPV modules to limit the operating temperature of the solar cells; decreasing the temperature differences between cells; decreasing temperature gradients across each cell; and ensuring reliability and decreasing costs. The design of HCPV solar receivers is evolving to decrease the thermal resistance of materials behind the solar cells. The addition of finned heat-exchangers is a simple way of improving heat dissipation, but many other alternatives are being investigated both for passive and active cooling [81].

The design of an HCPV cooler depends on many factors, which are not limited to the concentration and the outdoor conditions. First, the optics of the system usually play a fundamental role. With the most typical optical configurations in HCPV systems, in reflecting systems where no secondary is applied, the receiver is usually located between the sun and the mirrors. This means that the receiver must be as compact as possible to decrease shading. If a secondary reflector is present or if concentration is achieved through lenses, coolers would not create any risk of shadowing and large areas for cooling are usually available.

One of the main challenges of concentration optics is the decrease in acceptance angle as concentration ratio is increased due to etendue. Optical tolerance refers to all possible alignment uncertainties within the optical system including component misalignment, cell position uncertainty and tracking error. The acceptance angle or optical tolerance for high-concentration devices, such as parabolic dishes and Fresnel lenses, without additional optics can be expected to be very low ($\pm\approx 0.5^{\circ}$ or less) [82].

The preferred outline of a high-concentration optical system within an HCPV system consists of primary and secondary optics. The primary optics initially collect incident light and typical examples include Fresnel lens and the parabolic reflector. The secondary optics are of medium to low concentration and can be referred to as “receiver optics” when in optical contact with the PV. These secondary optics can increase the concentration of the system but are used more often with the aim of improving the system’s acceptance angle and the irradiance distribution on the PV cell. Receiver optics are introduced to a concentrator design which improve the irradiance distribution.

A high-concentration photovoltaic-thermal dish system was implemented in Switzerland [83]. The modular solar dish concentrator design was optimized for mass-production, structural rigidity, and scalability, with a high geometric concentration ratio of 1733x at each of its six receivers. Every receiver comprises 36 triple-junction CPV cells, interconnected in a unique hybrid parallel-serial scheme that mitigates mismatch losses caused by non-uniform irradiance distributions. The tested prototype was able to achieve an average solar radiative flux of 1374 suns on each of the receivers. It was noted that, the CPV-thermal system can deliver a solar-to-electricity conversion efficiency of 28.5% in PV-only mode and 26.6% in cogeneration mode while extracting heat at 89.8°C, and a power of 12.1 kW_{el} and 11.3 kW_{el}/21.5 kW_{th} respectively.

2.4.4 Spectral beam splitting

A way of obtaining high quality thermal energy while avoiding the overheating problems of solar cells in concentrated photovoltaic/thermal systems, is to introduce spectral splitting technology. The performance and the characterization of different CPV/T prototypes developed based on spectral beam splitting approach are illustrated in Table 2-5. The optical performance of filters cannot match the spectral response of solar cells perfectly and the complex optical structure contributes to much more optical loss and low optical efficiency. For this reason, the electric and thermal efficiencies of present studies on the SS-CPV/T systems are not so high.

In spectral splitting concentrating photovoltaic/thermal (SS-CPV/T) systems, the PV module and the thermal collector are decoupled by splitting the spectrum solar energy into two parts: the energy around the band gap is directed towards the PV unit to harvest electricity whilst the energy outside of this optimal band is conducted to the thermal unit to produce heat. This spectral decomposition approach offers a number of advantages such as: i) the quantity of sunlight energy dissipated as heat within the PV cells is reduced by illuminating the module with well suited light wavelengths. This helps to decrease the cell temperature and improve the performance of PV module; ii) the decomposition of sunlight allows photons with energy below the band gap that do not produce electricity to be directly accumulated as useful heat; and iii) the decoupling of the PV and thermal units of the receiver permits thermal output temperatures much higher than the PV cell operating temperature.

To achieve better solar conversion efficiencies, many spectral splitting methods were employed including the interference filter, liquid absorptive filter, holographic filter, luminescent filter, diffractive filter, combined interference and liquid absorptive filter, combined liquid and solid absorptive filter, and photovoltaics itself as a solid absorptive filter. Among a variety of spectral splitting methods, thin-film filters and absorptive liquid filters are the preferable spectral splitting methods in the developed SS-CPV/T systems due to their high optical efficiency, well matching with the concentrator and low cost.

At present, spectral beam splitting receivers have not yet evolved to the commercial level. Because the cost of PV systems utilizing spectral splitters is typically higher than the cost of standard PV systems. To offset this increase in cost, the optical efficiency of the spectral splitter and the

concentrating elements should be high enough to minimize the optical losses caused by the complex system designs and to improve the solar conversion efficiency.

Table 2-5. Summary of CPV/T prototypes developed based on spectral splitting approach

(Year) [Ref.]	PV cells	Concentrator	Aperture Area (m^2)	Geometric concentration ratio	spectral splitting medium	heat transfer fluid	T_Outlet fluid (°C)	Track system	Electric efficiency (%)	Thermal efficiency (%)
(2018) [84]	pc-Si	Truncated CPC (EMR)	N/A	15	water	water	50-70	no	5-10	50-55
(2016) [85]	mc-Si	Parabolic trough	2.4	42	propylene	water	37-68 (PV) 120-130 (thermal)	single axis	4-3.8	48-55
(2019) [86]	InGaP/GaAs (dual junction)	parabolic trough (primary) compound parabolic (secondary)	5	50	solar cells with integral side	molten salts	600	single axis	14	60
(2015) [87]	mc-Si	Linear	3.9	20	dichroic coating	water	100-220	single axis	12-29	N/A
(2018) [88]	mc-Si	Parabolic trough	5	14	gold & ITO particles + fluid	Duratherm S	60	single axis	5	61
(2016) [89]	mc-Si	linear fresnel	N/A	8	Cu_9S_5 nanoparticles	nanofluid	100-124	NO	22-24	33-42

2.5 Building integration PV/T systems

Building integrated photovoltaic (BIPV) and photovoltaic/thermal (BIPV/T) systems are powerful and versatile tools for achieving the ever-increasing demand for zero-energy and zero emission buildings.

'Building attached photovoltaic' (BAPV) systems are regarded as add-ons to the building. In further detail, they are not directly related to the building's structure and they only serve as a power generator. As for 'Building integrated photovoltaic' (BIPV), it is considered a functional part of the building structure and they are architecturally integrated into the building's design. Hence, the BIPV system serves as a building envelope material and power generator simultaneously. BIPVs have a great advantage compared to BAPVs, because they can reduce the total building material costs, especially since BIPVs do not require additional assembly components such as brackets and rails.

There are three principles for the integration of PV into buildings. This includes (i) weather skin (roof and façade integration), (ii) solar shading elements, and (iii) day lighting elements. BIPVs can also form semi-transparent elements of fenestration. BIPV with thermal energy recovery (BIPV/T) produces more energy than BIPV using the same roof or façade area. Thus, BIPV/T can increase the cost benefit of BIPV as long as the conversion of the thermal energy remains affordable. Table 2-6. illustrates the performance of building integration PV and PV/T systems in different climate conditions with different integration approaches.

It is also vitally important to ensure that the PV array can receive direct sunlight throughout the day during the winter without the shading out of sunlight by nearby obstacles (trees and buildings). In the northern hemisphere, solar panels will always work best if they are south facing. In the southern hemisphere, solar panels work best if they are north facing. The average efficiency drop of a solar panel mounted away from due south (due north in the southern hemisphere) is around 1.1% for every five degrees (see Figure 2-8).

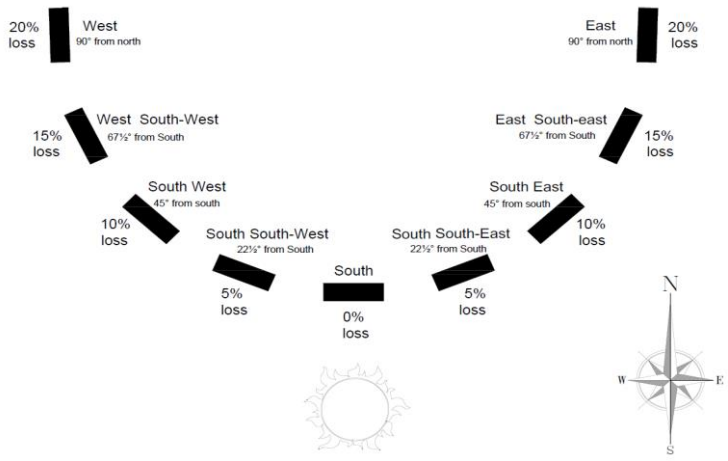

Figure 2-8. The approximate efficiency loss for solar panel mounted away from due south for northern hemisphere.

Based on the northern hemisphere, an optimum winter tilt angle for solar panels is the optimum angle for November and January. For the southern hemisphere, the optimum winter tilt is May and

July. The optimum tilt angle for winter setting can be calculated from Equation 2-8. While the optimum tilt angle for summer setting can be calculated from Equation 2-9.

$$90^{\circ} - \text{latitude} - 15.6^{\circ} = \text{optimum winter setting} \quad (2\text{-}8)$$

$$90^{\circ} - \text{latitude} + 15.6^{\circ} = \text{optimum summer setting} \quad (2\text{-}9)$$

Shading can also have a very significant impact on reducing the output power from the PV array owing to mismatching power losses between the PV modules. The mismatching power losses in PV systems depend on the PV array topology, physical location of the shaded area and the shading pattern on the PV module.

Table 2-6. Performance of building integration PV and PV/T systems in different climate conditions

Location, (study type), [Ref.]	Integration	PV Cell	Conclusion
Netherlands, (Simulation), [90]	Roof	c-Si	A 25 m^2 PV/T system and a ground coupled heat pump may cover the total heat demand for a typical Dutch one-family dwelling.
USA, (Experimental), [91]	Roof	a-Si	The solar absorption of the roof decreased to 0.38 from 0.75 after installation of the BIPV, lowering summertime daily mean roof upper surface temperatures by about 5 °C.
USA, (Experimental), [92]	Roof	c-Si	PV covered roof may cover up to 38% reduction in annual cooling load of the building.
Greece, (Simulation), [93]	Shading device	c-Si	Shading devices with integrated south facing PV can efficiently produce electricity which may be used for lighting.
Egypt, (Simulation), [94]	Ventilated BIPV facade	c-Si	Configurations of 60 mm gap depth BIPV wall were able to save 5700 kWh which is almost 30% of cooling loads. also, decreasing the CO_2 emissions each month by 250–300 kg.
USA, (Experimental), [95]	Roof	N/A	BIPV/T shows potential for increased electric efficiency of up to 5.3% over a naturally ventilated BIPV roof, reducing the negative effects of integration into the building façade.
Germany, Italy and Spain (Simulation), [96]	South-façade and roof	N/A	Varying the weather location and the building-plant configuration, the adoption of BIPVT panels produces a decrease of the primary energy demands from 67% to 89%.

2.5.1 Air based BIPV/T

To avoid the PV modules overheating when they are attached to the building skin, commonly an air gap between the PV and the building skin is left. This air gap can be closed cavity or open ended and can be ventilated mechanically or naturally.

A rigorous combined experimental and numerical approach was developed to assess the energy and thermal performance of the naturally ventilated PV façade systems in Turkey [97]. It was concluded that, the ventilation improves the efficiency of the PV façade system by up to 4%. Also, the fixed ventilation rates equal to 230 and 460 l/s on the back of each PV module increases the annual electricity generation of the system by up to 4.7 to 5.7%, respectively.

The techno-economic impact of retrofitting houses in the Canadian housing stock with PV and BIPV/T systems was evaluated using the simulation engine of the Canadian hybrid end-use energy and emission model [98]. The PV system was used to produce electricity and supply the electric demands of the house, with the excess electricity sold to the grid in a net-metering arrangement. The BIPV/T system produced electricity as well as thermal energy to supply the electric as well as the thermal demands for space and domestic hot water heating. The PV panels were installed on the available roof surface while the BIPV/T system was complemented with a heat pump, thermal storage tank, auxiliary heater, domestic hot water heating equipment and hydronic heat delivery system (see Figure 2-9). It was indicated that the PV system retrofit yielded 3% energy savings and 5% GHG emission reduction, while the BIPV/T system yielded 18% energy savings and 17% GHG emission reduction in the Canadian housing stock.

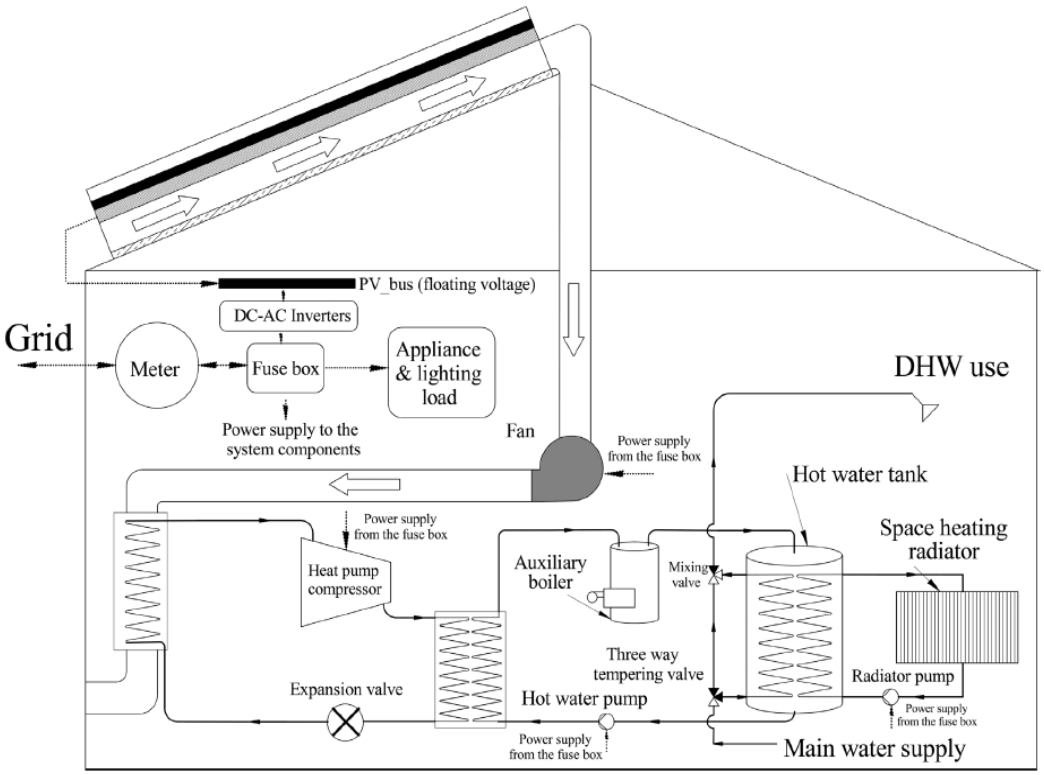

Figure 2-9. A typical house with BIPV/T system retrofitted [98].

2.5.2 Water based BIPV/T

A PV/T system comprised of a high efficiency multi-crystalline PV module and water based spiral flow absorber for BIPV/T application was tested in Malaysia [99]. It indicated that the BIPV/T system produced a primary energy saving efficiency between 73% and 81%. The PV/T combined energy efficiency varied between 55% and 62% whereas the variation in the PV/T exergy efficiency was from 12% to 14%.

2.5.3 Semi-transparent PV/T window

Semitransparent building-integrated photovoltaic windows can reduce solar heat gain promoting shading with the advantage of producing electricity. One of the drawbacks of this arrangement is that it can drastically reduce the amount of daylight gained by the indoor environment depending on the cell spacing and it also compromises the external view.

As the integration of photovoltaic modules into the building structure has an effect on the building's interior conditions, as it results in a variation of the thermal comfort due to the change of the thermal resistance of the envelope of the building structure. The temperature difference of indoor air temperature of buildings with BIPV and without BIPV can reach up to 4°C by combining orientation of building and the building material envelope. The orientation of the building must take into account its maximum natural ventilation which could reduce the temperature of the air inside by 3°C [100].

2.5.4 Bifacial BIPV modules

One study that focused on the performance of a bifacial BIPV module applied to a building envelope [101] indicated that the external wall reflectivity was the most important variable during the installation of the bifacial BIPV module. The distance between the bifacial module (glass-to-glass structure) and the building wall had a small impact on the module performance. In order to achieve higher performance by the bifacial BIPV modules, design conditions including reflectivity exceeding 50% and a transparent space ratio not less than 30% (depending on the properties of the exterior wall finishing material) must be considered. The multifunctional bifacial PV sun-shading achieved 37% more electric power compared to monofacial PV systems under the same installation conditions [102].

2.6 Commercial photovoltaic/thermal market products

Based on the market, most manufacturers supply liquid-based PV/T collectors. The LCPV/T systems such as Absolicon X10 PVT and Solarus are favorable with fluid temperature below 75 °C.

In 2018, the worldwide market survey of 26 PV/T collector manufacturers reported accumulated installed PV/T collector area of 1,075,247m^2, most manufacturers supply liquid based PV/T collectors (48 % uncovered flat plate collectors, 28 % covered flat plate collectors, 4 % vacuum tube collectors), while only 12 % of the manufacturers supply air collectors and 8 % concentrated collectors (see Figure 2-10). The distribution of the 26 PV/T manufacturers by country is illustrated in Figure 2-11. EndeF and Setolazar are the main PV/T manufacturers in Spain.

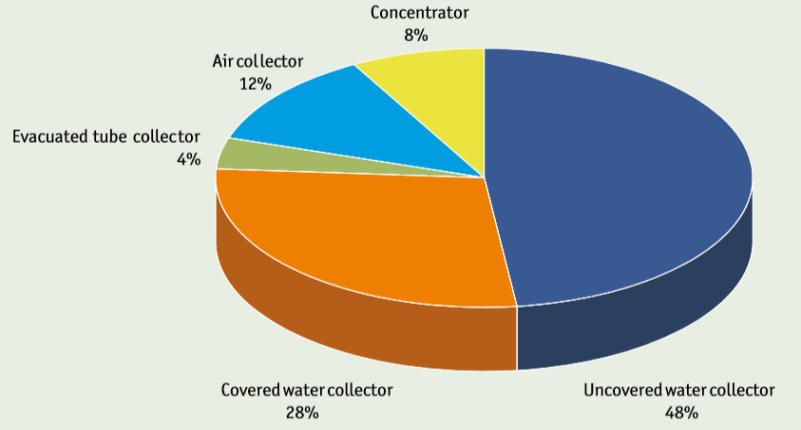

Figure 2-10. Distribution of photovoltaic/thermal manufacturers by collector type [103].

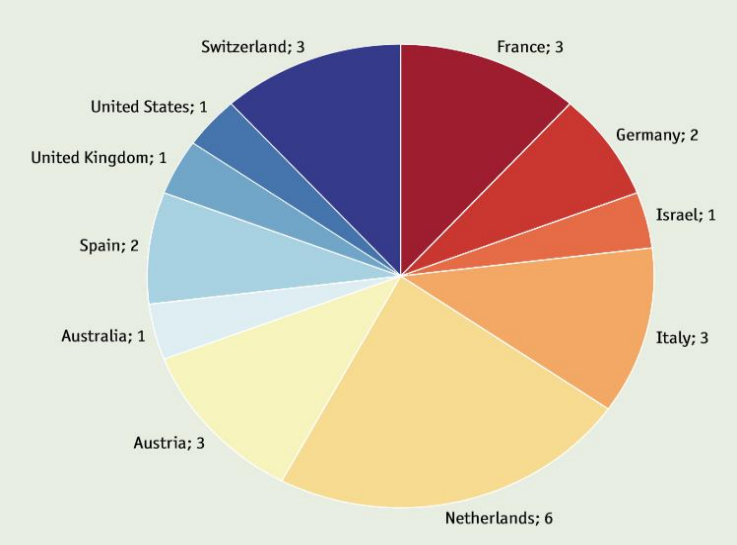

Figure 2-11 Distribution of photovoltaic/thermal manufacturers by country [103].

The installed water based PV/T systems counted approximately 118 million in 2017: about 63% for domestic hot water production in single-family houses, 28% attached to large domestic hot water systems for multifamily houses, hotels, hospitals, schools, etc., 6% for swimming pool heating, 2% for both domestic hot water and space heating, and the remaining counted for 1% and delivered heat to other application, including district heating networks, industrial process a thermally driven solar cooling applications [103].

The installation of 90 glass covered PVT panels were installed on the roof of a hotel in a luxury resort in Ibiza (Balearic Islands), covering a surface of 147.6 m^2 in 2017. This PV/T system is used for preheating of DHW and for self-consumption of electricity without feed-in the electricity grid (see Figure 2-12). The system produces 112,814 kWh/year of thermal energy and 34,600 kWh/year of electricity [104, 105].

Figure 2-12. Covered PV/T collectors in Spain (EndeF Spanish manufacturer) [105].

The 80 uncovered PV/T collectors were installed on the roof of the Marine Studies Center of Cádiz in Spain in 2018. The system is coupled to a reversible heat pump unit to complement the energy needs of the fish farm (see Figure 2-13). The annual energy generation is 67,240 kWh of thermal energy and 47,418 kWh of electricity [104, 106].

Figure 2-13. Uncovered PV/T collectors installed in Spain (Setolazar Spanish manufacture) [106].

For a cheese factory in Netherlands, the 88 LCPV/T collectors with a thermal capacity of 110 kW_{th} and electric power of 22 kW_{peak} were installed in 2017 (see Figure 2-14). In winter, the generated heat is used to preheat 8 m^3 water tank up to 30 °C while in summer, the tank is heated at 75°C. the collectors delivered 450 MWh of heat and 15 MWh of electricity during 2018 [104, 107].

Figure 2-14. LCPV/T system in north Holland for food industry (Solarus) [107].

The plant of 20 Absolicon X10 PVT collectors of 200 m^2 installed in 2011 in Harnosand, Sweden to generate heat for the district heating network and electricity for the electric power grid (see Figure 2-15). The system produces heat up to 75 °C of 80 kW_p and electricity production of 20 kWp [108].

Figure 2-15. Low concentrating Absolicon X10 PVT to generate heat for the district heating network and electricity for the electric power grid installed in Sweden [108].

2.7 Conclusion

This chapter has sought out to provide and up-to-date overview of hybrid photovoltaic/thermal techniques that included an introduction to PV cell generation and a review of theoretical analysis, investigative experiments and computer simulations of conventional, novel, and concentrated PV/T systems. All of PV/T based air, PV/T based water, PV/T based bi-fluid, PV/T based heat pipe, PV/T based nanofluid, PV/T-evaporator, PV/T based PCM, and thermoelectric integrated PV/T systems have displayed. All of low-, medium-, and high-concentrated PV/T system using and without using spectrum split techniques have overviewed. All of ventilated PV façade, air-based BIPV/T, water-based BIPV/T, semi-transparent PV/T window, multifunctional bifacial PV sun-shading have discussed.

Throughout the expanse of this review, the following conclusions were drawn:

- The large majority of current PV installations use single-junction modules, with multi-crystalline silicon cells having the largest market share because they are less expensive to produce than monocrystalline silicon cells, however they are slightly less efficient. A bifacial module produces 30% more electric power compared with a monofacial module since this cell type is harvesting sunlight from both front and rear sides. White ground has the highest albedo reflectance. The n-type structure-based heterojunction PV cell (mono-crystalline silicon) has a symmetrical structure and is bifacial without the need for additional process steps. However, there are not many commercially manufactured bifacial modules available due to a lack of standardized testing and modeling procedures that can accurately predict the performance of bifacial systems. Amorphous silicon and bifacial solar cells have better performance than mono or poly silicon at higher temperatures (drop in cell efficiency of 0.45% per °C rise for monofacial crystalline-silicon cells, 0.25% per °C for standard amorphous-silicon, and 0.22% per °C for bifacial cells. Multi-Junction cells comprised of III-V materials are typically used with high concentrating optics so that the cell cost becomes a small fraction of overall system cost. The most prominent Multi-Junction cell is a triple junction device that makes use of the p-n junction in $Ga_{0.5}$ $In_{0.5}$ P, $Ga_{0.99}$ $In_{0.01}$As and Ge with an average efficiency of 37% at 1000 W/m^2.
- The discrepancy between maintaining a satisfactory low operating temperature for the PV, and obtaining high-grade thermal energy, is considered the main limitation of PV/T systems. Glazing of PV/T collectors almost doubles the useful thermal output, but the electric efficiency drops owing to reflection losses. Temperature fluctuation in liquid-based PV/T is much less than in air based PV/T collectors when subjected to variation in solar radiation levels. The integration of nanofluid for cooling and as an optical filter in a single system, can significantly enhance PV/T system performance. Silicon carbide nanoparticles offer the best stability and the highest thermal conductivity compared to Al_2O_3 and CuO nanofluids. The large majority of PV/T installations is unglazed PV/T based water collectors. Amongst the various designs of PV/T based water collectors, the sheet-and-tube and roll bond designs appear to be the predominantly designs for domestic applications.
- Concentrator PV/T technology is an attractive approach to reduce the cost of solar PV modules as long as the cost of the reflector material is lower than the cell cost. The manufacturing costs and efficiency are the two key factors of concentrator cells. For building applications, LCPV systems are preferable due to their potential for non-tracking, high reliability and low cost. Further, Silicon-based cells fit well with LCPV solutions. The LCPV reduces the costs of production by up to 40%. The LCPV/T systems such as Absolicon X10 PVT and Solarus are favorable with fluid temperature below 75 °C.
- Building Integrated Photovoltaics (BIPVs) have a significant advantage compared to Building Attached Photovoltaics (BAPVs) because they can reduce the total building material costs. U-value and solar heat gain coefficient for thermal aspects and the visible light transmittance for optical ones are important parameters when replacing the building glazing by semi-transparent PV modules. The BIPV/T window has greater potential for reducing cooling load consumption

than conventional glass windows, however it also compromises the external view. Further, the solar absorption of the roof decreases after installation of the BIPV, lowering summertime daily mean roof upper surface temperatures by about 2-5 °C. Air based BIPV/T and ventilated PV façade systems have been widely applied to cool PV cells and to produce low grade thermal energy for residential applications, whilst water based BIPV/T systems have the highest overall efficiency and energy savings. The multifunctional bifacial PV sun-shading element ideally combines aesthetic appearance and significant cost reduction for solar electricity.

References

[1]- Green MA, Hishikawa Y, Warta W, Dunlop ED, Levi DH, Hohl-Ebinger J, Ho-Baillie AWH. Solar cell efficiency tables (version 50). Progress in Photovoltaics: Research and Applications 2017; 25: 668-676.
[2]- Khan J, Arsalan MH. Solar power technologies for sustainable electricity generation – A review. Renewable and Sustainable Energy Reviews 2016; 55: 414-425.
[3]- Castillo-Aguilella JE, Hauser PS. Multi-Variable Bifacial Photovoltaic Module Test Results and Best-Fit Annual Bifacial Energy Yield Model. IEEE 2016; 4: 498-506.
[4]- Khan MR, Hanna A, Sun X, Alam MA. Vertical bifacial solar farms: Physics, design, and global optimization. Applied Energy 2017; 206: 240-248.
[5]- Appelbaum J. Bifacial photovoltaic panels field. Renewable Energy 2016; 85: 338-343.
[6]- Aoyama T, Aoki M, Sumita I, Yoshino Y, Ogura A. Effect of glass frit in Metallization paste on the electrical losses in bifacial N-type crystalline Silicon solar cells. 43rd IEEE Photovoltaic Specialists Conference, USA; 2016, 16484211.
[7]- Singh JP, Guo S, Peters IM, Aberle AG, Walsh TM. Comparison of Glass/Glass and Glass/Backsheet PV Modules Using Bifacial Silicon Solar Cells. IEEE Journal of photovoltaics 2015; 5: 783-791.
[8]- EPRI - Program on technology innovation. Bifacial solar photovoltaic modules, (https://www.epri.com/#/pages/product/3002009163/); 2016 [Accessed 2017.02.01].
[9]- Deline C, MacAlpine S, Marion B, Toor F, Asgharzadeh A, Stein JS. Assessment of Bifacial Photovoltaic Module Power Rating Methodologies-Inside and Out. IEEE Journal of Photovoltaic 2017; 2: 575-580.
[10]- Sopian K, Ooshaksaraei P, Zaidi SH, Othman MY. Recent advances in air-based bifacial photovoltaic thermal solar collectors. In: Sayigh A, editor. Photovoltaics for Sustainable Electricity and Buildings: Springer Cham 2017: 161-176.
[11]- Y Bo, Song D, Sun Z, Liu K, Zhang Y, Rong D, Liu L. A study on electrical performance of N-type bifacial PV modules. Solar Energy 2016; 137: 129-133.
[12]- Zhang X, Zhao X, Smith S, Xu J, Yu X. Review of R&D progress and practical application of the solar photovoltaic/thermal (PV/T) technologies. Renewable and Sustainable Energy Reviews 2016; 1: 599-617.
[13]- Sopian K, Yigit KS, Liu HT, Kakaç S, Veziroglu TN. Performance analysis of photovoltaic thermal air heaters. Energy Conversion and Management 1996; 37: 1657-1670.
[14]- Othman MYH, Hussain F. Designs of various hybrid photovoltaic-thermal (PV/T) solar collectors. In: Sayigh A, editor. Photovoltaics for Sustainable Electricity and Buildings: Springer, Cham; 2017, p. 95-112.
[15]- Joshi AS, Tiwari A, Tiwari GN, Dincer I, Reddy BV. Performance evaluation of a hybrid photovoltaic thermal (PV/T) (glass-to-glass) system. International Journal of Thermal science 2009; 48: 154-164.

[16]- Elsafi A, Gandhidasan P. Comparative study of double-pass flat and compound parabolic concentrated photovoltaic–thermal systems with and without fins. Energy Conversion and Management 2015; 98: 59-68.
[17]- Aste N, del Pero C, Leonforte F. Water flat plate PV–thermal collectors: A review. Solar Energy 2014; 102: 98-115.
[18]- Hamid SA, Othman MY, Sopian K, Zaidi SH. An overview of photovoltaic thermal combination (PV/T combi) technology. Renewable and Sustainable Energy Reviews 2014; 38: 212-222.
[19]- Wu J, Zhang X, Shen J, Wu Y, Connelly K, Yang T, Tang L, Xiao M, Wei Y, Jiang K, Chen C, Xu P, Wang H. A review of thermal absorbers and their integration methods for the combined solar photovoltaic/thermal (PV/T) modules. Renewable and sustainable energy reviews 2017; 75: 839-854.
[20]- Kim J, Kim J. The Experimental Performance of an Unglazed PVT Collector with Two Different Absorber Types. International Journal of Photoenergy 2012: 312168. http://dx.doi.org/10.1155/2012/312168.
[21]- Zondag HA, de Vries DW, van Helden WGJ, van Zolingen RJC, van Steenhoven AA. (2003). The yield of different combined PV-thermal collector designs. Solar Energy 2003; 74: 253-269.
[22]- Chow TT, He W, Ji J. Hybrid photovoltaic-thermosyphon water heating system for residential application. Solar Energy 2006; 80: 298-306.
[23]- Ji J, Lu J, Chow T, He W, Pei G. A sensitivity study of a hybrid photovoltaic/thermal water-heating system with natural circulation, Applied Energy 2007; 84: 222-237.
[24]- Sandnes B, Rekstad J. A photovoltaic/thermal (PV/T) collector with a polymer absorber plate. Experimental study and analytical model. Solar Energy 2002; 72: 63-73.
[25]- Bai Y, Chow TT, Ménézo C, Dupeyrat P. Analysis of a Hybrid PV/Thermal Solar-Assisted Heat Pump System for Sports Center Water Heating Application. International Journal of Photoenergy 2012: 265838. http://dx.doi.org/10.1155/2012/265838.
[26]- Dupeyrat P, Ménézo C, Wirth H, Rommel M. Improvement of PV module optical properties for PV-thermal hybrid collector application. Solar Energy Materials and Solar Cells 2011; 95: 2028-2036.
[27]- Huang BJ, Lin TH, Hung WC, Sun FS. Performance evaluation of solar photovoltaic/thermal system. Solar Energy 2001; 70: 443-448.
[28]- Ji J, Guo C, Sun W, He W, Wang Y, Li G. Experimental investigation of tri-functional photovoltaic/thermal solar collector. Energy Conversion and Management 2014; 88: 650-656.
[29]- Bilbao JI, Sproul, AB, (2012). Experimental results of a PV/T-water for developing countries. Proceedings of the 50th annual conference, Australia Solar Energy Society 2012.
[30]- He W, Chow TT, Ji J, Lu J, Pei G, Chan L. Hybrid photovoltaic and thermal solar-collector designed for natural circulation of water. Applied Energy 2006; 83: 199-210.
[31]- Zondag HA, de Vries DW, van Helden WGJ, van Zolingen RJC, van Steenhoven AA. (2003). The yield of different combined PV-thermal collector designs. Solar Energy 2003; 74: 253-269.
[32]- Vittorini D, Castellucci N, Cipollone R, 2017. Heat recovery potential and electrical performances in-field investigation on a hybrid PVT module. Applied Energy 205, pp. 44-56.
[33]- Kazem HA. Evaluation and analysis of water-based photovoltaic/thermal (PV/T) system. Case Studies in Thermal Engineering 2019; 13: 100401.
[34]- Zhang X, Shen J, Zhao X, Xu Y, Nibeler B. Comparative Investigation of Solar Photovoltaic (PV) and Photovoltaic/Thermal (PV/T) Systems by both Laboratory and Field Experiments. In: Sayigh A, editor. Renewable Energy in the Service of Mankind Vol II: Springer, Cham; 2015: 673-682.
[35]- Bianchini A, Guzzini A, Pellegrini M, Saccani C. Photovoltaic/thermal (PV/T) solar system: Experimental measurements, performance analysis and economic assessment. Renewable Energy 2017; 111: 543-555.
[36]- Jarimi H, Abu Bakar MN, Othman M, Hj Din M. Bi-fluid photovoltaic/thermal (PV/T) solar collector: Experimental validation of a 2-D theoretical model. Renewable Energy 2016; 85: 1052-1067.

[37]- Othman MY, Hamid SA, Tabook MAS, Sopian K, Roslan MH, Ibarahim Z. Performance analysis of PV/T Combi with water and air heating system: An experimental study. Renewable Energy 2016; 86: 716-722.
[38]- Vats K, Tomar V, Tiwari GN. Effect of packing factor on the performance of a building integrated semitransparent photovoltaic thermal (BISPVT) system with air duct. Energy and Buildings 2012; 53: 159-165.
[39]- Jouhara H, Milko J, Danielewicz J, Sayegh MA, Szulgowska-Zgrzywa M, Ramos JB, Lester SP. The performance of a novel flat heat pipe based thermal and PV/T (photovoltaic and thermal systems) solar collector that can be used as an energy-active building envelope material. Energy 2016; 108: 148-154.
[40]- Jouhara H, Szulgowska-Zgrzywa M, Sayegh MA, Milko J, Danielewicz J, Nannou TK, Lester SP. The performance of a heat pipe based solar PV/T roof collector and its potential contribution in district heating applications. Energy 2017; 136: 117-125.
[41]- Sathe TM, Dhoble AS. A review on recent advancements in photovoltaic thermal techniques. Renewable and Sustainable Energy Reviews 2017; 76: 645–672.
[42]- Ni J, Li J, An W, Zhu T. Performance analysis of nanofluid-based spectral splitting PV/T system in combined heating and power application. Applied Thermal Engineering 2018; 129: 1160-1170.
[43]- An W, Li J, Ni J, Taylor RA, Zhu T. Analysis of a temperature dependent optical window for nanofluid-based spectral splitting in PV/T power generation applications. Energy Conversion and Management 2017; 151: 23-31.
[44]- Al-Waeli AHA, Sopian K, Chaichan MT, Kazem HA, Hasan HA, Al-Shamani AN. An experimental investigation of SiC nanofluid as a base-fluid for a photovoltaic thermal PV/T system. Energy Conversion and Management 2017; 142: 547–558.
[45]- Hassani S, Taylor RA, Mekhilef S, Saidur R. A cascade nanofluid-based PV/T system with optimized optical and thermal properties. Energy 2016; 112: 963-975.
[46]- Yazdanifard F, Ameri M, Ebrahimnia-Bajestan E. Performance of nanofluid-based photovoltaic/thermal systems: A review. Renewable and Sustainable Energy Reviews 2017; 76: 323-352.
[47]- Al-Waeli AHA, Chaichan MT, Kazem HA, Sopian K. Comparative study to use nano-(Al_2O_3, CuO, and SiC) with water to enhance photovoltaic thermal PV/T collectors. Energy Conversion and Management 2017; 148: 963–973.
[48]- Wang Z, Qiu F, Yang W, Zhao X. Applications of solar water heating system with phase change material. Renewable and Sustainable Energy Reviews 2015; 52: 645-652.
[49]- Ma T, Yang H, Zhang Y, Lu L, Wang X. Using phase change materials in photovoltaic systems for thermal regulation and electrical efficiency improvement: A review and outlook. Renewable and Sustainable Energy Reviews 2015; 43: 1273-1284.
[50]- Yang X, Sun L, Yuan Y, Zhao X, Cao X. Experimental investigation on performance comparison of PV/T-PCM system and PV/T system. Renewable Energy 2018; 119: 152-159.
[51]-Hosseinzadeh M, Sardarabadi M, Passandideh-Fard M. Energy and exergy analysis of nanofluid base photovoltaic thermal system integrated with phase change material. Energy 2018; 147: 636-647.
[52]- Kamel RS, Fung AS, Dash PRH. Solar systems and their integration with heat pumps: A review. Energy and Buildings 2015; 87: 395-412.
[53]- Zhou J, Zhao X, Ma X, Qiu Z, Ji J, Du Z, Yu M. Experimental investigation of a solar driven direct-expansion heat pump system employing the novel PV/micro-channels-evaporator modules. Applied Energy 2016; 178: 484-495.
[54]- Wang G, Quan Z, Zhao Y, Sun C, Deng Y, Tong J. Experimental study on a novel PV/T air dual-heat-source composite heat pump hot water system. Energy and Buildings 2015; 108: 175-184.
[55]- Sporn P, Ambrose E. The heat pump and solar energy. Proc of the world symposium on applied solar energy phoenix, US1955.
[56]- He W, Zhou J, Hou J, Chen C, Ji J. Theoretical and experimental investigation on a thermoelectric cooling and heating system driven by solar. Applied Energy 2013; 107: 89-97.

[57]- He W, Zhou J, Chen C, Ji J. Experimental study and performance analysis of a thermoelectric cooling and heating system driven by a photovoltaic/thermal system in summer and winter operation modes. Energy Conversion and Management 2014; 84: 41-49.
[58]- Sala G, Luque A. Past Experiences and New Challenges of PV Concentrators. In: López AL, Andreev VM, editors. Concentrator Photovoltaics: Springer Series in Optical Sciences; 2007, p. 1-23.
[59]- Steiner M, Gerstmaier T, Bett AW. Concentrating photovoltaic systems. In: Pearsall N, editor. The Performance of Photovoltaic (PV) Systems: Elsevier; 2017, p. 297-320.
[60]- Wang G, Chen Z, Hu P, Cheng X. Design and optical analysis of the band-focus Fresnel lens solar concentrator. Applied Thermal Engineering 2016; 102: 695-700.
[61]- Paul DI. Theoretical and Experimental Optical Evaluation and Comparison of Symmetric 2D CPC and V-Trough Collector for Photovoltaic Applications. International Journal of Photoenergy 2015: 693463. http://dx.doi.org/10.1155/2015/693463.
[62]- Varieras RV, Wang J, King, DL. System performance considerations for low concentration linear-focus silicon-based photovoltaic modules. 38th IEEE Photovoltaic Specialists Conference. USA; 2012. doi: 10.1109/PVSC-Vol 2.2013.6656791.
[63]- Yu YM, Yu MJ, Tang RS. A mathematical procedure to predict optical performance of CPCs. IOP Conference Series: Earth and Environmental Science 2016; 40: 012006.
[64]- Yousef MS, Abdel Rahman AK, Ookawara S. Performance investigation of low – Concentration photovoltaic systems under hot and arid conditions: Experimental and numerical results. Energy Conversion and Management 2016; 128: 82–94.
[65]- Sellami N, Mallick T. Optical efficiency study of PV Crossed Compound Parabolic Concentrator. Applied Energy 2013; 102: 868-876.
[66]- Sellami N, Mallick TK, McNeil DA. Optical characterisation of 3-D static solar concentrator. Energy Conversion and Management 2012; 64: 579-586.
[67]- Baig H, Sellami N, Mallick TK. Performance modeling and testing of a Building Integrated Concentrating Photovoltaic (BICPV) system. Solar Energy Materials & Solar Cells 2015; 134: 29-44.
[68]- Jakobsen ML, Thorsteinsson S, Poulsen PB, Rødder PM, Rødder K. Vertical reflector for bifacial PV-panels. 43rd IEEE Photovoltaic Specialists Conference. USA; 2016: 16484138. doi: 10.1109/PVSC.2016.7750136.
[69]- Al-Shohani WAM, Al-Dadah R, Mahmoud S, Algareu A. Optimum design of V-trough concentrator for photovoltaic applications. Solar Energy 2016; 140: 241-254.
[70]- Kunnemeyer R, Anderson TN, Duke M, Carson JK. Performance of a V-trough photovoltaic/thermal concentrator. Solar Energy 2014; 101: 19-27.
[71]- Michael JJ, Iqbal SM, Iniyan S, Goic R, 2018. Enhanced electrical performance in a solar photovoltaic module using V-trough concentrators. Energy 148, pp. 605-613.
[72]- Solanki C, Sangani C, Gunashekar D, Antony G, 2008. Enhanced heat dissipation of V-trough PV modules for better performance. Solar Energy Materials and Solar Cells 92, pp. 1634-1638.
[73]- Yousef M, Abdel Rahman A, Ookawara S, 2016. Performance investigation of low – Concentration photovoltaic systems under hot and arid conditions: Experimental and numerical results. Energy Conversion and Management 128, pp. 82–94.
[74]- Al-Shohani W, Al-Dadah R, Mahmoud S, Algareu A, 2016. Optimum design of V-trough concentrator for photovoltaic applications. Solar Energy 140, pp. 241-254.
[75]- Solanki CS, Sangani CS, Gunashekar D, Antony G. Enhanced heat dissipation of V-trough PV modules for better performance. Solar Energy Materials and Solar Cells 2008; 92: 1634-1638.
[76]- Jaaz AH, Hasan HA, Sopian K, Ruslan MHBH, Zaidi SH. Design and development of compound parabolic concentrating for photovoltaic solar collector: Review. Renewable and Sustainable Energy Reviews 2017; 76: 1108-1121.
[77]- Conventry JS. Performance of a concentrating photovoltaic/thermal solar collector. Solar Energy 2005; 78: 211-222.
[78]- Canavarro D, Chaves J, Collares-Pereira M. New second-stage concentrators (XX SMS) for parabolic primaries; Comparison with conventional parabolic trough concentrators. Solar Energy 2013; 92: 98-105.

[79]- Skouri S, Ali AB, Bouadila S, Ben Salah M, Ben Nasrallah S. Design and construction of sun tracking systems for solar parabolic concentrator displacement. Renewable and Sustainable Energy Reviews 2016; 60: 1419-1429.
[80]- Ahmed MH, Rady M, Amin AMA, Montagnino FM, Paredes F. Comparison of thermal and optical performance of Linear Fresnel and Parabolic Trough Concentrator. Renewable Energy Research and Applications. Italy; 2015: 15807286.
[81]- Rodrigo P, Micheli L, Almonacid F. The high-concentrator photovoltaic module. In: Pérez-Higueras P, Fernández E, editors. High concentrator photovoltaics: Springer, Cham; 2015, p. 115-151.
[82]- Shanks, K., Senthilarasu S, Mallick TK. High-Concentration optics for photovoltaic applications. In: Pérez-Higueras P, Fernández E, editors. High concentrator photovoltaics: Springer, Cham; 2015, p. 85-113.
[83]- Schmitz M, Wiik N, Ambrosetti G, Pedretti A, Paredes S, Ruch P, Michel B, Steinfeld A. A 6-focus high-concentration photovoltaic-thermal dish system. Solar Energy 2017; 155: 445–463.
[84]- Zhang G, Wei J, Xie H, Wang Z, Xi Y, Khalid M. Performance investigation on a novel spectral splitting concentrating photovoltaic/thermal system based on direct absorption collection. Solar Energy 2018; 163: 552-563.
[85]- Stanley C, Mojiri A, Rahat M, Blakers A, Rosengarten G. Performance testing of a spectral beam splitting hybrid PVT solar receiver for linear concentrators. Applied Energy 2016; 168: 303-313.
[86]- Widyolar B, Jiang L, Ferry J, Winston R, Kirk A, Osowski M, Cygan D, Abbasi H. Theoretical and experimental performance of a two-stage (50X) hybrid spectrum splitting solar collector tested to 600 °C. Applied Energy; 239: 514-525.
[87]- Mojiri A, Stanley C, Taylor RA, Kalantar-zadeh K, Rosengarten G. A spectrally splitting photovoltaic-thermal hybrid receiver utilising direct absorption and wave interference light filtering. Solar Energy Materials and Solar Cells 215; 139: 71-80.
[88]- Otanicar T, Dale J, Orosz M, Brekke N, DeJarnette D, Tunkara E, Roberts K, Harikumar P. Experimental evaluation of a prototype hybrid CPV/T system utilizing a nanoparticle fluid absorber at elevated temperatures. Applied Energy 2018; 228: 1531-1539.
[89]- An W, Wu J, Zhu T, Zhu Q. Experimental investigation of a concentrating PV/T collector with Cu9S5 nanofluid spectral splitting filter. Applied Energy 2016; 184: 197-206.
[90]- Bakker M, Zondag HA, Elswijk MJ, Strootman KJ, Jong MJM. Performance and costs of a roof-sized PV/thermal array combined with a ground coupled heat pump. Solar Energy 2005; 78: 331-339.
[91]- Ban-Weiss G, Wray C, Delp W, Ly P, Akbari H, Levinson R. Electricity production and cooling energy savings from installation of a building-integrated photovoltaic roof on an office building. Energy and Buildings 2013; 56: 210-220.
[92]- Dominguez A, Kleissl J, Luvall JC. Effects of solar photovoltaic panels on roof heat transfer. Solar Energy 2011; 85: 2244-2255.
[93]- Mandalaki M, Zervas K, Tsoutsos T, Vazakas A. Assessment of fixed shading devices with integrated PV for efficient energy use. Solar Energy 2012; 86: 2561-2575.
[94]- Elsayed MS. Optimizing thermal performance of building-integrated photovoltaics for upgrading informal urbanization. Energy and Buildings 2016; 116: 232-248.
[95]- Corbin CD, Zhai ZJ. Experimental and numerical investigation on thermal and electrical performance of a building integrated photovoltaic–thermal collector system. Energy and Buildings 2010; 42: 76-82.
[96]- Buonomano A, Calise F, Palombo A, Vicidomini M. BIPVT systems for residential applications: An energy and economic analysis for European climates. Applied Energy 2016; 184: 1411-1431.
[97]- Shahrestani M, Yao R, Essah E, Shao L, Oliveira AC, Hepbasli A, Biyik E, del Caño T, Rico E, Lechón JL. Experimental and numerical studies to assess the energy performance of naturally ventilated PV façade systems. Solar Energy 2017; 147: 37–51.
[98]- Asaee SR, Nikoofard S, Ugursal VI, Beausoleil-Morrison I. Techno-economic assessment of photovoltaic (PV) and building integrated photovoltaic/thermal (BIPV/T) system retrofits in the Canadian housing stock. Energy and Buildings 2017; 152: 667-679.

[99]- Ibrahim A, Fudholi A, Sopian K, Othman MY, Ruslan MH. Efficiencies and improvement potential of building integrated photovoltaic thermal (BIPVT) system. Energy Conversion and Management 2014; 77: 527-534.
[100]- Akata AMEA, Njomo D, Agrawal B. Assessment of building integrated photovoltaic (BIPV) for sustainable energy performance in tropical regions of Cameroon. Renewable and Sustainable Energy Reviews 2017; 80: 1138-1152.
[101]- Kang J, Kim J, Kim J. Design Elements and Electrical Performance of a Bifacial BIPV Module. International Journal of Photoenergy 2016; 6943936: 1-10. http://dx.doi.org/10.1155/2016/6943936.
[102]- Hezel R. Novel Applications of Bifacial Solar Cells. Progress in photovoltaics: research and applications 2003; 11: 549-556. https://doi.org/10.1002/pip.510.
[103]- Weiss W, Spork-Dur M. Solar Heat Worldwide Edition 2019. AEE – Institute for Sustainable Technologies; 2019. Available from: (https://www.iea-shc.org/Data/Sites/1/publications/Solar-Heat-Worldwide-2019-Summary.pdf). Accessed 19.06.2019.
[104]- Weiss W, Spork-Dur M. Solar Heat Worldwide - Global Market Development and Trends in 2018. IEA Solar Heating & Cooling Programme; 2019. Available from: (https://www.iea-shc.org/Data/Sites/1/publications/Solar-Heat-Worldwide-2019.pdf). Accessed 19.06.2019.
[105]- Endef PV/T manufacturer. Available from: (www.endef.com).
[106]- Setolazar PV/T manufacturer. Available from: (www.setolazar.es).
[107]- Solarus low concentrating PV/T. Available from: (www.solarus.com).
[108]- Absolicon X10 PVT. Available from: (http://www.absolicon.com).

Chapter 3. Experimental performance, modeling validation and dynamic simulation of photovoltaic systems

Throughout the literature reviewed in Chapter 2, the commercial polycrystalline PV, monocrystalline PV and air-based PV/T modules are selected to investigate their energy generation profiles.

This chapter investigates the experimental generation profiles of the selected PV systems and presents the validated PV models using TRNSYS dynamic simulation modelling environment to explore their dynamic performance under different climate conditions. Two approaches to improve the electric power generated from the selected PV modules are investigated. The first approach investigates the effect of coating the polycrystalline PV modules by aluminum nanoparticles on the electricity produced and the panel temperature. The second approach aims to modify the selected monocrystalline PV module to LCPV/T system to obtain high quality thermal energy (fluid stream temperature of up to 90 ° C) with operating the solar cells at favorable temperature. By heating up the useful fluid leaving the PV/T into the linear parabolic concentrator and inserting this combination between V-trough mirrors, this stream could be heated up to 90 °C. Meanwhile, the PV cell temperature is kept below 75 °C. This makes the system useful for operating thermally driven air conditioning. The laboratory test of attaching V-trough mirrors to the PV module, is carried out to identify the most appropriate reflector tilt angle and reflector width. The outdoor test of the developed LCPV/T and the selected PV modules are performed to validate the energy production from the selected PV models. The dynamic simulation of the selected monocrystalline, polycrystalline PV and air-based PV/T modules and the developed LCPV/T is carried out in nine climate conditions. The climate conditions and locations are Mediterranean (Tarragona, Spain), subtropical hot (Cairo, Egypt), tropical rainforest (Colombo, Sri Lanka), moderately continental (Geneva, Switzerland), subtropical hot (Kuwait), humid subtropical (Miami, USA), subarctic (Quebec, Canada) and humid continental (Wiscasset, USA).

3.1 Experimental characterization of the selected photovoltaic systems

The selected commercial PV modules are the polycrystalline PV, monocrystalline PV and air-based polycrystalline PV/T. The experimental set-up of the polycrystalline PV (Eurener-235) module and air-based PV/T (Ecomesh-265) collector which are installed on the roof of a building in Elche, Spain with an inclination angle of 45° and at an azimuth angle 0° (facing the south) is presented. The experimental set-up of the polycrystalline (JAP6-60-270) and monocrystalline (JASOLAR-290) PV modules which are installed on the roof of a building in Cairo, Egypt with an inclination angle of 30° and at an azimuth angle 0° (facing the south) is presented. The performance impact of coating PV module by 5% Al_2O_3 nanoparticles-glycerin based on two typical installed polycrystalline (JAP6-60-270) modules in Cairo, Egypt is investigated. The micro-inverter (Enecsy model: SMI-480W-60-UL) is installed in the experiment set-up in Spain and its power conversion efficiency of 95% is considered in experiment set-up in Cairo.

3.1.1 Characterization of the photovoltaic systems and micro-inverter

The selected commercial PV modules involve the polycrystalline PV (Eurener-235), the polycrystalline PV (JAP6-60-270), the polycrystalline air-based PV/T (Ecomesh-265), and the monocrystalline PV (JASOLAR-290). The technical characteristics of the selected modules at the standard test conditions of irradiance of 1000W/m^2 and cell temperature of 25℃ are presented in Table 3-1.

Table 3-1. Technical characteristics of the selected commercial PV and PV/T modules

Technical characteristics	Polycrystalline PV	Polycrystalline PV	Polycrystalline air-based PV/T	Monocrystalline PV
PV Model	Eurener-235	JAP6-60-270	Ecomesh-265	JASOLAR-290
$P_{PV,Peak}$ (W)	235	270	265	290
A_{PV} (m^2)	1.65	1,64	1.62	1,64
η_e (%)	14.08	16.28	16.61	17.5
I_{SC} (A)	8.40	9.15	9.06	9.57
V_{OC} (V)	37.32	38.27	38.58	39.46
I_{peak} (A)	7.83	8.65	8.40	9.12
V_{peak} (V)	30.07	31.23	31.65	31.80

The specifications of the micro-inverter (Enecsy model: SMI-480W-60-UL) are shown in Table 3-2.

Table 3-2 Technical specifications micro-inverter model (SMI-480W-60-UL)

Micro-inverter (SMI-480W-60-UL)	Unit	Value
Nominal input power	W	480
Maximum/minimum DC input voltage	V	44/20
Maximum output power	W	450
Nominal AC output current	A	1.88
Nominal output voltage	V	240
Peak Efficiency	%	94.5
Power factor	-	> 0.95

3.1.2 Experimental set-up of the photovoltaic and photovoltaic/thermal modules

The purpose of this experiment is to obtain the daily generation profile (electric and thermal power generated) from the PV panel along with the irradiance, module temperature, ambient air humidity and ambient air relative humidity. The experimental set-up of the polycrystalline PV (Eurener-235) module and air-based PV/T (Ecomesh-265) collector which are installed on the roof of a building in Elche, Spain with an inclination angle of 45° and at an azimuth angle 0° (facing the south) is presented.

The shunt resistors are used to measure the electrical power converted to electricity by the PV panels. The pyranometer (model 6B manufactured by KIPP & ZONEN) is used to measure the incident solar radiation for one-year monitoring at inclination angle of 45°C, azimuth of 0° (facing the same direction as the PV) and it has the measurement errors of 1%. A data acquisition (Hewlett Packard 34972A Agilent) unit is used to monitor multiple signals (temperatures, voltage, frequency) during the test period (see Figure 3-1). The low-cost microcontroller Arduino data logger is installed to monitor the outdoor humidity and air temperature using the DHT11 sensor and to measure the PV back surface temperature and the air temperature leaves the PV/T collector using DS18B20 sensors.

(a)

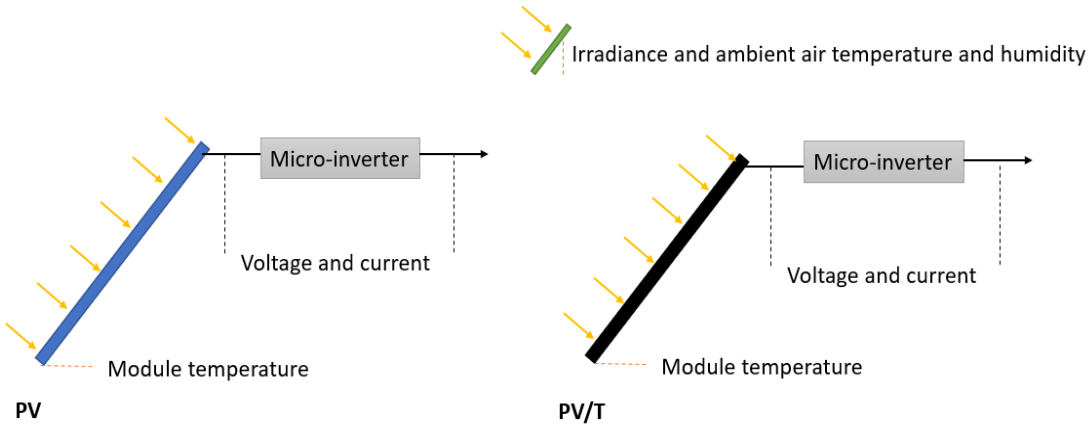

(b) (c)

Figure 3-1. a) Experiment layout of the PV and air-based PV/T modules in Spain; b) schematic of experiment outputs from the PV; and c) schematic of experiment outputs from the PV/T.

3.1.3 Experimental set-up of polycrystalline and monocrystalline photovoltaic modules

The purpose of this experiment is to obtain the daily generation profile from the PV panel along with the irradiance, module temperature, ambient air humidity and ambient air relative humidity. The selected polycrystalline (JAP6-60-270) and monocrystalline PV modules (JASOLAR-290) are tested in Cairo, Egypt with an inclination angle of 30° and at an azimuth angle 0° (see Figure 3-2). The micro-inverter efficiency of 95% is considered in this experiment. The preparation of Al_2O_3 nanoparticles for coating the PV surface is performed on two identical polycrystalline PV modules (JAP6-60-270).

(a)

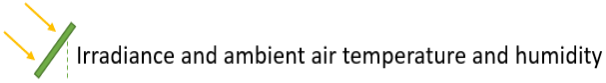

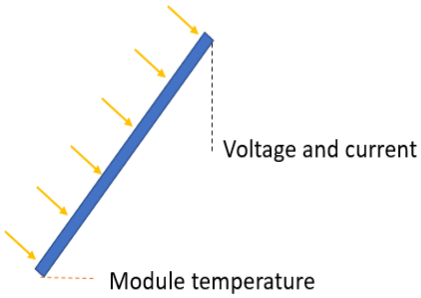

Monocrystalline PV modules

(b)

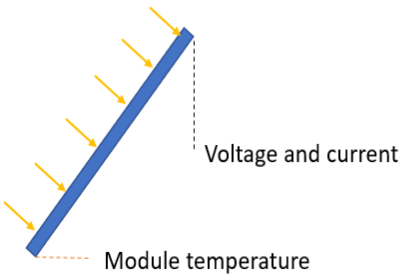

Polycrystalline PV modules

(c)

Figure 3-2. a) Outdoor test of the polycrystalline and monocrystalline PV modules in Cairo; schematic of experiment outputs from b) the monocrystalline PV; and c) the polycrystalline PV.

The PV panel voltage, current, efficiency and solar radiation are obtained by a solar system analyzer (Prova-1011). This PV analyzer features a remote solar detector connected by Bluetooth wireless for irradiance measurement. The electric specifications of this PV analyzer are shown in Table 3-3 for the ambient temperature of 23°C±5°C and irradiance ≥ 800 W/m².

Table 3-3. Main electric specifications of the PV analyzer (Prova-1011)

Prova-1011	Range	Resolution	Accuracy
DC Voltage measurement	1 - 1000 V	0.01V / 0.1V / 1V	±1% ± (1% of V_{oc} ± 0.1V)
DC Current measurement	0.1 - 12 A	1mA / 10mA	±1% ± (1% of I_{sc} ± 9mA)
DC Current simulation	0.1 - 12 A	1mA / 10mA	±1% ± 9mA
Irradiance measurement	0 - 2000 W/m²	1 W/m²	± 3 % ± 20 dgts

The performance comparison of PV module before and after cleaning is conducted. The two monocrystalline PV modules (JASOLAR-290) are used in this test under the same outdoor conditions. One panel is maintained without cleaning for 7 days and the second has been cleaned.

3.1.4 Preparation of aluminum nanoparticles for coating the polycrystalline module

The purpose of this experiment is to explore the effect of coating the PV module by Al_2O_3 nanoparticles on the power generated and module temperature as a function of the time. The polycrystalline module is coated by Al_2O_3 nanoparticles with a diameter of 40 nm is mixed with the liquid glycerin of 60 ml for a volumetric concentration of 5%. The investigation is performed on two typical polycrystalline modules (JAP6-60-270). A brush is used to coat one panel and the second is maintained without coating (see Figure 3-3).

(a)

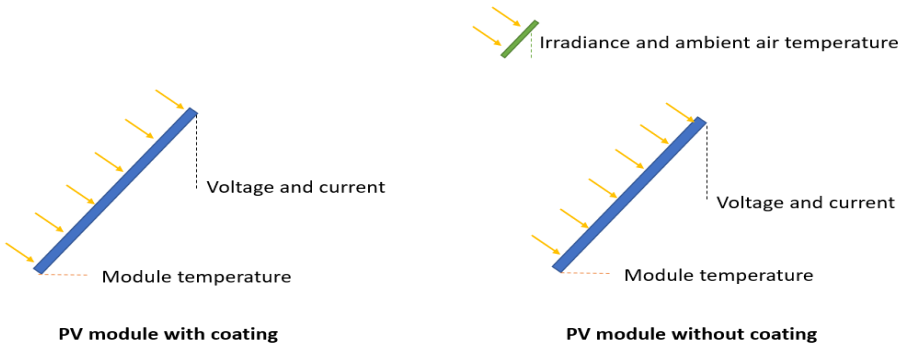

(b) (c)

Figure 3-3. a) Coating the polycrystalline module by 5% Al_2O_3 nanoparticles-glycerin; schematic of experiment outputs from b) the coated PV; and c) the PV without coating.

3.2 The proposed low-concentrated photovoltaic/thermal system

This section aims to modify the selected commercial monocrystalline PV module (Table 3-1) to the water-based LCPV/T system based on the literature reviewed in chapter 2. The main purpose of this design configuration is to obtain high quality thermal energy (fluid stream temperature of up to 90 ° C) with operating the solar cells at favorable temperature. By heating up the useful fluid leaving the PV/T into the linear parabolic concentrator and inserting this combination between V-trough mirrors, this stream could be heated up to 90 °C. Meanwhile, the PV cell temperature is kept below 75 °C. This makes the system useful for operating thermally driven air conditioning. The laboratory test of attaching V-trough mirrors to the PV module, is carried out to identify the most appropriate reflector tilt angle and reflector width. The outdoor test of the developed LCPV/T and the selected PV module are performed to their energy production at the same operation conditions. The effect of modifying the selected PV module to water-based LCPV/T is performed outdoors on two identical monocrystalline PV modules (JASOLAR-290) and laboratory tested using three identical small polycrystalline PV modules in Cairo, Egypt.

3.2.1 Laboratory test of V-trough concentrated photovoltaic system

The aim of this laboratory test is to ensure the impact of attaching mirrors to the PV module and define the most appropriate reflector tilt angle. In the laboratory test, the PV module of 0.17 m^2 is inserted between 2 mirrors (0.18 m^2 each mirror) and with a reflector tilt angle of 60° from the horizontal of the PV surface (vertex angle 30°). The technical characteristics of the small 20 W polycrystalline are described in Table 3-4. The three identical small polycrystalline PV modules represents PV without reflector, PV with one-reflector an PV with V-trough reflector. The distance between the PV panel and the solar simulator is 70 cm for the three modules (see Figure 3-4).

Table 3-4. Technical characteristics of the 20 W polycrystalline laboratory PV module

PV module laboratory tested	Unit	Value
Module dimensions (L×W)	mm×mm	495 × 350
Nominal power	W	20
Rated voltage	V	17.5
Rated current	A	1.14
Open-circuit voltage	V	21.9
Short circuit current	A	1.22

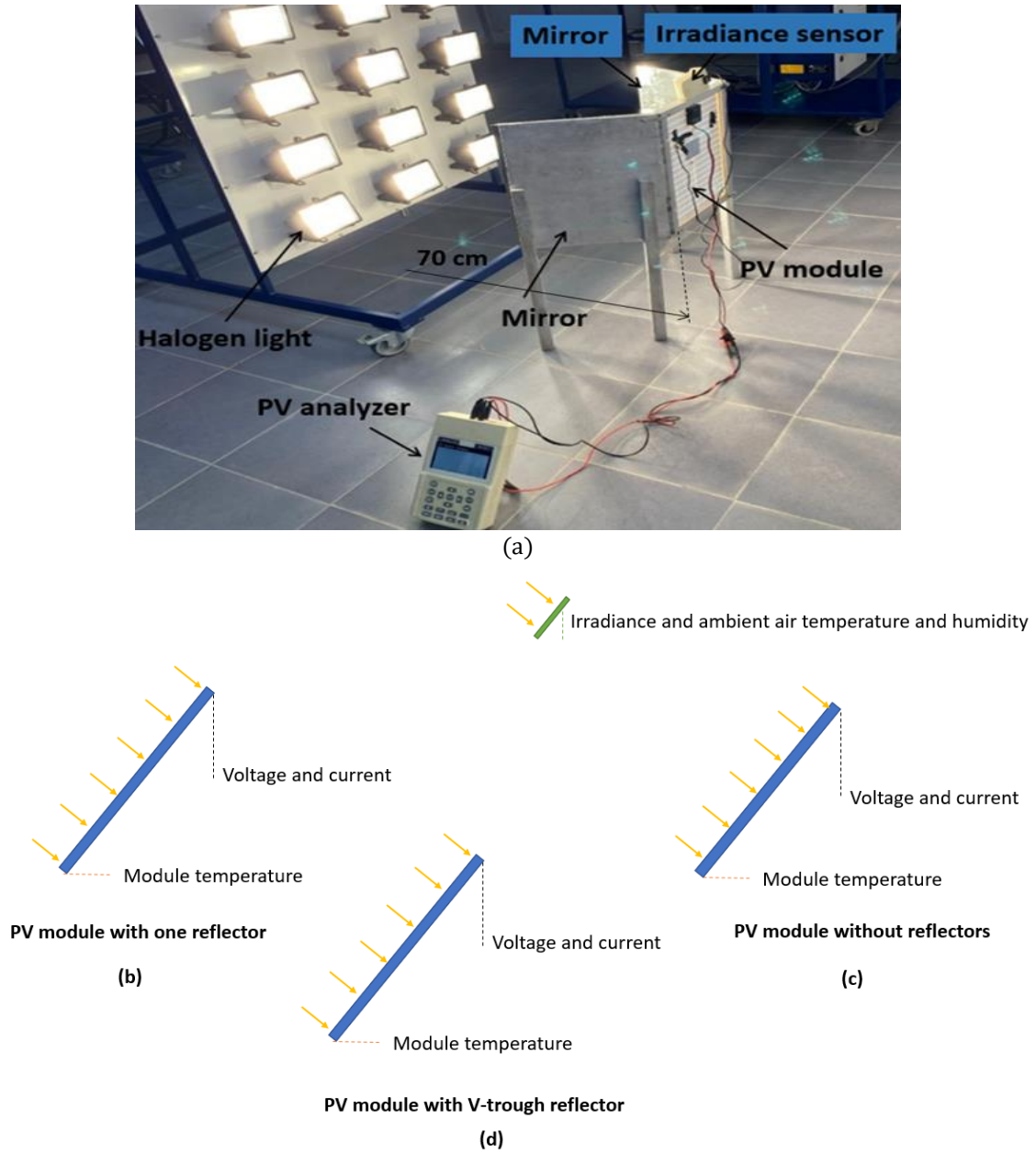

Figure 3-4. a) The laboratory test of the small PV module fitted with V-trough concentrator; experiment outputs from b) PV with one mirror; b) PV without mirrors and c) PV with V-trough.

3.2.2 Design and implementation of low-concentrated photovoltaic/thermal system

For the proposed design of the LCPV/T system, the JASOLAR-290 monocrystalline PV module with an area of 1.64 m^2 (1.65 ×0.99) is modified to LCPV/T (see Figure 3-5). This LPV/T system consists of two flat reflectors fixed on the PV module and placed as a V letter. The PV module is cooled using the sheet-and-tube heat exchanger beneath the module. The heat exchanger is used to cool the PV modules and preheat the water before entering the concentrated linear parabolic. The geometric concentration ratio of the LCPV/T is 2 for the V-trough reflector and 6 for the linear parabolic concentrator. Each mirror attached to the receiver frame using 2 hinges with locker to investigate the reflector inclination angle. This LCPV/T features a better thermal performance by using a red

copper HX instead of aluminum HX. The thermal conductivity is around 210 W/m·K for the aluminum and 400 W/m·K for the copper.

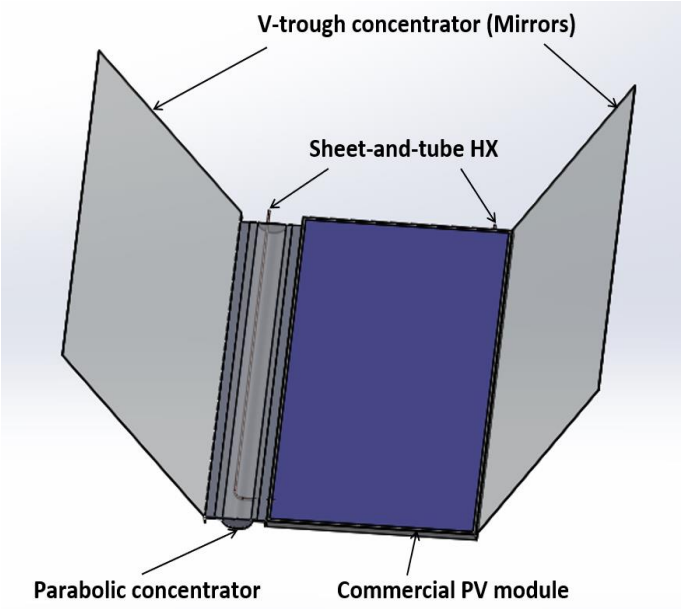

Figure 3-5. Schematic 3-D modelling of the proposed LCPV/T system.

The sheet-and-tube heat exchanger is made of copper with a pipe diameter 8 mm and sheet thickness of 1 mm and has an area of 1.38 m^2 with a bended coil of 17 identical tubes. The tubes are bonded to the absorber plate using horizontal fillet lead with 2 mm bond width arc. Figure 3-6.a shows the dimension in mm of the designed heat exchanger beneath the PV module linked with the pipe extended in linear parabolic concentrator. Figure 3-6.b shows the dimension in mm of the designed linear parabolic where the copper pipe from the PV/T is passed in a high absorptive coating with a thickness of 1 mm. Figure 3-6.c shows the attaching of the heat exchanger beneath the commercial PV modules. The direct contact technique is used along with a wood frame of 3 mm thickness that presses the sheet-and-tube HX beneath the PV module and fixed into the aluminum frame. Figure 3-6.d shows the concentrated parabolic (150 cm length and 12 cm aperture width) attached to the PV module and the heat exchanger. The serpentine copper tube beneath the PV goes into the parabolic concentrator made of 2 mm stainless steel coated with silver for heat upgrading under the V-trough concentrator. Also, a 4 mm glass sheet is used to close the aperture opening and the reflectors are adjusted at a reflector tilt angle (θ_R). The modified LCPV/T is installed on the roof of a building in Cairo, Egypt with an inclination angle of 30° and at an azimuth angle 0°. The main parameters of the developed LCPV/T are shown in Table 3-5.

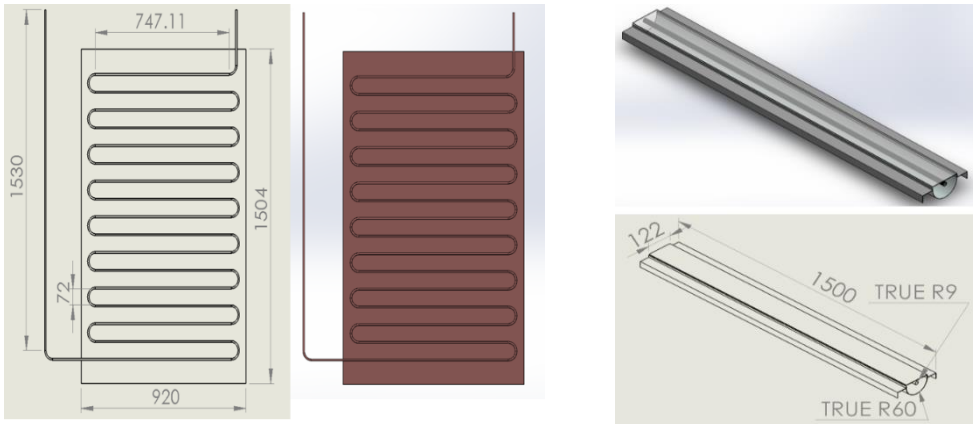

(a) (b)

(c) (d)

Figure 3-6. Description of the proposed LCPV/T system: a) sheet-and-tube HX; b) linear parabolic; c) manufacturing and assembling; and d) implementation.

Table 3-5. Main parameters of the developed LCPV/T unit

Parameters of the LCPV/T	Unit	Value
Length of fluid channel	m	14.5
Diameter of fluid channel	mm	8
Number of tubes bonded to the absorber	-	17
Bond width	mm	2
Fluid thermal capacitance	kJ/(m.k)	4.19
Area of PV module	m^2	1.64
PV efficiency at STC	%	18
Thickness of photovoltaic cells	mm	2
Thermal conductivity of copper	W/(m.k)	403
Concentration ratio of V-trough	-	2
Concentration ratio of linear parabolic	-	6

3.2.3 Experimental set-up of low-concentrated photovoltaic/thermal system

The purpose of this experiment is to obtain the daily generation profile (electric and thermal power generated) of the LCPV/T system to provide a validated model that will be simulated in different climate conditions. The new LCPV/T design configuration aims to obtain high quality thermal energy (fluid stream temperature of up to 90 ° C) with operating the solar cells at favorable temperature. This makes the system useful for operating thermally driven air conditioning. By varying the reflector tilt angle from 30° to 80° from the PV surface, the most appropriate angle is defined. This outdoor test is performed on Two typical monocrystalline modules (Table 3-1), the first one is modified to the proposed design of LCPV/T system and the second one does not present any modifications.The selected monocrystalline module and the developed LCPV/T are installed on the roof of a building in Cairo, Egypt to investigate the effect of modifying the PV module to the designed LCPV/T system (see Figure 3-7).

The PV panel voltage, current, efficiency and solar radiation are obtained by a solar system analyzer (Prova-1011). The micro-inverter efficiency of 95% is considered in this experiment. The ambient air temperature, ambient humidity, water mass flow, fluid entering temperature, fluid leaving temperature are measured and recorded in real-time using an Arduino data logger. The Arduino Mega 2560 is a low-cost microcontroller board with 54 digital input/output pins, 16 analog inputs and 4 serial ports. The Arduino was powered via a USB regulator of 5 V.

The fluid mass flow rate is controlled using a valve before the pump and is measured using YF-S402 flow meter before entering the tank of 50 liters. For the developed LCPV/T, the water flow rate is adjusted at 0.5 l/min. The fluid temperature entering the LPV/T is measured using temperature sensor (T1), the fluid temperature leaving the PV/T and entering the linear parabolic concentrator is obtained by temperature sensor (T2) while, the fluid temperature leaving the CPV/T is measured by temperature sensor (T3) (see Figure 3-7).

The hardware of this Arduino datalogger with monitoring sensors is described as it follows:

- The SD shield is connected to a mega Arduino microcontroller via the connection of CS to D53, SCK to D52, MOSI to D51, and MISO to D50 on the Arduino.
- The air temperature and humidity are detected by using the DHT11 sensor that contains two measurement components for humidity and temperature. The DHT11 sensor includes four pins. The 1st pin is connected to +5V on the Arduino, the 2nd pin is connected to D8 on the Arduino, the 3rd pin is a free pin without connection, and the 4th pin is connected to Arduino GND. A 4.8K pull-up resistor is also linked between VDD and the 2nd pin.
- The water temperature is measured by using a waterproof DS18B20 sensor that provides 9-bit to 12-bit Celsius temperature measurements in the preferable temperature range of -55 to 125 °C. As such, the sensor cable ends in three junctions. The GND pin of the DS18B20 digital thermometer connects to the Arduino GND, the VDD pin of the DS18B20 connects to the Arduino +5V, the Data pin of the DS18B20 is connected to the D3 pin on the Arduino, and a pull-up resistor of 4.7 KΩ is linked between the VDD and data pins. Another two DS18B20 water temperature sensors are connected and their data pin are connected to D4 and D5 on the Arduino.

- The water flow meter YF-S402 is interfaced with the Arduino via 3 pins. The GND pin of the YF-S402 connects to the Arduino GND, the VDD pin of the YF-S402 connects to the Arduino +5V, the Data pin of the YF-S402 is connected to the D2 pin on the Arduino. The Arduino is powered by a 5V USB. The main characteristics of the flow meter are shown in Table 3-6.

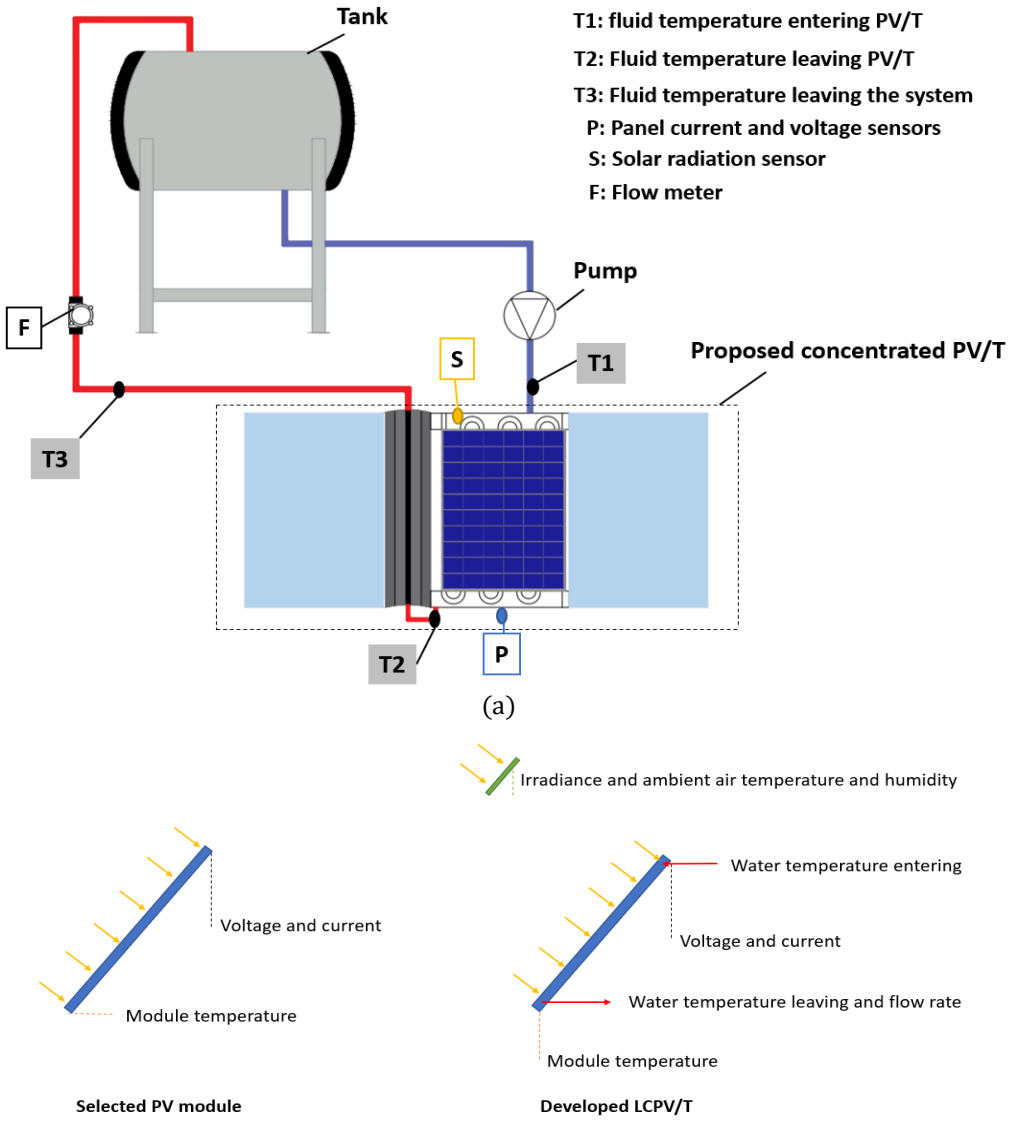

Figure 3-7. a) Experimental set-up of the designed LCPV/T system; schematic of experiment outputs from b) the selected PV module; and c) the modified PV to LCPV/T system.

Table 3-6. Main specifications of the water flow meter (YF-S402)

YF-S402-flow meter	Unit	Value
Operating voltage	V (DC)	3.5-24
Operating flow rate	l/min	0.3-6
Maximum temperature	°C	120
Error percentage	%	± 2
Water pressure	MPa	≤0.8

3.3 Experimental profiles of the selected and developed photovoltaic systems

This section illustrates the experimental profiles of the PV and PV/T that presented in section 3.1, and the developed low-cost LCPV/T system that presentenced in section 3.2. The experiments of the PV systems (PV, PV/T and LCPV/T) have been performed in the Spain and Cairo climate locations. The experimental performance of the polycrystalline PV (Eurener-235) module and air-based PV/T (Ecomesh-265) collector has been registered for typical days in Spain. The experimental performance of the polycrystalline (JAP6-60-270) and monocrystalline (JASOLAR-290) PV modules and the modified installed PV to LCPV/T has been registered for typical days in Egypt. Firstly, the solar radiation on the PV surface monitored for one year in two climates is presented. Secondly, the hourly electricity generation from the polycrystalline module and the natural ventilated air-based collector registered in Spain is presented. Thirdly, the hourly electricity generation from the polycrystalline and monocrystalline PV modules with the same module area registered in Egypt is presented. Fourthly, the impact of coating the PV surface by Al_2O_3 nanoparticles based on two typical polycrystalline modules (JAP6-60-270) is evaluated. Fifthly, the effect of modifying the selected PV module to LCPV/T system based on two typical monocrystalline modules (JASOLAR-290) is presented, the first one is modified to the proposed design of LCPV/T system and the second one does not present any modifications. The experimental evaluation of the proposed design (section 3.2) of the LCPV/T (including laboratory tests and real outdoor conditions) is presented.

3.3.1 Mean daily tilted radiation in Spain and Egypt based on one-year monitoring

The solar radiation on the collector surface has been monitored for one year in Spain and Egypt. Figure 3-8 shows the mean daily solar radiation on the PV surface for the recorded data of 2018-2019 in Elche, Spain and 2019-2020 in Cairo, Egypt.

Results show that the maximum mean daily radiation on the PV surface is 6.7 kWh/m² in Spain and 7.2 kWh/m². The average mean daily radiation on the PV surface is 5.6 kWh/m² in Spain and 6.2 kWh/m² in Egypt.

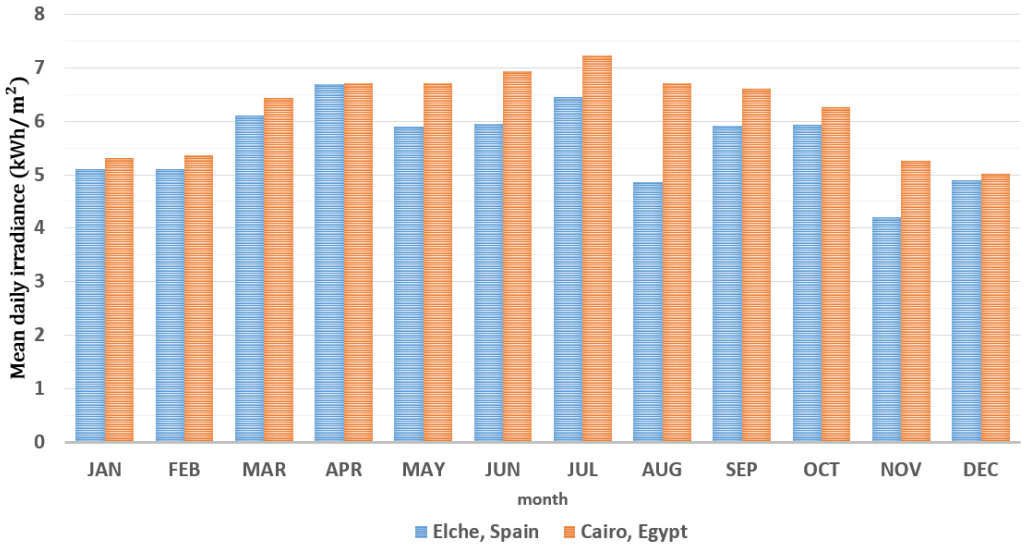

Figure 3-8. Mean daily tilted solar radiation on the PV surface in Elche (Spain) and Cairo (Egypt).

The yearly solar radiation on the collector surface is around 3.1 MWh/m² in 2018-2019 for Spain and 3.5 MWh/ m² in 2019-2020 for Egypt.

3.3.2 Daily generation profiles of polycrystalline photovoltaic and photovoltaic/thermal

The hourly performance of the 235 W polycrystalline module (Eurener-235) and the 265 W natural ventilated air-based collector (Ecomesh-265) (section 3.1.2) is shown in Figure 3-9. The readings are registered based on a time step of 1 minute in a typical day.

Results show that the daily energy generation is 1.6 kWh for natural ventilated air-based PV/T and 1.2 for the polycrystalline module under the same climate conditions in Elche, Spain.

The performance of the 265 W natural ventilated air-based PV/T collector (Ecomesh 265) is investigated in another typical day (see Figure 3-10). Figure 3-10 illustrates the ambient humidity and temperature, solar radiation, electricity produced and the measured temperature beneath the natural ventilated air-based polycrystalline PV/T module (Ecomesh 265). The readings are registered based on a time step of 30 minutes.

Results showed that the daily electricity generated from one natural ventilated air-based PV/T collector (Ecomesh 265) is 1.56 kWh and the daily solar radiation on the PV surface is 6.78 kWh/m² (daily electric efficiency of 14%) in the typical day of 21/02/2019. The maximum temperature measured beneath the PV panel of the natural ventilated air-based PV/T collector (Ecomesh 265) is 56 °C at maximum tilted radiation of 1085 W/m². The maximum and minimum ambient air temperature are 26 °C and 9 °C. However, the minimum temperature measured beneath the PV panel of the natural ventilated air-based PV/T collector (Ecomesh 265) is 5.5 °C at night.

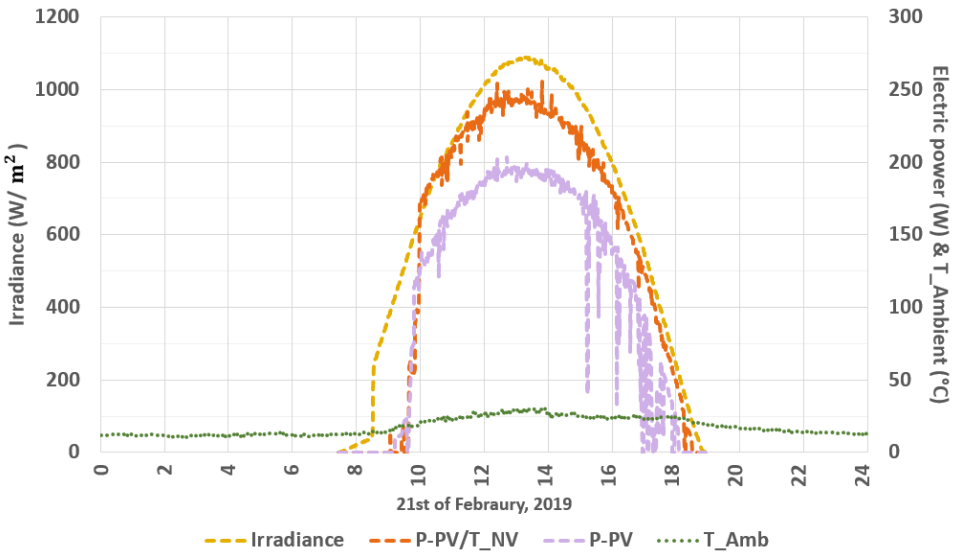

Figure 3-9. Electric power generated from the 235 W polycrystalline PV module and the 265 W natural ventilated air-based PV/T collector in Spain.

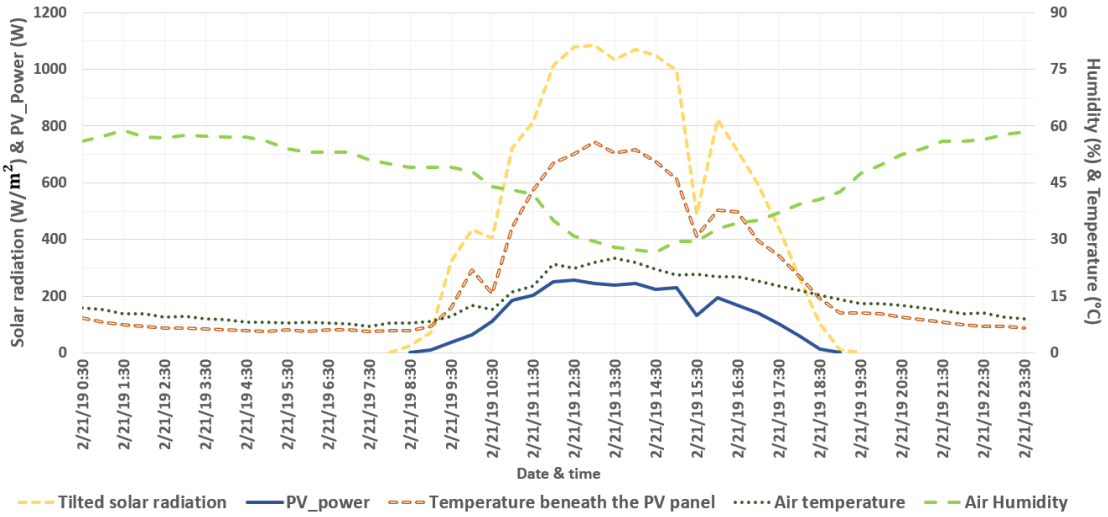

Figure 3-10. Temperature beneath PV panel of the 265 W natural ventilated air-based PV/T collector in Spain.

The temperature fluctuation by using the air-based PV/T is so high. The outlet air temperature from the PV/T has limited applications. The precise control is required for a forced ventilation and sometimes when the irradiance and ambient temperature are low, the air could be cooled instead of being heated.

3.3.3 Performance of polycrystalline and monocrystalline systems

Figure 3-11 shows the performance of the polycrystalline (JAP6-60-270) and the monocrystalline PV modules (JASOLAR-290) with the same module area in Cairo, Egypt (section 3.1.3).

Results show that the maximum solar conversion efficiency is 13.1% for the monocrystalline PV modules (JASOLAR-290) and 12.3% for the polycrystalline (JAP6-60-270). The minimum solar conversion efficiency is 7.3% for the polycrystalline (JAP6-60-270) and 7.5% for the monocrystalline PV modules (JASOLAR-290).

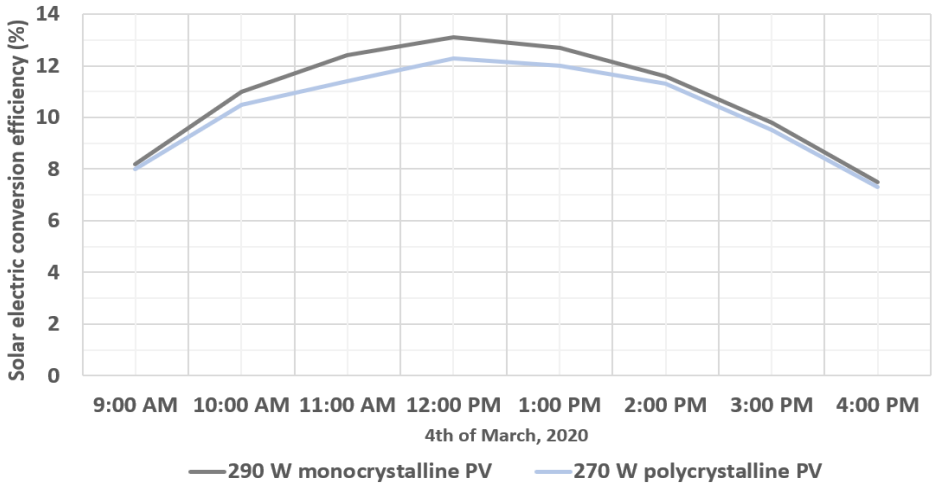

Figure 3-11. Solar conversion efficiency (%) of the polycrystalline and monocrystalline PV modules with the same area in Cairo, Egypt.

Also, results show that the maximum solar conversion efficiency of the monocrystalline PV module (JASOLAR-290) is 13.1% for the cleaned module and 11% for the soiled module under the same ambient conditions (See Figure 3-12). The mean ambient temperature was around16 °C during the test day.

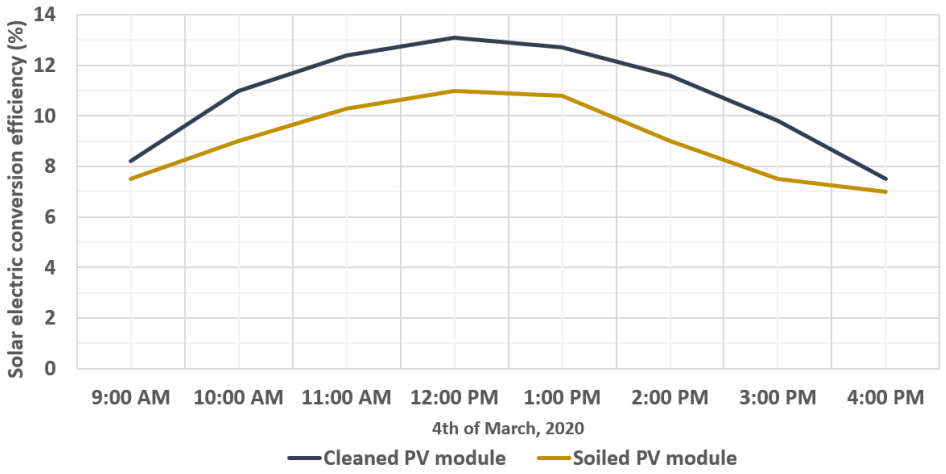

Figure 3-12. Solar conversion efficiency (%) of the soiled and cleaned monocrystalline PV modules.

The monocrystalline PV module produces more electricity compared to the polycrystalline module with the same module area and under the same operation conditions. The monocrystalline PV module improves the solar electric conversion efficiency by almost 1% compared to the polycrystalline module. By cleaning the monocrystalline PV surface, the electric conversion efficiency is improved by almost 2%.

3.3.4 Impact of coating the PV surface by Al_2O_3 nanoparticles

The effect of coating the PV surface by Al_2O_3 nanoparticles on the module temperature and electric power produced (section 3.3.4) is shown in Figure 3-13. This experiment is performed on two identical selected polycrystalline (JAP6-60-270) modules under the same conditions. The module temperature and electric efficiency of the first PV module with Al_2O_3 coating are represented by (T-PV-C_ Al_2O_3) and (EFF-C_ Al_2O_3), respectively. The module temperature and electric efficiency of the second PV module without coating are represented by (T-PV-NC) and (EFF-NC), respectively. During the first day after adding the Al_2O_3 coating, the efficiency of the module is improved from 12.97% to 13.79% and the module temperature is reduced from 43.9 to 41.1. However, after 6 days the electric efficiency is only improved from 12.63% to 12.65% and the module temperature is only reduced from 36.7 to 36.6 at the same outdoor test conditions in Cairo, Egypt.

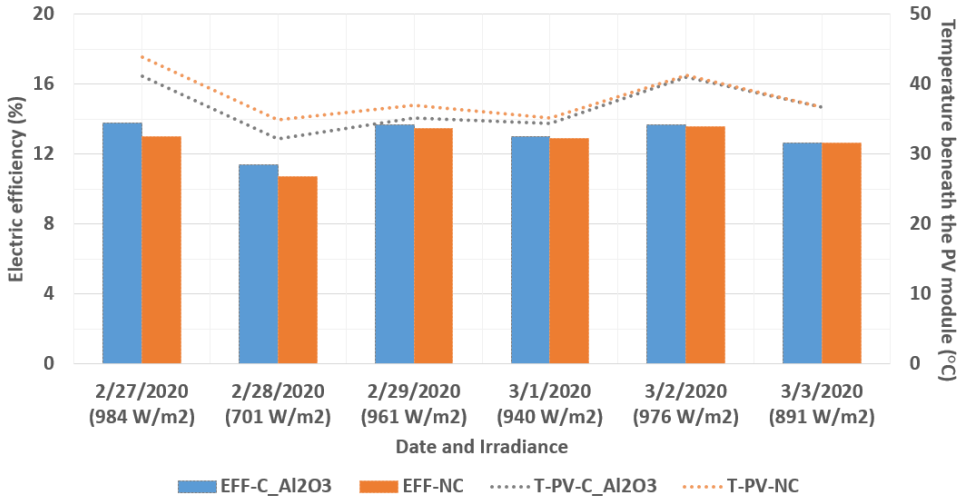

Figure 3-13. Variation of module temperature and electric efficiency of PV module with Al_2O_3 coating and the no coating (NC) module in function of the solar radiation and coating days.

Coating the PV modules by Al_2O_3 nanoparticles-glycerin is improving the electric power generation from the PV module with reducing the module temperature. However, the impact of coating the PV module by Al_2O_3 nanoparticles-glycerin remains for limited time and get reduced with the time. The electric efficiency of the polycrystalline PV module is improved by almost 1% after coating its surface by Al_2O_3 nanoparticles-glycerin. However, after 6 days the electric efficiency is almost the same compared to the PV module without coating.

3.3.5 Daily generation profile of the developed low-concentrated photovoltaic/thermal system

The indoor performance of the small PV module (0.17 m^2) in different situations under the laboratory test (section 3.2.1) is 7.6% for module without mirrors, 9.1% for module with one mirror and 9.9% for module with V-trough mirrors (see Table 3-7). The ambient temperature was around 16 °C during the test.

Table 3-7. Electric efficiency of the small PV module with V-trough mirrors (laboratory test)

PV module configurations	Electric efficiency (%)
PV module without mirrors	7.6
PV module with one mirror	9.1
PV module with V-trough mirrors	9.9

The outdoor performance of the modified monocrystalline PV module (JASOLAR-290) with an area of 1.64 m^2 to the LCPV/T with an area of 3.9 m^2 (section 3.2.2) is investigated in Cairo, Egypt. By varying the reflector tilt angle from 30° to 80° from the PV surface, the maximum fill factor and solar electric conversion efficiency is achieved at angle 60°. The maximum panel electric efficiency of 16.69% is measured at angle 60°. The minimum fill factor and PV electric efficiency is measured at angle 30°.

The performance of two typical monocrystalline (Table 3-1) PV modules, the first one is modified to the LCPV/T system (section 3.2.2) and the second one does not present any modifications are compared.

Results show that the minimum and maximum electric efficiencies are 12.68% and 17.27% for LCPV/T and 11.91%- 13.72% for the PV panel, respectively in a typical day. The highest electric improvement is about 3.6% for 60 min. From 10 am to 4 pm, the maximum electric power is 295.2 W for the LCPV/T system and 217.7 W for the PV panel, the electric energy produced is 1.51 kW for the LCPV/T system and 1.12 kW for the PV panel (see Figure 3-14). The maximum tilted radiation on the PV panel surface without reflector in this typical day is 980 W/m^2.

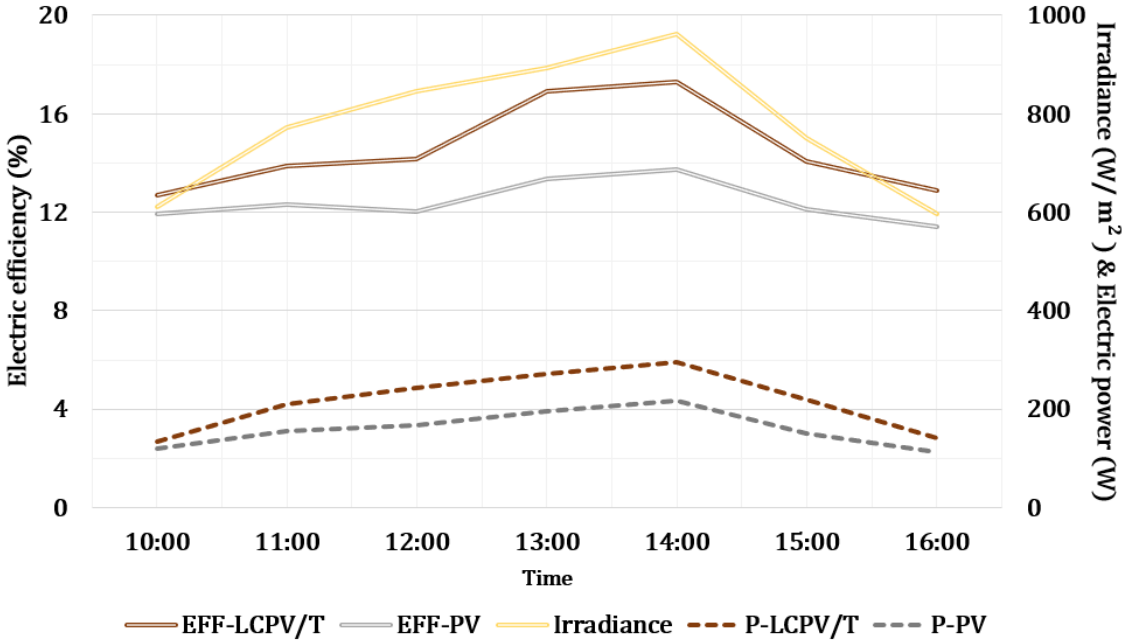

Figure 3-14. Variation of PV and LCPV/T efficiencies and irradiance and electric power in function of the hourly sunlight in Cairo, Egypt.

The hourly solar conversion efficiency of the selected monocrystalline PV module and the modified monocrystalline module to water based LCPV/T system are shown in Table 3-8.

Table 3-8. Electric efficiency of the monocrystalline PV module and the modified one to LCPV/T

Electric efficiency (%) Hourly (6/3/2020)	Selected monocrystalline PV	Modified monocrystalline to LCPV/T
10:00 AM	11.9	12.7
11:00 AM	12.3	13.8
12:00 PM	12.0	14.2
1:00 PM	13.4	16.9
2:00 PM	13.7	17.3
3:00 PM	12.1	14.1
4:00 PM	11.4	12.9

For another typical day in March with the maximum irradiance of 931 W/m² (measured at point above the PV panel without reflector) and ambient temperature (TA) of 25.5 °C, the maximum outlet temperature leaving the LCPV/T (T3) is 66.3 °C and fluid temperature recovered from the PV panel (T2) is 54.6 °C when the inlet water temperature (T1) is 23.2 °C and the water flow rate is 0.5 l/min (see Figure 3-15). The average thermal efficiency of the LCPV/T system is around 48%. The maximum thermal power of the LCPV/T is around 1.5 kW_t.

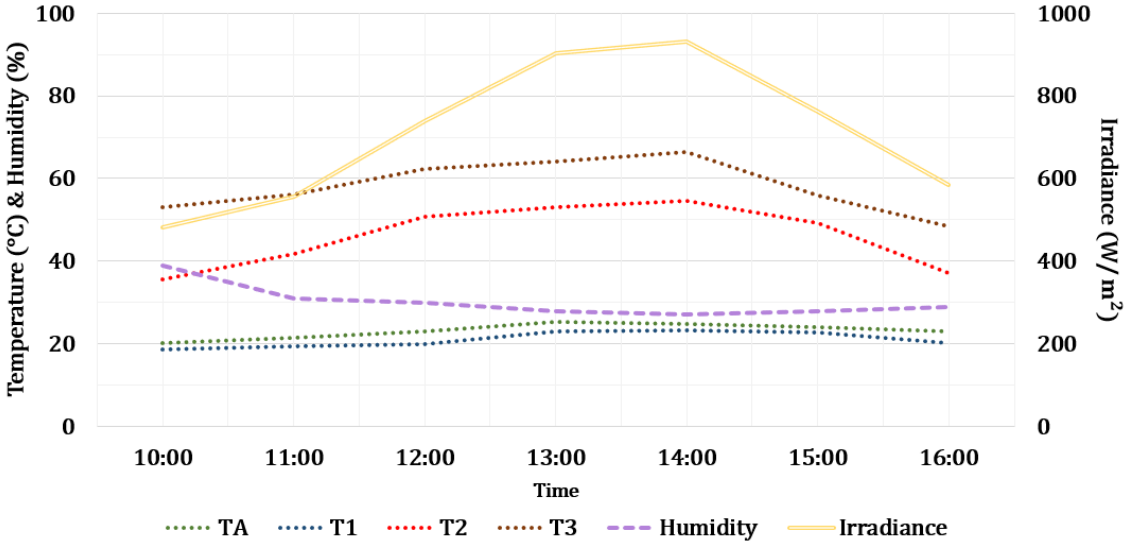

Figure 3-15. Temperatures of water entering the heat exchanger below the PV panel (T1), fluid entering the linear parabolic (T2) and fluid leaving the LCPV/T (T3), and ambient temperature (TA), humidity and irradiance in Cairo, Egypt.

The thermal performance of the developed water based LCPV/T is shown Table 3-9 with illustrating the water entering the heat exchanger below the PV panel (T1), fluid entering the linear parabolic (T2) and fluid leaving the LCPV/T (T3).

Table 3-9. Temperatures at three point on the developed water based LCPV/T system

Temperature (°C) Hourly (8/3/2020)	Fluid entering the LCPV/T (T1)	Fluid entering the linear parabolic (T2)	Fluid leaving the LCPV/T (T3)
10:00 AM	18.7	35.7	53.1
11:00 AM	19.5	41.8	56.2
12:00 PM	19.8	50.6	62.4
1:00 PM	23.1	53.1	64.1
2:00 PM	23.2	54.6	66.3
3:00 PM	22.8	49.2	55.8
4:00 PM	20.1	37.1	48.5

The electric efficiency of the selected monocrystalline PV after the modification to LCPV/T system is improved by almost 3.6% with the water flow rate of 0.5 l/min. the temperature lift in the LCPV/T is around 43 °C. The developed LCPV/T is able to operate thermally driven air conditioning at a

temperature level of 75-88 °C. The main characteristics of the LCPV/T based on the experiments are shown in Table 3-10 at ambient temperature of 26 °C and irradiance of 980 W/m^2.

Table 3-10. Main characteristics of the developed LCPV/T system

LCPV/T characteristics	Unit	Value
Nominal electric efficiency	%	17.8
Nominal thermal efficiency	%	50.2
Water flow rate	l/min	0.5
Inlet water temperature	°C	20.4
LCPV/T total area	m^2	3.91
PV module area	m^2	1.64
Nominal electric power	W	410
Nominal thermal power	kW	1.86

3.4 Modeling of energy performance of photovoltaic systems

This section incorporates the Transient System Simulation (TRNSYS) [1] environment that assesses the dynamic performance of the PV modules, PV/T collectors and the developed LCPV/T system based on the data sheet provided by the manufacture and the investigated performance of photovoltaic systems. The registered solar radiation, ambient temperature and ambient humidity from the experiments are introduced to the TRNSYS environment to validate the experimental energy generated from the polycrystalline and polycrystalline PV modules, air-based PV/T collector and the developed LCPV/T with simulated energy generated from the PV, PV/T and LCPV/T models. The irradiance, ambient temperature, fluid inlet temperature and fluid flow rate are introduced as input variables to the model to calculate the output current, voltage, fluid outlet temperature and useful thermal energy.

3.4.1 Photovoltaic modules

There are many different approaches to model PV systems. A PV panel has a very distinct current- voltage curve that needs to be accounted for when modeling the PV system.

This I-V curve has three distinct points of interest which can be used in modeling to calculate parameters (diode reverse saturation current, module photocurrent module, series resistance, module shunt resistance, modified ideality factor) of the dynamic model (TRNSYS, TYPE 194). The first point is the short circuit current point, at which the voltage is zero and the current is equal to the short circuit current (I_{SC}). The second point of interest is the Maximum Power Point (MPP). At this point the maximum power is generated by the PV panel. The current has a value of I_{MPP} while the maximum voltage is V_{MPP}. The third of interest is an open circuit voltage point in which the current is zero and the voltage is at open current voltage. Each of these voltages and currents are distinct to the particular PV array and are detailed on the manufacturer's data sheet. Some equivalent circuits have been proposed to characterize the non-linear behavior of crystalline silicon PV. Some authors suggest

using a two-diode model due to the good results attainable even in low light conditions, but it requires the extraction of seven parameters and the use of two exponential terms. The one-diode two-resistance model, commonly known as the five-parameters model, is currently the most diffuse option for PV simulations due to a very good accuracy in most environmental conditions, avoiding the extraction of two parameters respect to the two diodes models, and fast and robust convergence of the algorithms.

The model of Type 194 is based on the five-parameter equivalent circuit model (see Figure 3-16), it will be used for modelling poly- and mono- crystalline silicone PV modules to validate their performance and simulate their models under different situations.

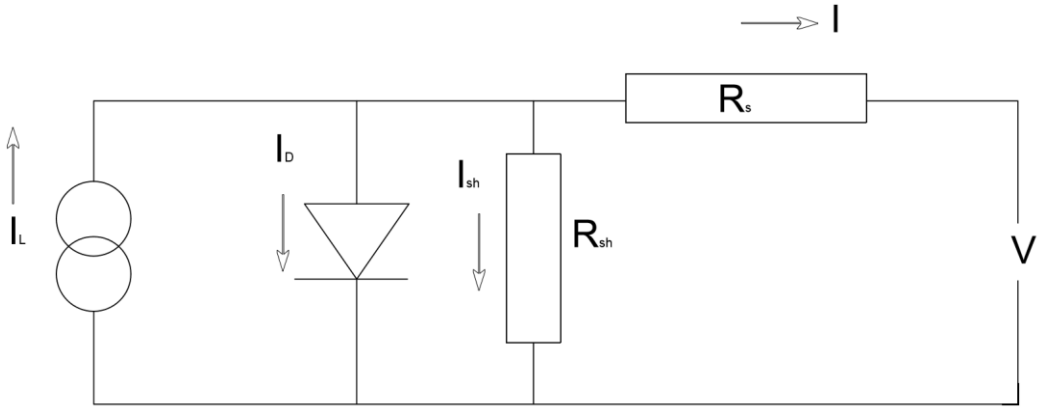

Figure 3-16. The five-parameter equivalent circuit model of PV panel.

The variation of irradiance and PV cell temperature changes the current-voltage (I-V) characteristics. The TRNSYS dynamic PV model calculates the current-voltage curve as a function of the environmental conditions based on the five parameters that are obtained from the nominal operation conditions provided by the manufacturer (see Table 3-11).

The current-voltage equation for the circuit is shown in Figure 3-16 and described by Equation 3-1:

$$I = I_L - I_o\left[e^{\frac{V+IR_s}{a}} - 1\right] - \frac{V+IR_s}{R_{sh}} \qquad (3\text{-}1)$$

Where the I_L (light current), I_o(the diode reverse saturation current, R_s (series resistance), and R_{sh} (shunt resistance) are provided, the modified ideality factor (a) is determined by Equation 3-2:

$$a = \frac{N_s\, n_1\, k\, T_c}{q} \qquad (3\text{-}2)$$

These five parameters are functions of the irradiance and the PV cell temperature and they are obtained at the reference standard test conditions of 1000 W/m^2 and 25 °C. The maximum power point current and voltage, the short circuit current and the open circuit voltage are available from the supplied PV module datasheet. The temperature coefficient of the open circuit voltage (β_{Voc}) is used to determine the fifth parameter at the reference condition and the short circuit current (α_{Isc}) is used when the cell is operating out of the reference conditions.

Table 3-11. Main parameters, inputs and outputs of the PV module model

Main parameters of PV model (TRNSYS-TYPE 194)	Highlights
Module short-circuit current at reference conditions	Obtained from the datasheet provided by the producer (main characteristics of the selected PV modules) that presented in Table 3-1.
Module open-circuit voltage at reference conditions	
Reference temperature	
Reference insolation	
Module voltage at max power point and reference conditions	
Module current at max power point and reference conditions	
Temperature coefficient of Isc at (ref. cond)	
Temperature coefficient of Voc (ref. cond.)	
Module temperature at NOCT	
Ambient temperature at NOCT	
Insolation at NOCT	
Module area	
Product tau-alpha for normal incidence	
Semiconductor bandgap	
Module series resistance	
Main inputs	
Total incident radiation	Obtained from the experimental performance under different situations.
Ambient temperature	
Main outputs	
Voltage at MPP	Directly obtained from the model outputs using unit converters
Current at MPP	
Electric power at MPP	
Array temperature	
Outputs by inserted equation	
Electric efficiency	The ratio between electric power produced and incident radiation.

3.4.2 Photovoltaic/thermal collector

The model of the selected natural ventilated air-based PV/T (Table 3-1) relies on the TRNSYS 17 mathematical reference of type 560 and type 561 as a reference coding for PV/T collector and air heating collector. Figure 3-17 shows the structure of the selected natural ventilated air-based PV/T collector.

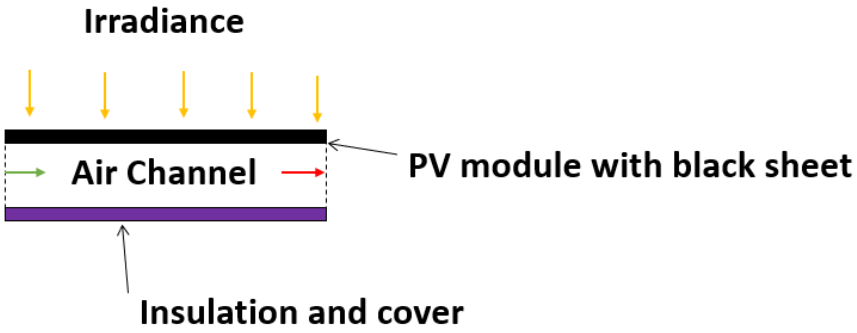

Figure 3-17. Schematic of the selected natural ventilated air-based PV/T.

Type 561 models an un-glazed solar collector that passes air behind the absorbing plate. The thermal model of this collector relies on algorithms supplied by [2]. The general first-order differential equation for the fluid in a solar thermal collector is given by Equation 3-3:

$$C\frac{dT}{dt} = A \cdot F\left(S - U_L(T - T_a)\right) - \dot{m}\, C_p\, (T - T_{in}) \qquad (3\text{-}3)$$

C is the capacitance of the collector including the fluid [W/K], A is the collector area [m²], F is the collector fin efficiency factor [-], U_L is the overall thermal loss coefficient of the collector per unit area, T is Temperature of the collector fluid at any point [°C], T_a is the ambient air temperature [°C], $\dot{m}$ is the fluid flow rate through the collector [kg/h], C_p is the specific heat of the fluid [kJ/kg.K], and T_{in} is the fluid temperature entering the collector [°C].

Type 560 defines the water-based PV/T model which has the dual purpose of creating power from embedded photovoltaic (PV) cells and providing heat to a fluid stream passing through tubes bonded to an absorber plate located beneath the PV cells. PV/T Model 560 relies on linear factors relating the efficiency of the PV cells to the cell temperature and it also relies on the incident solar radiation. The cells are assumed to be operating at their maximum power point condition.

The energy balance on the PV module surface is given by Equation 3-4 [2]:

$$0 = S - h_{outer}(T_{PV} - T_{amb}) - h_{rad}\left(T_{PV} - T_{sky}\right) - \frac{(T_{PV} - T_{abs})}{R_T} \qquad (3\text{-}4)$$

S is the net absorbed solar radiation [kW], h_{outer} is the heat transfer coefficient from the top of PV module to the ambient air [W.m².K], T_{PV} is the PV cell temperature [°C], T_{amb} is the ambient temperature [°C], h_{rad} is the radiative heat transfer coefficient from the top of the PV module to the sky [W.m².K], T_{sky} is the sky temperature [°C], T_{abs} is the absorber plate temperature [°C], and R_t is the resistance to heat transfer from the PV module to the absorber plate [h.m².K/kJ]. The main parameters, inputs and outputs of the air-based PV/T collector model are described in Table 3-12.

Table 3-12. Main parameters, inputs and outputs of the air-based PV/T collector model

Main parameters of PV/T model (TRNSYS-TYPE 560 & 561)	Highlights
Collector length	Obtained from the datasheet provided by the producer (main characteristics of the selected air-based PV/T collector) that presented in Table 3-1.
Collector width	
Absorber plate thickness	
Thermal conductivity of the absorber	
Reflectance	
Emissivity	
Fluid specific heat	
PV efficiency at reference condition	
Efficiency modifier - temperature	
Efficiency modifier - radiation	
1st order IAM coefficient	
Packing factor	
Collector loss coefficient	
Thermal conductance between cells and absorber	
Main inputs	
Incident solar radiation	Obtained from the experimental performance under different situations.
Ambient temperature	
Inlet flowrate	
Inlet fluid temperature	
Main outputs	
Temperature at the collector outlet	Directly obtained from the model outputs using unit converters
Useful thermal energy gain	
PV power	
PV efficiency	

3.4.3 Low-concentrated photovoltaic/thermal systems

The model of the implemented LCPV/T relies on the TRNSYS 17 mathematical reference of type 50 and type 536 as a reference coding for LCPV/T and linear parabolic concentrator. The model is the operation of the type 50 and type 536 together based on the I-V curves experimentally obtained under different situation (see Figure 3-18). The optical analysis of the V-trough CPV was performed in [3] and the energy and exergy of the linear parabolic trough PV/T collector was analyzed in [4]. The main parameters, inputs and outputs of the water-based LCPV/T collector model are described in Table 3-13.

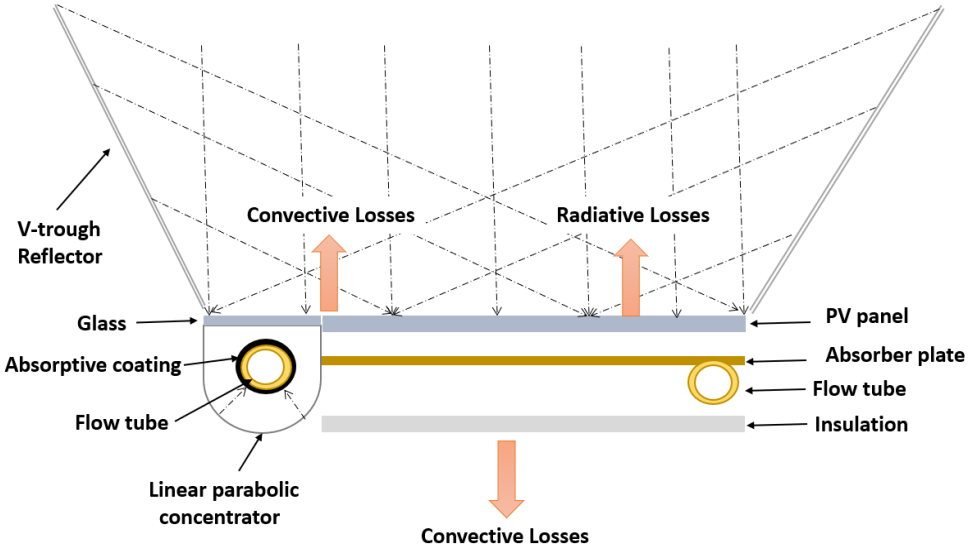

Figure 3-18. Schematic of the dynamic modelling of the developed LCPV/T system.

The geometrical concentration factor is based on the ratio between lens area (A_{lens}) and cell area (A_{cell}) as represented by Equation 3.5. The experimental concentration ratio (CR_{exp}) can be calculated by Equation 3-6 that describes the ratio between the short circuit current of the PV module with and without reflector. The operation efficiency can be calculated by Equation 3-7 that describes the ratio between the CR_{exp} and the geometric efficiency ($C_{geometrical}$).

$$C_{geometrical} = \frac{A_{lens}}{A_{cell}} \quad (1)$$

$$CR_{exp} = \frac{I_{sc}(\text{with reflector})}{I_{sc}(\text{without reflector})} \quad (2)$$

$$OE = \frac{CR_{exp}}{C_{geometrical}} \quad (3)$$

The thermal efficiency of the system can be calculated from Equation 3-8:

$$\eta_{th} = \frac{m \cdot C_p \cdot \Delta T}{IRR_c \cdot A_c} \quad (3\text{-}8)$$

The thermal efficiency (η_{th}) is represented as the ratio between the useful heat power and the irradiance on the surface. m: water mass flow rate, Cp: specific heat capacity and $\triangle T$: temperature difference.

Table 3-13. Main parameters, inputs and outputs of the water based LCPV/T collector model

Main parameters of LCPV/T model (TRNSYS-TYPE 536 & 50)	Highlights
Collector area	Main characteristics of the selected air-based PV/T collector that presented in Table 3-10.
Nominal PV power	
Nominal thermal efficiency	
Fluid thermal capacitance	Main parameters of the developed LCPV/T unit that presented in Table 3-5.
Collector loss coefficient	
Number of tubes	
Diameter of fluid channel	
PV efficiency at reference conditions	
Length of fluid channel	
Area of PV panel	
Concentration ratio of V-trough	
Concentration ratio of linear parabolic	
Main inputs	
Incident solar radiation	Obtained from the experimental performance under different situations.
Ambient temperature	
Inlet flowrate	
Inlet fluid temperature	
Main outputs	
Temperature at the collector outlet	Directly obtained from the model outputs using unit converters
Useful thermal energy gain	
PV power	
PV efficiency	

3.5 Performance validation of photovoltaic models based on the experimental data

This section illustrates the modelling validation of the selected PV systems based on the experimentally obtained data under different situation. The incident solar radiation and ambient temperature that were obtained experimentally are used in the model as inputs along with the water inlet temperature and the water flow rate. The energy generated from the models of the polycrystalline PV, monocrystalline PV and air-based PV/T that were selected in Table 3-1 and the developed water-based LCPV/T system that was presented in Table 3-5 and Table 3-10 are compared with the experimental generation profiles of the selected PV systems (section 3.1 and section 3.2).

Error percentage is given by Equation 3-9:

$$\text{ERROR}\ (\%) = \frac{|E_{model} - E_{EXP}|}{E_{EXP}} \times 100 \qquad (3\text{-}9)$$

The error percentage is given by the absolute difference between the energy generated from PV model and the energy generated from the experimental investigated PV module divided by the experimental investigated PV module.

3.5.1 Polycrystalline PV module

The total electricity production for the 235 W polycrystalline module (Eurener-235) is 1.17 kWh for the experimental module and 1.13 kWh for the modeled module with a performance reduction factor of 21% based on the panel age of 7 years. The irradiance, ambient outdoor temperature (T_Amb) are registered as environmental parameters to the model. Figure 3-19 shows the power production experimentally (P_PV_EXP) from the 235 W polycrystalline PV module and the power obtained from the modelled module. The maximum solar radiation for this day is about 1110 W/m^2 and the maximum outdoor temperature is 30.5 °C, while the maximum power production is 211 W for the experimental module and 202 W for the model module.

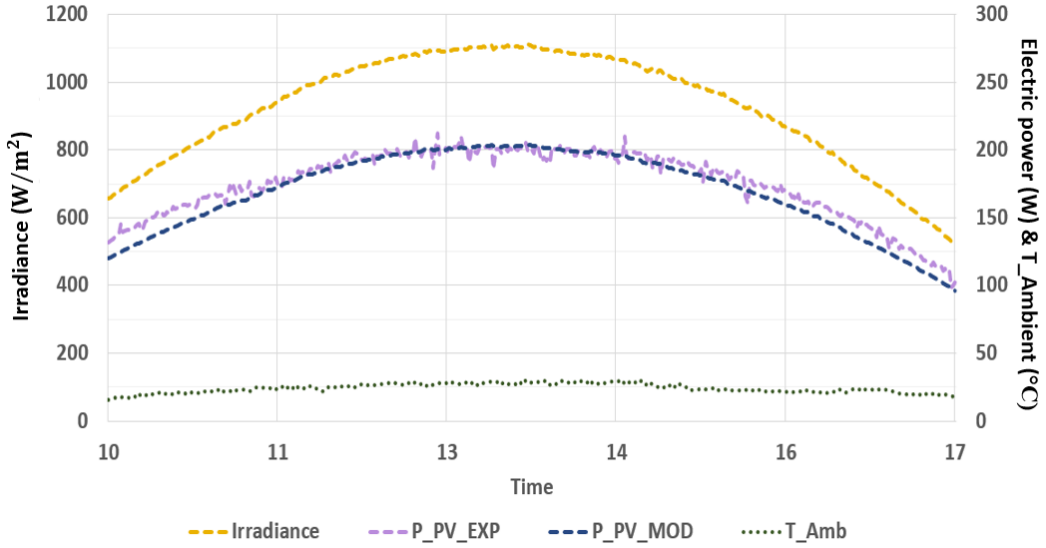

Figure 3-19. Comparison of the electricity generated from the experimental polycrystalline PV (P_PV_EXP) module and the modelled PV (P_PV_MOD) module.

The model of the polycrystalline module generates the same electricity generated from the experimental investigated module with daily error percentage of 3.4 %. One of the reasons of this error percentage is the degradation based on the panel age.

3.5.2 Natural ventilated air-based PV/T collector

The total electricity production for the 265 W air-based PV/T (Ecomesh 265) module is 1.42 kWh for experimental module and 1.32 kWh for modeled module during the monitoring period from 10 am to 5 pm. The irradiance and ambient temperature (T_Amb) were registered to the model. The Power production experimentally (P_PV_EXP) from the 265 W air-based collector vs power obtained from the modelled module are shown in Figure 3-20. The maximum solar radiation for this day is about 1089 W/m^2 and the maximum outdoor temperature is 30.7 °C, while the maximum power production is 255 W for the experimental module and 234 W for the model module.

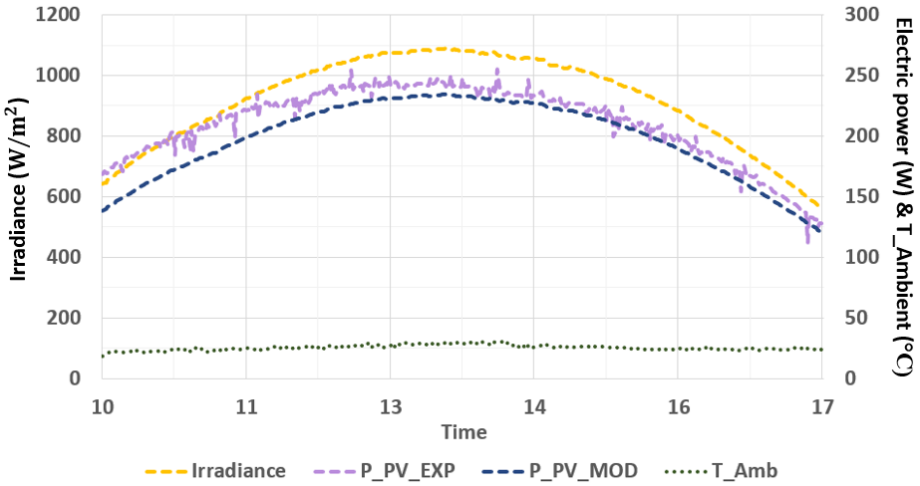

Figure 3-20. Electricity generated the 265 W air-based PV/T module: power production experimentally registered (P_PV_EXP) vs power obtained from the modelled (P_PV_MOD) module.

The model of the natural-ventilated air-based PV/T module generates the same electricity generated from the experimental investigated module with daily error percentage of 7.5 %. The reasons of this error percentage are the degradation based on the panel age and the undefiled wind speed for the natural ventilated air-based PV/T collector.

3.5.3 Monocrystalline PV module

The total electricity production for the 290 W monocrystalline module (JASOLAR-290) is 1.55 kWh for experimental module and 1.53 kWh for modeled module during the monitoring period from 10 am to 4 pm. The irradiance and ambient outdoor temperature (T_Amb) were registered to the model. The Power production experimentally (P_PV_EXP) from the 290W monocrystalline module vs power obtained from the modelled module are shown in Figure 3-21. The maximum solar radiation for this day is about 950 W/m² and the maximum outdoor temperature is 27 °C, while the maximum power production is 240 W for the experimental module and 249 W for the model module.

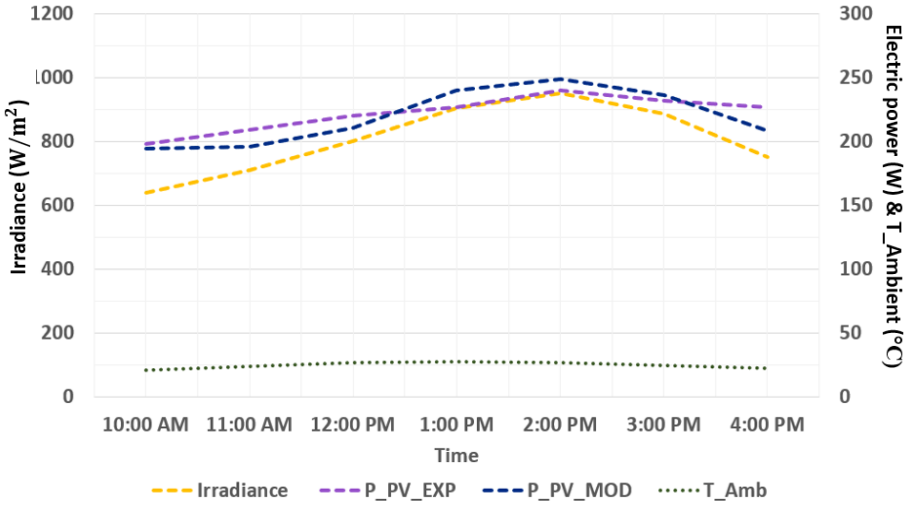

Figure 3-21. Power production experimentally registered (P_PV_EXP) vs power obtained from modelled module of the 290 W monocrystalline PV module.

The model of the monocrystalline PV module generates the same electricity generated from the experimental investigated module with daily error percentage of 1.2 %. One of the reasons of this error percentage is the degradation based on the panel age.

3.5.4 Modified monocrystalline module to low-concentrated photovoltaic/thermal system

The total electricity production for the developed LCPV/T system (section 3.2) is 1.63 kWh for experimental module and 1.70 kWh for modeled system during the monitoring period from 11 am to 4 pm. The irradiance, ambient temperature, outdoor humidity and the concentration factor were registered to the model. The power production experimentally (P_PV_EXP) and the power obtained from the modelled system (P_PV_MOD) using the registered environmental inputs (irradiance ambient air temperature) are shown in Figure 3-22.

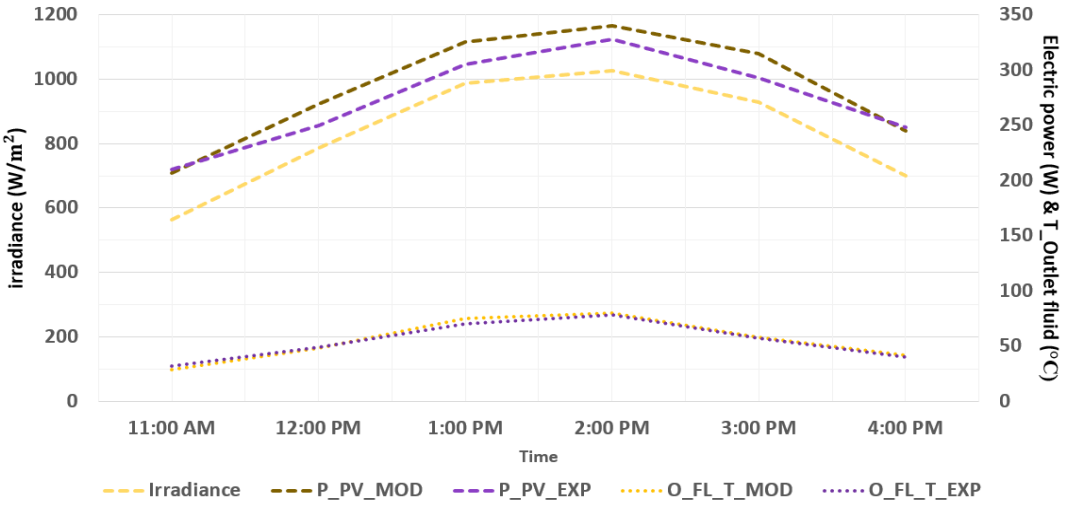

Figure 3-22. Power and outlet water temperature from the experimentally registered (P_PV_EXP) system and (O_FL_T_EXP) vs power and outlet fluid temperature of the modelled LCPV/T system.

The maximum solar radiation for this day was about 1072 W/m^2 and the maximum outdoor temperature is 28 °C. The water inlet temperature is about 24 °C and the maximum power production was 328 W for the experimental system and 340 W for the system model. For this typical day, the maximum outlet temperature was 78 °C for the experimental system and 80 °C for the system model. The maximum useful thermal power from the LCPV/T system was 1.95 kW for the system model and 1.88 kW for the experimental system. The daily useful thermal energy from the LCPV/T system was 6.56 kWh for modeled system and 6.35 kWh for the experimental system. The thermal efficiency was around 45% for the experimental system and 47% for the experimental LCPV/T system.

The model of the developed LCPV/T generates the same electricity generated from the experimental investigated system with daily error percentage of 1.3 %. The model of the developed LCPV/T generates the same thermal energy generated from the experimental investigated system with daily error percentage of 3.7%. The reasons of this error percentage are the degradation based on the panel age and the undefiled diffuse radiation.

The validated models will be simulated in the following section to investigate their energy performance in nine climate conditions.

3.6 Energy generation from photovoltaic systems in different climate conditions

The performance of the selected polycrystalline (Eurener-235), monocrystalline (JASOLAR-290) PV modules, air-based PV/T (Ecomesh-265), and the developed LCPV/T are shown in different climate conditions. The classification of the selected 9 locations with different climate conditions is illustrated in Table 3-14. Tarragona (Spain) is Mediterranean climate, Cairo (Egypt) is Subtropical hot climate, Colombo (Sri Lanka) is Tropical rainforest, Geneva (Switzerland) is Moderately continental, Kuwait (Kuwait) is Subtropical hot, Miami (USA) is Humid subtropical, Quebec (Canada) is Subarctic, and Wiscasset (USA) is Humid continental.

Table 3-14. Classification of the selected climate regions

Location	Classification
Tarragona (Spain)	Mediterranean
Cairo (Egypt)	Subtropical hot
Colombo (Sri Lanka)	Tropical rainforest
Geneva (Switzerland)	Moderately continental
Kuwait (Kuwait)	Subtropical hot
Miami (USA)	Humid subtropical
Quebec (Canada)	Subarctic
Wiscasset (USA)	Humid continental

The average annual maximum and minimum temperature are 21.3 °C and 13.0 °C for Tarragona, 27.0 °C and 15.0 °C for Cairo, 30.5 °C and 24.0 °C for Colombo, 12.0 °C and 4.0 °C for Geneva, 34.0 °C and 20.0 °C for Kuwait, 28.0 °C and 20.0 °C for Miami, 9.0 °C and -0.8 °C for Quebec, 15.0 °C and 6.0 °C for Wiscasset. The maximum mean monthly temperature is 41 °C for Kuwait in August, while the minimum mean monthly temperature is -11 °C for Quebec in January. The average maximum annual relative humidity is 80% for Colombo, while the minimum is 40% for Kuwait.

Cooling degree days (CDD) are a measure of how much (in degrees), and for how long (in days), outside air temperature was higher than a specific base temperature that calculated for (25 °C) at each location. Heating degree days (HDD) are a measure of how much (in degrees), and for how long (in days), the outside air temperature was lower than a specific base temperature that calculated for (21 °C) at each location. Degree days are basically a simplified representation of the ambient air temperature data, also the degree days are calculated easily by using a calculator which requires identifying the location and the base temperature. Figure 3-23 illustrates the annual heating and cooling degree days of the specified locations. The maximum annual heating degree days is 6285 HDD (see Figure 3-23.a), while maximum annual cooling degree days is 2179 CDD for Kuwait (see Figure 3-23.b).

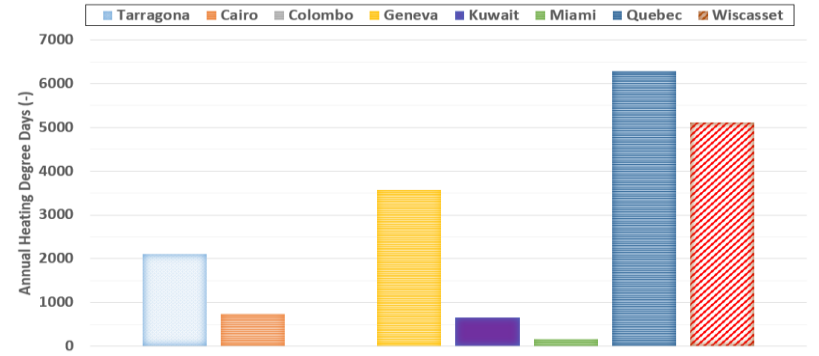

(a)

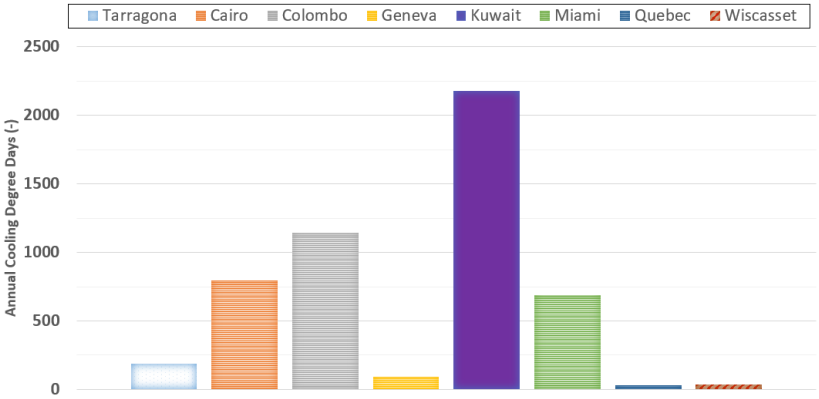

(b)

Figure 3-23. Average annual degree days of the specified locations: a) heating degree days, and b) cooling degree days.

The average monthly daylight of the specified locations is shown in Table 3-15. The maximum average daylight is 362 hours for Tarragona in July, 339 hours for Cairo in May, 318 hours for Colombo in December, 342 hours for Geneva in July, 352 hours for Kuwait in June, 333 hours for Miami in July, 348 hours for Quebec in July, and 336 hours for Wiscasset in July. The maximum average daylight is 3699 hours for Kuwait, while the minimum is 2867 hours for Geneva.

Table 3-15. Average monthly daylight hours of the specified locations

Month	Average hours of daylight (hours)							
	Tarragona	Cairo	Colombo	Geneva	Kuwait	Miami	Quebec	Wiscasset
JAN	228	264	313	94	273	289	206	173
FEB	233	264	279	164	259	276	219	152
MAR	297	306	310	261	300	328	296	278
APR	317	305	297	299	304	325	302	286
MAY	350	339	307	333	339	309	310	306
JUN	346	325	291	336	352	317	321	313
JUL	362	311	304	342	348	333	348	336
AUG	344	309	306	326	341	325	317	329
SEP	295	300	301	291	327	293	269	280
OCT	274	279	313	219	325	296	229	200
NOV	231	266	304	117	276	278	152	182
DEC	230	260	318	85	255	278	167	113

The system tilt angle is adjusted at 45° in Tarragona, Quebec and Wiscasset, 30° in Cairo and Geneva, 60° in Colombo, and 40° in Kuwait and Miami based on the annual energy production per year at different inclination angles.

The electricity produced (E_{PV}) from the polycrystalline PV (Eurener-235) and the module temperature (T_{PV}) are shown in Table 3-16 for typical summer and winter days in different climate conditions.

Table 3-16. Energy generation from the polycrystalline PV module in different climate conditions

Polycrystalline PV	Typical summer day		Typical winter day	
Eurener-235 W	Daily E_{PV} (kWh)	Average T_{PV} (°C)	Daily E_{PV} (kWh)	Average T_{PV} (°C)
Tarragona	1.28	39	1.03	26
Cairo	1.19	40	1.19	26
Colombo	0.65	39	1.14	26
Geneva	1.31	32	0.13	2
Kuwait	1.11	49	1.01	18
Miami	0.96	38	0.62	32
Quebec	1.19	49	1.05	-18
Wiscasset	1.28	32	0.20	-1

The electricity produced (E_{PV}) from the monocrystalline PV (JASOLAR-290) and the module temperature (T_{PV}) are shown in Table 3-17 for typical summer and winter days in different climate conditions.

Table 3-17. Energy generation from the monocrystalline PV module in different climate conditions

Monocrystalline PV	Typical summer day		Typical winter day	
JASOLAR-290 W	Daily E_{PV} (kWh)	Average T_{PV} (°C)	Daily E_{PV} (kWh)	Average T_{PV} (°C)
Tarragona	2.11	36	1.56	23
Cairo	1.56	38	1.49	24
Colombo	1.11	36	1.92	24
Geneva	2.13	29	0.13	1
Kuwait	1.83	46	1.43	16
Miami	1.83	37	1.43	28
Quebec	1.91	45	1.46	-19
Wiscasset	2.06	27	0.24	-1

The maximum temperature difference (Delta T) refers to the difference between air temperature leaving the collector and air temperature entering the collector. In the typical winter day, the temperature difference is 0 °C for Geneva and Wiscasset (solar radiation is not sufficient to produce heat) and the fluid flow pump is switched off. The inlet air temperature is adjusted at 15 °C and mass flow is adjusted at 0.01 kg/s during the typical winter day. On the other hand, the inlet air temperature is adjusted at 20 °C and mass flow is adjusted at 0.01 kg/s during the specified typical summer day. The electricity produced (E_{PV}) from the air-based PV/T (Ecomesh-265) and the fluid temperature difference ($T_{out} - T_{in}$) are shown in Table 3-18 for typical summer and winter days in different climate conditions.

Table 3-18. Performance of the air-based PV/T collector in different climate conditions

Air-based PV/T	Typical summer day		Typical winter day	
Ecomesh-265	Daily E_{PV} (kWh)	$T_{out} - T_{in}$ (°C)	Daily E_{PV} (kWh)	$T_{out} - T_{in}$ (°C)
Tarragona	1.79	10	1.27	9
Cairo	1.57	10	1.53	10
Colombo	1.79	7	1.27	11
Geneva	1.78	10	0.1	0
Kuwait	1.57	10	1.15	8
Miami	1.28	8	0.77	6
Quebec	1.57	9	1.15	7
Wiscasset	1.72	9	0.18	0

The maximum temperature difference (Delta T) refers to the difference between water temperature leaving the collector and water temperature entering the collector. In the typical winter day, the temperature difference is 0 °C for Geneva and Wiscasset (solar radiation is not sufficient to

produce heat) and the fluid flow pump is switched off. The inlet temperature is adjusted at 15 °C and mass flow is adjusted at 0.5 l/min during the specified typical winter day. On the other hand, the inlet temperature is adjusted at 24 °C and mass flow is adjusted at 0.5 l/min in the typical summer day. The electricity produced (E_{PV}) from the water-based LCPV/T (modified monocrystalline PV module to LCPV/T system) and the fluid temperature difference ($T_{out} - T_{in}$) are shown in Table 3-19 for typical summer and winter days in different climate conditions.

Table 3-19. Performance of the water based LCPV/T system in different climate conditions

The developed	Typical summer day		Typical winter day	
LCPV/T	Daily E_{PV} (kWh)	$T_{out} - T_{in}$ (°C)	Daily E_{PV} (kWh)	$T_{out} - T_{in}$ (°C)
Tarragona	2.51	47	1.86	38
Cairo	2.07	54	1.74	44
Colombo	1.27	41	2.23	43
Geneva	2.39	49	0.14	0
Kuwait	2.28	49	1.78	41
Miami	2.01	51	1.66	32
Quebec	2.16	52	1.71	34
Wiscasset	2.43	54	0.27	0

From the outlook of this chapter, the mean daily electric energy generated is, 1.2 kWh_e for the 235 W polycrystalline (1.65 m^2), 2.14 kWh_e for the 290 W monocrystalline module (1.64 m^2), 1.6 kWh_e for the 265 W air based PV/T (1.64 m^2), and 2.61 kWh_e for the LCPV/T (3.9 m^2)based on the 290 W monocrystalline module. The electric and thermal energy during the specified winter and summer typical days of the developed LCPV/T system are in the range of 1.6-2.7 kWh_e and 4.5-7.1 kWh_t, respectively.

3.7 Conclusion

This chapter elaborated on the experimental generation profiles of the selected PV systems and presents the validated PV models using TRNSYS dynamic simulation modelling environment to explore their dynamic performance under different climate conditions. Two approaches to improve the electric power generated from the selected PV modules have been investigated. The first approach investigated the effect of coating the polycrystalline PV modules by aluminum nanoparticles on the electricity produced and the panel temperature. The second approach modified the selected monocrystalline PV module to LCPV/T system to obtain high quality thermal energy (fluid stream temperature of up to 90 ° C) with operating the solar cells at favorable temperature. This makes the system useful for operating thermally driven air conditioning. The laboratory test of attaching V-trough mirrors to the PV module, was carried out to identify the most appropriate reflector tilt angle and reflector width. The outdoor test of the developed LCPV/T and the selected PV modules were performed to validate the energy production from the selected PV models. The

dynamic simulation of the selected monocrystalline, polycrystalline PV and air-based PV/T modules and the developed LCPV/T was carried out in nine climate conditions.

By adding the Al_2O_3 coating on the monocrystalline surface, the efficiency of the module is increased 0.81% for the first day and only 0.03% after six days while the module temperature is reduced 2.8 °C for the first day and 0.2 °C after six days at the same outdoor operating conditions.

The electric solar conversion efficiency of the modified PV module fitted with V-trough mirrors is increased under the laboratory test and the outdoor test. By modifying the installed monocrystalline PV module to the water based LCPV/T system, the electric efficiency is increased 3.55%. The temperature of the outlet water stream from the LCPV/T systems can exceed 80 °C while the PV module is kept below 75 °C in summer (solar radiation of 1020 W/m^2 and ambient temperature of 28 °C) and exceeds 50 °C in winter (solar radiation of 850 W/m^2 and ambient temperature of 15 °C).

The dynamic modeling of the PV, PV/T and LCPV/T systems based on the experimentally obtained irradiance and ambient temperature has been deployed and validated under different situation. The mean daily electric energy generated is, 1.2 kWh_e for the 235 W polycrystalline (1.65 m^2), 2.14 kWh_e for the 290 W monocrystalline module (1.64 m^2), 1.6 kWh_e for the 265 W air based PV/T (1.64 m^2), and 2.61 kWh_e for the LCPV/T (3.9 m^2)based on the 290 W monocrystalline module. The electric and thermal energy during the specified winter and summer typical days of the developed LCPV/T system are in the range of 1.6-2.7 kWh_e and 4.5-7.1 kWh_t, respectively.

The dynamic models of PV, PV and the developed LCPV/T produces the same energy from the experimental investigated system with mean daily error of 5%. The reasons of this error percentage are the degradation of the PV module based on the panel age, the undefined wind speed and the undefined diffused radiation.

The outlet water from the LCPV/T system can be used to supply absorption chillers for hot climates at 70-90 °C, desiccant systems at 50-65 °C for high humidity climates, water heaters at 35-45 °C, and evaporator-heat pump at 25-35 °C.

References

[1]- University of Wisconsin, Solar Energy Laboratory, TRNSYS 17: A Transient System Simulation Program, 2012, http://www.trnsys.com/. Accessed on April 26, 2020.

[2]- Duffie JA and Beckman WA. 2006. Solar engineering of thermal process. Willey, Canada.

[3]- Ustaoglu A, Ozbey U, Torlaklı H, 2020. Numerical investigation of concentrating photovoltaic/thermal (CPV/T) system using compound hyperbolic –trumpet, V-trough and compound parabolic concentrators. Renewable Energy 152, pp.1192-1208.

[4]- Valizadeh M, Sarhaddi F, Adeli M, 2019. Exergy performance assessment of a linear parabolic trough photovoltaic thermal collector. Renewable Energy 138, pp. 1028-1041.

Chapter 4. Energy performance of photovoltaic/thermal systems for handling the electricity, cooling and heating loads in buildings incorporated into the micro-grid and thermal district network

Throughout the experimental energy performance and the validated models presented in Chapter 3, the energy generation profiles of the selected polycrystalline PV, monocrystalline PV and air-based PV/T modules and the developed LCPV/T system are explored. This chapter examines the use of on-site energy production from the validated models along with the integration of efficient cooling and heating systems.

Two proposed bidirectional integration configurations of the LCPV/T system with buildings incorporated into the electricity microgrid and district thermal network are investigated. The integration of the LCPV/T system into the 4th generation heating network (supply temperatures below 70 °C) is dynamically performed using direct heat exchanger and reversible electric water-to-water heat pump for heating and cooling in the warm climate. The integration of the LCPV/T system into the cooling network (supply temperatures around 7 °C) is dynamically performed using the thermal and electric chillers for mainly cooling in the extremely hot climate.

The two proposed configurations along with the traditional configurations of PV driven electric air-to-water HP, PV driven electric chiller and PV/T assisted air-to water HP are modelled. Moreover, the performance of these five solar configurations are compared with the conventional cooling (air-cooled chiller) and heating (gas boiler) systems.

Two case study buildings in hot and warm climate conditions are selected. The two case study buildings are dynamically operated to characterize the thermal demand of the buildings and match the energy demand and on-site energy generation. The first case study building is an existing laboratory building that belongs to the university campus of the URV in Tarragona. The second case study building is an existing university building that belongs to the university campus of the BUE in Cairo.

The design of the grid-tie photovoltaic system has been taken the available roof area, the distance between module rows, the building's orientation and the fulfilment of building's demands into consideration. The cooling and heating systems are sized to meet the case building's demands.

The solar contribution index, monthly bill saving, CO_2 emissions reduction and the payback of the PV, PV/T and LCPV/T systems coupled with cooling and heating systems in the two case buildings are presented. The proposed method incorporates dynamic modeling simulation environments (DesignBuilder/EnergyPlus engine and TRNSYS dynamic modelling environment) to investigate the match between energy production and consumption hourly, daily, monthly and yearly.

4.1 Modelling of the energy performance of solar cooling and heating systems

The dynamic modelling simulation of integrating the selected PV, PV/T and the developed LCPV/T that were presented and validated in Chapter 3 is performed here for the two case buildings. These two case buildings are incorporated into the modern district cooling and heating network and the electricity micro-grid. The following five integration configurations of solar cooling and heating

systems are modelled and dynamically simulated along with conventional cooling (air-cooled chiller) and heating (gas boiler) systems. These five integration configurations are: i) the LCPV/T coupled with compression and absorption chillers for cooling; ii) the LCPV/T coupled with water-to-water HP for cooling and heating; iii) the PV/T assisted air-to-water HP for heating; iv) the PV driven air-cooled electric chiller for cooling; and v) the PV driven air-to-water HP for cooling and heating.

4.1.1 Configurations of the selected and developed photovoltaics for cooling and heating

The proposed two bidirectional integration configurations of the LCPV/T system with the microgrid and modern district cooling and heating network for providing buildings with electricity, cooling and heating are shown in Figure 4-1.

Figure 4-1.a shows the integration of LCPV/T system into the 4th generation district heating network (supply temperatures below 70 °C) using direct heat exchanger and the cooling network using the thermal and electric chillers for mainly cooling of buildings. In extremely hot climate (summer), the useful heat from the LCPV/T in the range of 75-88 °C is being used to drive the air-cooled absorption chiller that is connected to the building with the air-cooled electric chiller. The useful heat from the water based LCPV/T in the range of 55-65 °C and the water stream leaving the thermal chiller at the same temperature range, are being imported to the district hot network. The stream leaves the network after releasing its heat to enter the LCPV/T system at 30 °C.

Figure 4-1.b shows the integration of the developed LCPV/T system into the modern district cooling and heating network using the reversible water-to-water HP. In cold climates, the water at the temperature range of 18-25 °C is being heated up by the LCPV/T system. The water reaches a temperature level of 45-50 °C to supply heating directly to the building through a fan coil or 30-40 °C to be used as heat source for the HP.

The performance of i) LCPV/T with compression and absorption chillers for cooling (Figure 4-1.a); ii) LCPV/T with water-to-water HP for cooling and heating (Figure 4-1.b); iii) PV/T with air-to-water HP for heating (Figure 4-1.c); iv) PV with air-cooled chiller for cooling (Figure 4-1.d); and v) PV with air-to-water HP for cooling and heating(Figure 4-1.e). Moreover, the performance of both configurations of the LCPV/T system for space cooling and heating are compared with the conventional cooling (air-cooled chiller) and heating (gas boiler) systems.

This evaluation of integrating LCPV/T with buildings into the modern district cooling and heating network is carried out hourly, monthly, yearly and in summer and winter typical days in the hot and warm climates. The size of the solar generation system is limited by the availably roof area. The space cooling and heating system is sized to meet the cooling and heating demands of the existing case buildings using the fan coil system.

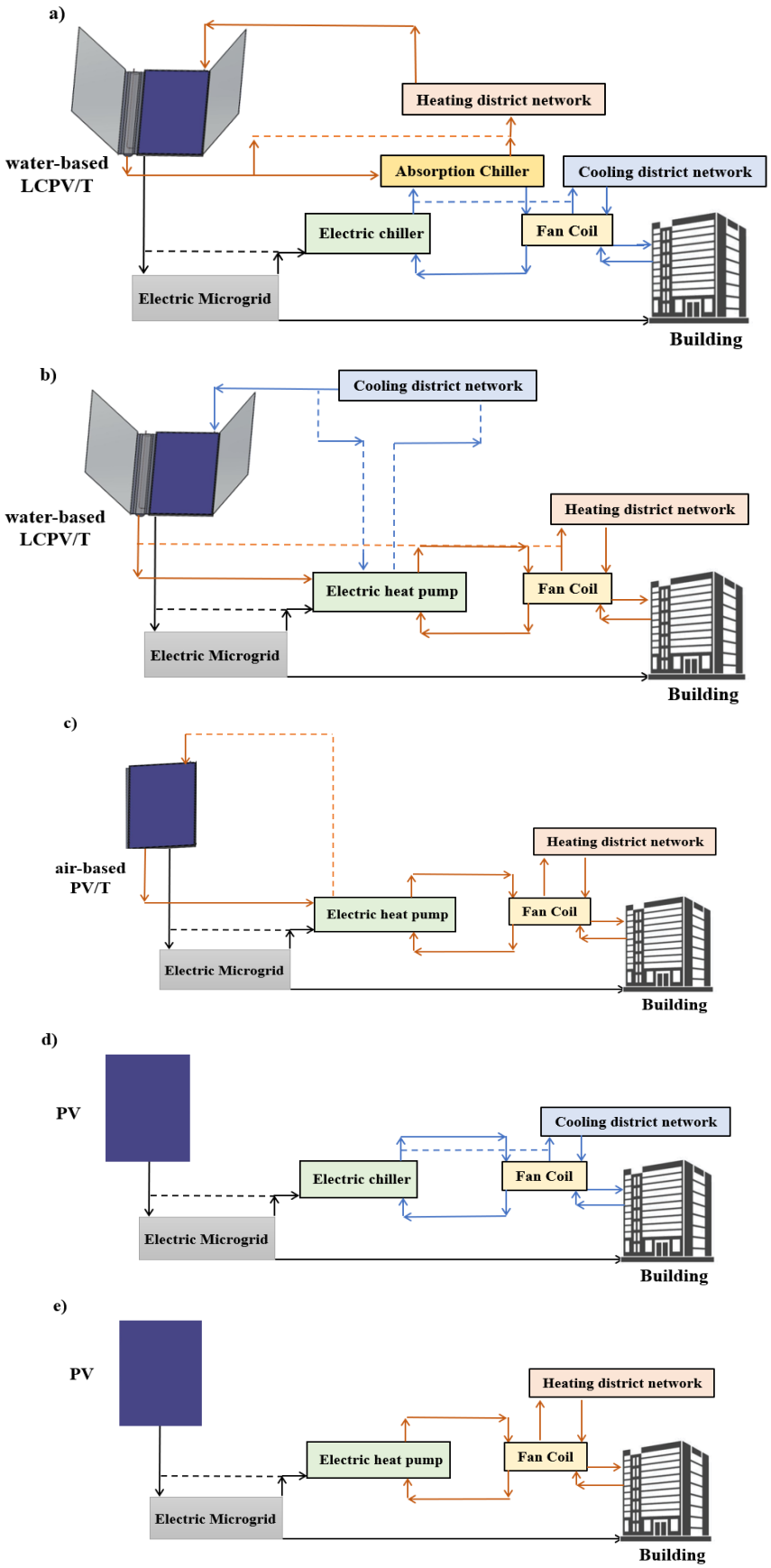

Figure 4-1. Configurations of solar cooling and heating systems with electricity microgrid, and thermal networks: a) LCPV/T with compression-absorption chillers; b) LCPV/T with water-to-water HP; c) PV/T assist air-to-water HP, d) PV with electric chiller, and e) PV with air-to-water HP.

4.1.2 Modelling of different configurations of solar cooling and heating systems in buildings

DesignBuilder/EnergyPlus engine and TRaNsient System Simulation (TRNSYS) dynamic simulation environment are the two simulation tools used for the model. They are two linked environments that are used for analyzing the match between energy consumption and energy production in the selected buildings.

From Chapter 3, the main parameters, inputs and outputs of the PV module model (TRNSYS-TYPE 194) was shown in Table 3-11, the main parameters, inputs and outputs of the air-based PV/T collector model (TRNSYS-TYPE 560 & 561) was shown in Table 3-12, and the main parameters, inputs and outputs of the water based LCPV/T collector model (TRNSYS-TYPE 536 & 50) was shown in Table 3-13.

The DesignBuilder/EnergyPlus engine is used for characterizing the thermal demand of the building in a one-year operation and then the building's sensible heating and cooling loads are uploaded on TRNSYS 17 dynamic modelling simulation environment using 2-pipe console unit (Type 673). The main parameters, inputs and outputs of 2-pipe console unit model is shown in Table 4-1.

The dynamic simulation environment then takes the energy rate control loads attained from a building model and converts them into temperature-level controls by adding or subtracting heat from a flow stream. The hot fluid stream is supplied by the water-to-water HP (Type 927) in the proposed case, the air-to-water heat pump (Type 941) and the gas boiler (Type 751) in the comparative case. On the other hand, the chilled fluid stream is supplied by the air-cooled water chiller (Type 655) and the single stage hot water air cooled absorption chiller that modelled by assuming the COP of 0.76 and using the nominal conditions provided by the suppler as the minimum operation temperature of 75 °C and the cooling capacity of 2.5 kW (PURIX-A25s, Chapter 1, Table 1-2) in the proposed case, and the air-cooled electric chiller in the comparative case. The water pipes (Type 31) and the pump (Type 114) are used in the cooling and heating pipelines.

Table 4-1. Main parameters, inputs and outputs of 2-pipe console unit model

Main parameters of 2-pipe console unit (TYPE 673)	Highlights
Rated fan power (kW)	14 (building A) & 95 (building B)
Rated cooling capacity (kW)	166 (Building A) & 1155 (Building B)
Rated heating capacity (kW)	181 (Building A)
Fluid specific heat (kJ/kg.K)	4.190
Main inputs	
Inlet fluid temperature	Temperature from the building
Total fluid flowrate	Based on the cooling and heating system
Main outputs	
Outlet fluid temperature	Directly obtained from the model outputs
Outlet flowrate	.
Fan power	

The main parameters, inputs and outputs of air-to-water HP model (TRNSYS-TYPE 941) is shown in

Table 4-2 and the main parameters, inputs and outputs of water-to-water HP model (TRNSYS-TYPE 927) is shown in Table 4-3.

Table 4-2. Main parameters, inputs and outputs of air-to-water HP model

Main parameters of air-to-water HP (TRNSYS-TYPE 941)	Highlights
Rated cooling capacity	Obtained from the datasheet provided by the producer
Rated cooling power	
Rated heating capacity	
Rated heating power	
Total air flowrate	
Main inputs	
Inlet liquid temperature	Obtained from the sized HP system
Inlet liquid flowrate	
Inlet Air Temperature	Experimentally from Chapter 3
Main outputs	
Exiting Fluid Temperature	Directly obtained from the model outputs
Exiting Fluid Flowrate	
Heat Pump Power	.

Table 4-3. Main parameters, inputs and outputs of water-to-water HP model

Main parameters of water-to-water HP (TRNSYS-TYPE 927)	Highlights
Rated cooling capacity	Obtained from the datasheet provided by the producer
Rated cooling power	
Rated heating capacity	
Rated heating power	
Main inputs	
Inlet source temperature	Obtained from the sized HP system
Source flowrate	
Inlet load temperature	
Load flow rate	
Main outputs	
Outlet Source temperature	Directly obtained from the model outputs
Source flowrate	
Outlet load temperature	.
Load flowrate	
Heat pump power	

The main parameters, inputs and outputs of the gas boiler model (TRNSYS-TYPE 751) is shown in Table 4-4 and the main parameters, inputs and outputs of air-cooled electric chiller model (TRNSYS-TYPE 655) is shown in Table 4-5.

Table 4-4. Main parameters, inputs and outputs of gas boiler model

Main parameters of gas boiler (TRNSYS-TYPE 751)	Highlights
Rated capacity (kW)	181 (Building A)
Main inputs	
Inlet fluid temperature	Return temperature from the building
Inlet fluid flowrate (kg/s)	6.5
Set point temperature (°C)	45
Main outputs	
Outlet fluid temperature	Directly obtained from the model
Outlet fluid flowrate	outputs
Required boiler energy input	.

Table 4-5. Main parameters, inputs and outputs of air-cooled electric chiller model

Main parameters of electric chiller (TRNSYS-TYPE 655)	Highlights
Rated capacity (kW)	166 (Building A) & 1155 (Building B)
Rated COP (-)	1.9 (Building A) & 2.5 (Building B)
Fluid specific heat (kJ/kg.K)	4.190
Main inputs	
Chilled water inlet temperature	Return temperature from the building
Chilled water flowrate (kg/s)	3 (Building A) & 13.8 (Building B)
Set point temperature (°C)	7
Ambient temperature	Experimentally from Chapter 3
Main outputs	
Outlet fluid temperature	Directly obtained from the model
Fluid flowrate	outputs
Chiller power	.

The thermostats (Type 1503 for cooling mode and Type 1502 for heating) are used to switch the cooling and heating system on/off. In cooling mode, the system (chiller in the existing case and heat pump in the proposed case) operates till the building's return stream drops below 7 °C. As for heating mode, the system (gas boiler in the existing case, air-to-water HP in the comparative case and heat pump in the proposed case) operates till the building's return stream exceeds 40 °C. This control function is activated before the building's operating time by one hour in order to assure a comfortable temperature for the occupants and to prevent the compressor from initiating and thus meeting a high load capacity.

The HP part load capacity ratio is determined by using a part load performance calculator (Type 43). The recorded hourly reading for the building's lights and equipment load is uploaded on TRNSYS dynamic simulation environment using a data reader (Type9). The power condoning management device (Type 175) is then used to connect the HP, equipment and lights loads with the PV systems.

The PV system contains PV modules, PV/T collectors, LCPV/T systems and a grid-tie inverter with maximum power tracking device (Type 48). The fluid-based PV/T and LCPV/T systems have a mass flow rate of 0.02 kg/s for air-based and 0.5 l/min for water-based PV/T collectors. A controller for temperature valve (Type 953) is included to avoid cooling the fluid in the PV/T and LCPV/T systems instead of heating it when the fluid temperature is higher than the PV cells temperature. The modification of commercial PV modules to LCPV/T systems and the dynamic modeling validation of the PV, PV/T and LCPV/T systems for visualizing their energy use, have been previously presented in Chapter 3.

The results are recorded and plotted by model (Type 25C) and (Type 65C). The matching equation and calculations of solar power systems (PV, PV/T and LPV/T), air-conditioning systems (air-to-water HP, air-cooled chiller, water-to-water HP, thermal chiller, gas boiler) and building loads, are inserted into the model.

The size of the solar generation system is limited by the availably roof area. The space cooling and heating system is sized to meet the cooling and heating demands of the existing case buildings using the fan coil system.

The following proposes control mechanisms and scenarios that are capable of balancing supply and demand with the connection to the microgrid and the modern water district network. Three control mechanisms are examined. Firstly, the heat pump or the electric-thermal chiller system follows the thermal building demand when the immediate capacity of the LCPV/T system is not enough, seeing that the electricity for heat pump or the electric chiller is imported from the local grid (no thermal exchange with water network). Secondly, the heat pump or the electric-thermal chiller system follows the building thermal demand when the LCPV/T power is low. In this method, the heat pump or the electric-thermal chiller system is switched off and the water network supplies the thermal energy. Finally, the heat pump or the electric chiller continuously operates at full load to provide thermal energy for the building and the water network (immediate excess PV power is exported to local grid while immediate required power is imported from the local grid).

The effectiveness of integrating PV, PV/T and LCPV/T systems, electric chillers and heat pump units into the electricity microgrid and the modern heating/cooling district network for providing different case buildings (different activities and building size) with cooling, heating and electricity, is evaluated hourly, monthly, yearly and on typical summer and winter days in different climate conditions. The impact of the PV system type on the solar contribution index, the effect of the electricity and thermal energy exporting scheme on the payback period of different types of grid-tie PV systems, the monthly bill before and after the implementation of the proposed configuration with different control mechanisms, the impact of different integration scenarios on the payback of different of the designed roof-mounted PV systems for the case study buildings, the CO_2 emissions reduction by implementing the different types of grid-tie PV systems are evaluated.

4.1.3 Energy flow of low-concentrated photovoltaic/thermal assisted absorption chiller

The performance of the air-cooled absorption chiller (PURIX-A25s, Chapter 1, Table 1-2), with a cooling capacity of 2.5 kW, hot water driven temperature of 75 °C and COP of 0.76, is investigated

along with the developed LCPV/T system. To predict the dynamic performance of this air-cooled absorption chiller, the catalog data is imported to TRNSYS environment. The air flow rate of the air-cooled absorption chiller is adjusted at 500 m^3/h. The average flow rate at the evaporator is around 7.2 l/min for a temperature lift of 5 °C.

The maximum thermal and electric power from one unit of LCPV/T is 1.9 kW_t and 395 W_e, respectively. The average daily electric energy produced from the developed LCPV/T is around 1.6-2.7 kWh_e and the average daily thermal energy is around 4.5-7.1 kWh_t (Chapter 3).

An air-cooled absorption chiller (PURIX-A25s) machine requires two LCPV/T units to attain favorable operation conditions. Assuming the LCV/T integration operation losses are of 10%, the maximum thermal and electric power from two units of LCPV/T is around 3.5 kW_t and 711 W_e.

The average nominal COP of the air-cooled electric chillers (small capacity) based on the datasheet provided by different suppliers is around 3 while the nominal COP of the air-cooled absorption chiller (PURIX-A25s) is 0.76 at hot water driven temperature of ≥ 75 °C.

The solar fraction index indicates the percentage of PV produced energy in regards of the total energy demanded in a specific period of time (Equation 4-1).

$$\text{Solar Fraction (\%)} = \frac{\text{PV electricity generation}}{\text{Energy consumption}} \times 100 \qquad (4\text{-}1)$$

The solar fraction highly depends on the environmental conditions (ambient temperature and solar radiation intensity). However, it depends only slightly on the return water stream temperature from the fan coil in the building.

The maximum water temperature supplied from the LCPV/T is adjusted at 88 °C and the minimum operation temperature of the absorption chiller is adjusted at 70 °C. The air-cooled chiller unit is driven by 2 LCPV/T units.

4.2 Case study buildings in warm and hot climate conditions

Two case study buildings in warm and hot climate conditions are dynamically operated to characterize the thermal demand of the buildings and match the building energy demand and on-site energy generation. The first case study building is an existing laboratory building that belongs to the university campus of the URV in Tarragona, Spain. The second case study building is an existing university building that belongs to the university campus of the BUE in Cairo, Egypt.

4.2.1 Characteristics of the case building A (medium-size office building, warm climate)

An existing office building incorporated in a local grid and a water network of a university campus located in Tarragona. To characterize the thermal demand of the building located at 41.13° N and 1.24° E, a dynamic building energy simulation engine (DesignBuilder/EnergyPlus) is used (see Figure 4-2). The area of the two-storey building is 2627 m^2 with a ceiling height of 3.5 m. It consists of seventy zones (i.e. offices, laboratories, bathrooms, etc.). The main classifications of building's construction elements are described in Table 4-6, while the building occupancy schedules are presented in Table 4-7. The number of occupants within the building is 292 people. The heating thermostat setting is adjusted to 21 °C and the cooling thermostat setting is adjusted to 25 °C. The

case building works for 5 days a week minus the Holidays/Closings that are presented in Table 4-8. The construction materials are defined based on the construction year and the location of the building.

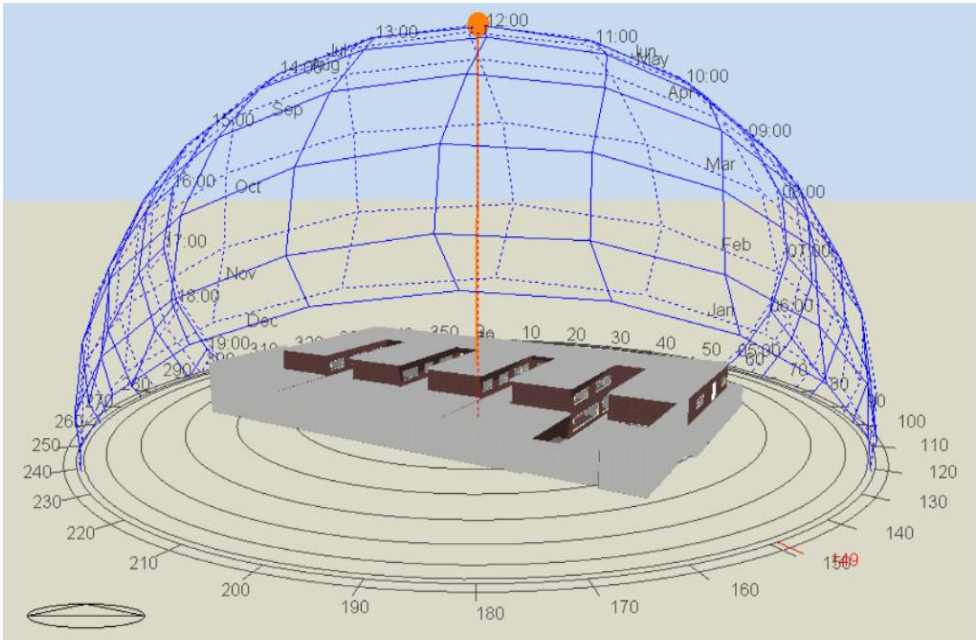

Figure 4-2. Case study A: building physical model.

Table 4-6. Main characterization of the building construction (case building A)

Construction element	Characterization	Value
Walls	U-value (W/m².K)	1.061
Floor	U-value (W/m².K)	0.695
Roof	U-value (W/m².K)	0.486
Glazing	U-value (W/m².K)	1.960
	Light transmission	0.744
	Total solar transmission	0.691
	Window-to-wall ratio (%)	30

Table 4-7. Occupancy schedule of the case building A

Time of the day	Weekdays	Weekends	Holidays
From 00:00 to 06:00	0	0	0
From 06:00 to 08:00	0.25	0	0
From 08:00 to 09:00	0.75	0.01	0.05
From 09:00 to 13:00	1	0.08	0.08
From 13:00 to 15:00	0.3	0	0.01
From 15:00 to 18:00	1	0	0
From 18:00 to 20:00	0.2	0	0
From 20:00 to 24:00	0	0	0

Table 4-8. Annual holidays for the case building A

Month	Holidays
January	From 1 to 6
February	-
March	30
April	2
May	1
June	24
July	31
August	From 1 to 26
September	11
October	12
November	1
December	6, 8, 23, 25, 26, 31

4.2.2 Characteristics of the case building B (large-size university building, hot climate)

An existing university building with interdisciplinary research facilities incorporated in a local grid and a water network of a university campus located in Cairo, Egypt was chosen.

To characterize the thermal demand of the building located at 30.12° N and 31.39° E, a dynamic building energy simulation engine (DesignBuilder/EnergyPlus) is used (see Figure 4-3). The area of the four-storey building is 16,109 m^2 with a ceiling height of 3.5 m. It consists of 190 zones (i.e. research centres, laboratories, lecture halls, classrooms, bathrooms, etc.). The main classifications of building's construction elements are described in Table 4-9, while the building occupancy schedules are presented in Table 4-10. The number of occupants within the building is 1482 people. The heating thermostat setting is adjusted to 21°C and the cooling thermostat setting is adjusted to 25 °C. The case building works for 6 days a week minus the Holidays/Closings that are presented in Table 4-11.

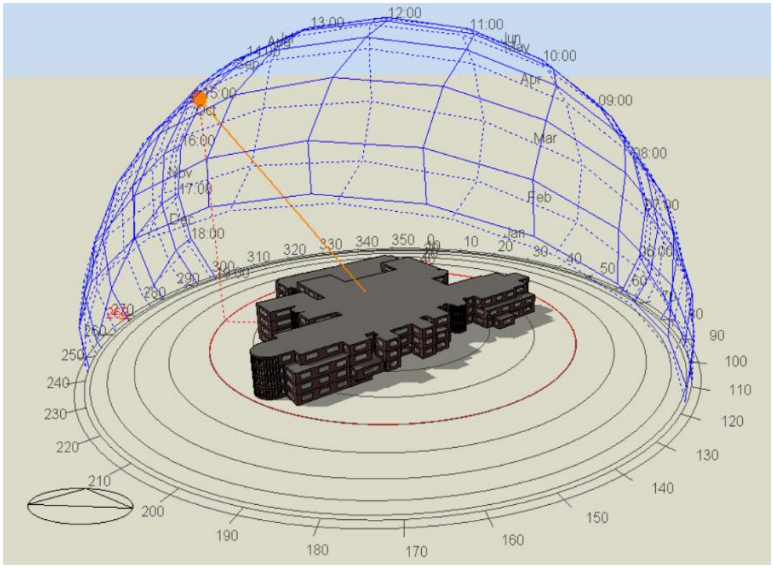

Figure 4-3. Case study B: building physical model.

Table 4-9. Main characterization of the building B construction

Construction element	Characterization	Value
Walls	U-value (W/m².K)	1.684
Floor	U-value (W/m².K)	0.896
Roof	U-value (W/m².K)	0.648
Glazing	U-value (W/m².K)	3.779
	Total solar transmission	0.72
	Window-to-wall ratio (%)	40

Table 4-10. Occupancy schedule of the case building B

Time of the day	Weekdays	Weekends	Holidays
From 00:00 to 06:00	0	0	0
From 06:00 to 08:00	0.10	0	0
From 08:00 to 09:00	0.65	0	0
From 09:00 to 13:00	0.98	0.1	0.08
From 13:00 to 15:00	0.51	0	0.09
From 15:00 to 18:00	0.36	0	0
From 18:00 to 20:00	0.09	0	0
From 20:00 to 24:00	0	0	0

Table 4-11. Annual holidays for the case building B

Month	Holidays
January	From 1 to 8 and 25
February	-
March	12
April	From 19 to 26
May	1, 24, 25, 26, 27
June	30
July	23
August	From 1 to 31
September	-
October	6
November	-
December	23, 25, 26, 31

4.2.3 Load profile of the case study buildings

4.2.3.1 building A

The significantly referenced Energy Consumption Guide (ECG) provides benchmarks for power load density in general offices, varying from 10 to 18 W/m² [1].

In this case study, the electricity consumption from the building's equipment and lighting was documented by the URV in 2016 hourly (see Figure 4-4) and monthly (see Figure 4-5). It was found that the maximum hourly lighting and equipment consumption was estimated to be 29.6 kW (about 11.3 W/m²). As the case building is a laboratory office type, the power demand for the equipment was almost 24 hours a day. The maximum and minimum monthly electricity consumption by the lights and equipment are 12.7 MWh and 5.4 MWh, respectively. The average monthly electricity by the lights and equipment is 10.4 MWh. The thermal demand for a whole year of dynamic operation of the occupied building, considering the lighting and equipment consumption readings with a radiant fraction of 0.5.

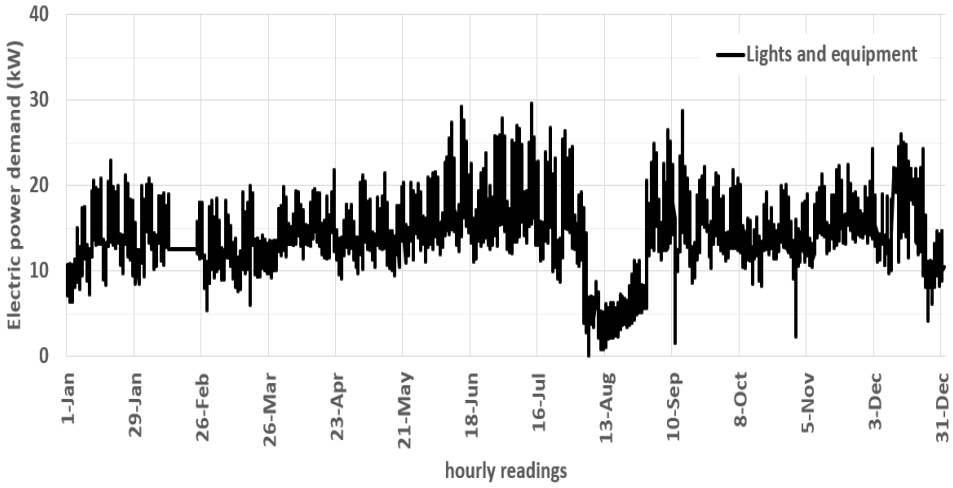

Figure 4-4. Hourly load profile recorded for the building's equipment and lighting during one-year operation for case building A.

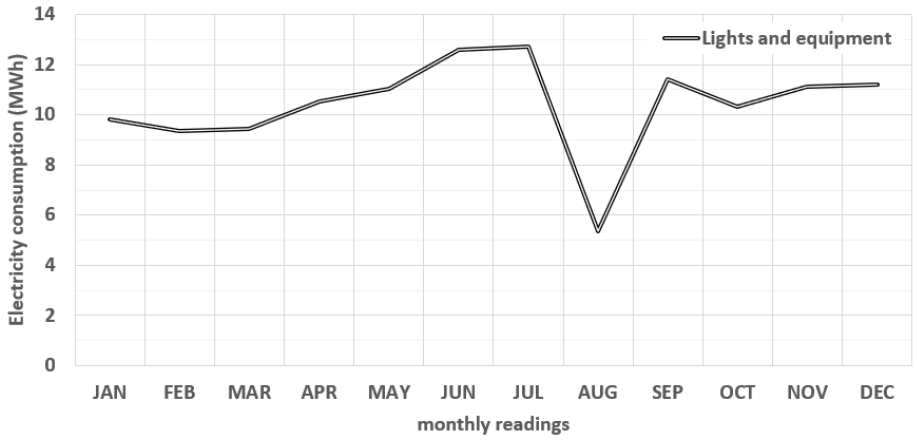

Figure 4-5. Monthly load profile recorded for the building's equipment and lighting during one-year operation for building A.

According to a one-year dynamic operation of the case building, the maximum sensible cooling load is 114.3 kW and the maximum sensible heating load is 116.2 kW (see Figure 4-6).

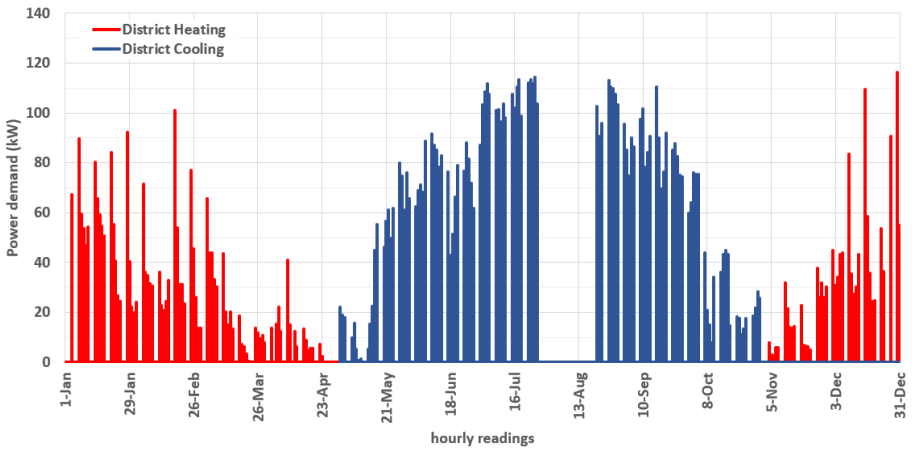

Figure 4-6. The district cooling and heating demand of the case building A.

The performance comparison is made between the HP cooling/heating unit driven by LCPV/T and the traditional system (gas boiler for heating and air cooled chiller for cooling), including factors like the operation costs considering the natural gas price of 0.08 €/kWh and electricity tariff of 0.12€/kWh. Furthermore, a performance analysis of the heat pump is applied in full-mode operation, including the COP and load capacity for cooling and heating. The yearly operation cost is 4,125€ for the sized water-to-water HP and 4,509€ for the air-to-water HP, while the yearly operation cost of the gas boiler for heating and air-cooled chiller for cooling is 5,266 €.

The monthly load profile for the building base case's cooling and heating system (water chiller and natural gas boiler) is shown in Figure 4-7. The maximum COP of this chiller is 1.9 and the maximum boiler efficiency is 75%. The cooling demand starts from May to October while the heating demand starts from November to April. The maximum energy required by the gas boiler is 5.18 MWh in January and the minimum energy required is 0.51 MWh in April, while the maximum energy consumed by the air-cooled chiller is 8.86 MWh in July and the minimum energy consumed by the chiller is 1.52 MWh in October. The total energy required by the boiler is 16.11 MWh and the total electricity consumption by the air-cooled chiller is 26.12 MWh. The average monthly electricity consumption by the air-cooled chiller is 4.35 MWh. The maximum hourly energy required by the boiler is 110 kWh for heating the case building A in the typical winter day, while the maximum hourly electricity power consumed by the air-cooled chiller is 50 kW for cooling the case building A.

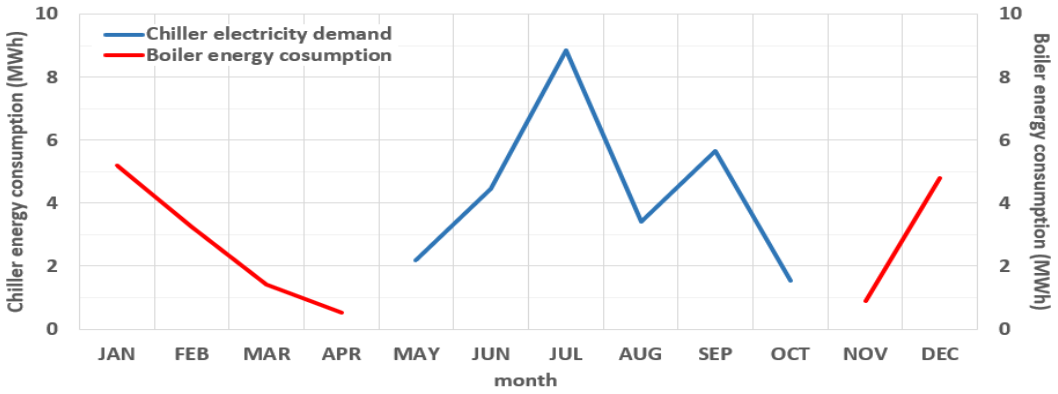

Figure 4-7. Monthly load profile for base case cooling and heating system (water chiller and natural gas boiler) for case building A.

The case building A achieves its cooling and heating loads through the connection to the campus' chilled/hot water network supplied by a natural gas boiler and an air-cooled water chiller in the current case. For this reason, a boiler of 161.2 kW heating capacity and a water chiller of 147 kW cooling capacity are considered in the simulation model for delivering the primary energy consumption of the building in the current case.

The integration of an efficient air-to-water heat pump is investigated on the case building A. The heat pump of 147 kW cooling capacity and 161.2 kW heating capacity is selected. In cooling and heating modes the airflow rate is set at 40,000 m^3/hr., while the water flow rate is set at 23,732 kg/hr. The main characteristics of the investigated air-to-water HP unit are shown in Table 4-12.

Table 4-12. Technical characteristics of the selected reversible heat pump (CYAN-Swegon)

ETON-Swegon-16.2	Unit	Value
Cooling Mode		
Nominal capacity	kW	147
Power input	kW	62
EER	-	2.37
ESEER	-	3.66
Evaporator ingoing-outgoing temperature	°C	12/7
External air temperature	°C	35
Heating mode		
Nominal capacity	kW	161.2
Power input	kW	62.3
COP	-	2.59
Condenser ingoing-outgoing temperature	°C	40/45
External air temperature	°C	7

Meanwhile, the heat pump system based on 3 units of water-to-water HP (CRIMSONMAX-63-Swegon) is investigated on the case building A. The main characteristics of the reversible water-to-water heat pump of a cooling capacity of 66.3kW with a power input of 12.1 kW and a heating capacity of 68.4 kW with a power input of 11.6 kW is shown in Table 4-13.

Table 4-13. Main characteristics of the water-to-water heat pump (CRIMSONMAX-63-Swegon)

CRIMSONMAX-63-Swegon	Unit	Value
Cooling Mode		
Nominal capacity	kW	66.3
Power input	kW	12.1
EER	-	5.47
Evaporator ingoing temperature	°C	18
Condenser ingoing temperature	°C	30
Heating mode		
Nominal capacity	kW	68.4
Power input	kW	11.6
COP	-	5.89
Condenser ingoing temperature	°C	35
Evaporator ingoing temperature	°C	10

4.2.3.2 building B

In this case study, the electricity consumption from the building's equipment and lighting was simulated hourly and monthly (see Figure 4-8). It was found that the maximum hourly lighting and equipment consumption was estimated to be 405 kW (about 25.1 W/m^2). The maximum and

minimum monthly electricity consumption by the lights and equipment are 107 MWh and 50 MWh, respectively. The average monthly electricity by the lights and equipment is 92 MWh. The thermal demand for a whole year of dynamic operation of the occupied building, considering the lighting and equipment consumption readings with a radiant fraction of 0.5.

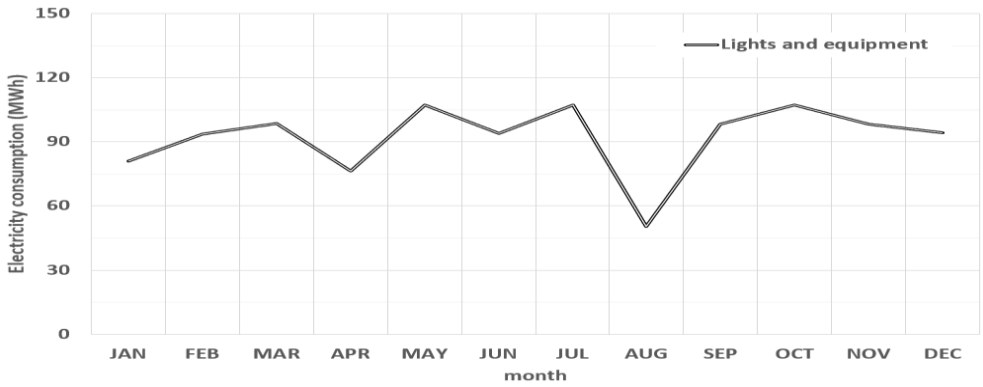

Figure 4-8. Monthly load profile recorded for the building's equipment and lighting during one-year operation for building B.

According to a one-year dynamic operation of the case building B, the maximum sensible cooling load is 953 kW and the maximum sensible heating load is 600 kW (see Figure 4-9). The cooling demand starts from March to November, while the heating demand starts from December to March. In the current case, the building is cooled by Air cooled chiller with a COP of 2.5 and no heating systems are attached.

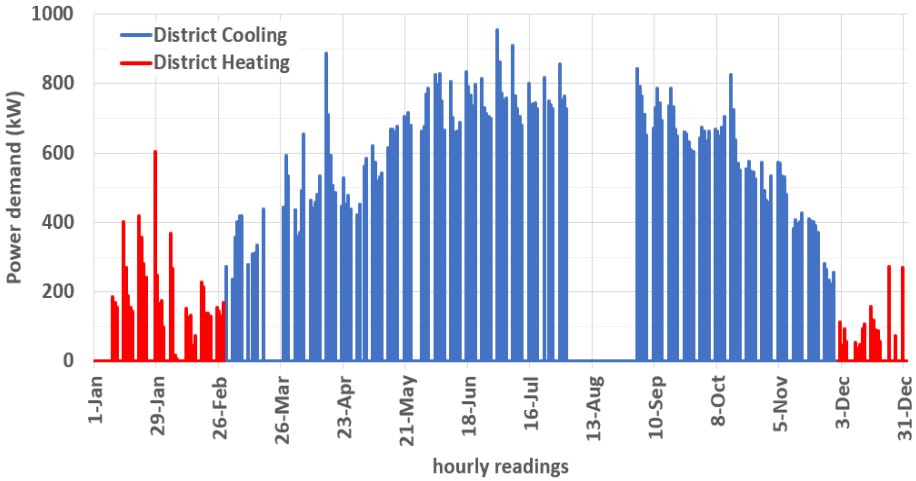

Figure 4-9. The district cooling and heating demand of the case building B.

The hourly electric power demanded by the air-cooled chiller for cooling the case building B is shown in Figure 4-10. The maximum hourly power demand is 630 kW in July. The chiller is switched on from March to July and from September to November and switched off in August holiday. The maximum monthly electricity consumption for cooling the case building is 126 MWh, the minimum is 24.4 MWh and the average is 70.5 MWh.

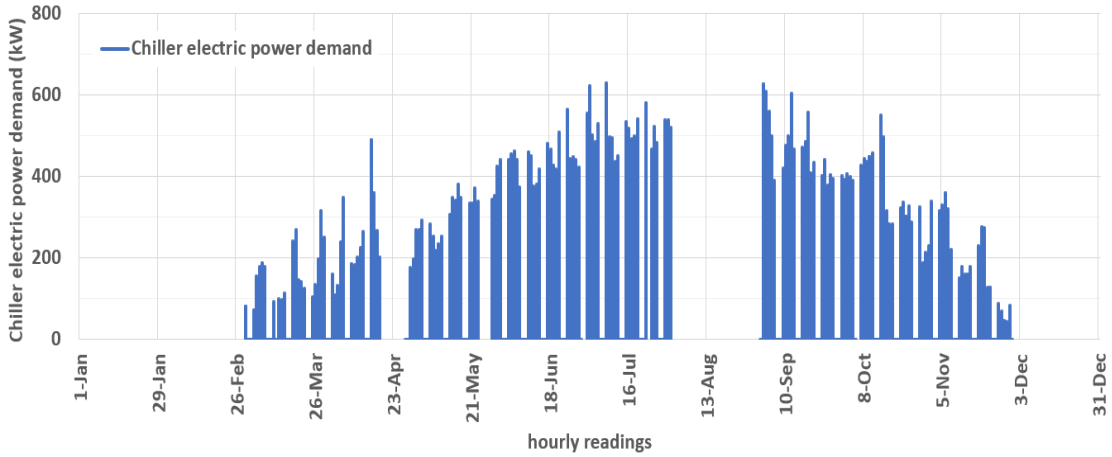

Figure 4-10. Hourly electric power demand by the air-cooled chiller for cooling the case building B.

The impact of integrating the two air-cooled electric chillers model GHA-B3160A ES-EC-34 in the case building B is investigated. Each unit has a nominal cooling capacity of 1,054 kW with total electric power input of 308 kW and the two chillers are used to represent the existing air-cooled chiller systems. The technical characterization of this electric chiller is shown in Table 4-14.

Table 4-14. Technical characteristics of the selected air-cooled chiller (GHA-B3160A ES-EC-34)

GHA-B3160A ES-EC-34	Unit	Value
Refrigerant		R134a
Total cooling capacity	kW	1045.5
Nominal Power input	kW	308.1
Power circuit voltage	V/Ph/Hz	400/3/50
Control circuit voltage	V/Ph/Hz	230/1/50
E.E.R.	-	3.42
E.S.E.E.R.	-	5.66
Compressors type		Screw
Inlet water temperature	℃	12
Outlet water temperature	℃	6
Ambient temperature	℃	35

Meanwhile, the air-cooled absorption chiller (PURIX-A25s) is investigated on the case building B. The air-cooled absorption chiller (PURIX-A25s) machine is driven by two LCPV/T systems (from section 4.1.3).

4.3 Design and sizing of solar power system for the case study buildings

The design of the grid-tie photovoltaic system takes the available roof area, the distance between module rows, the building's orientation, and the fulfilment of building's demands into consideration. The cooling and hating systems are sized to meet the building's demands.

Based on a one-year dynamic simulation of the specified PV technologies at different inclination angles, while considering the climate and weather parameters of the building location, the maximum solar energy captured is around a tilt angle of 30° in Cairo (Egypt) and 40° in Tarragona (Spain).

4.3.1 Available roof area

The roof area is about 1,330 m^2 for case building A and 5,100 m^2 for case building B. Considering an available area of 75% for roof-mounted PV installations, the maximum area is 998 m^2 for case building A and 3825 m^2 for case building B.

4.3.2 Minimal distance between PV rows

The PV system is comprised of rows of PV modules with distance d between every row. Each module is inclined with an angle (module tilt angle) β_α from the horizontal surface. The module has length L and faces the sun by azimuth angle γ_s and sun altitude angle α_s (see Figure 4-11).

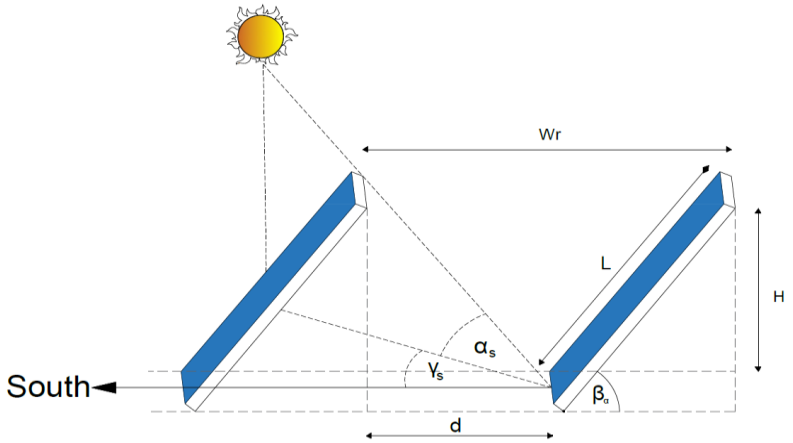

Figure 4-11. South facing (northern hemisphere) tilted two rows of photovoltaic system on a horizontal surface.

PV installers use different guidelines to define the minimal distance between rows [2, 3]. Ordinarily, it is defined by the sun's altitude angle that can be determined at noon or any earlier hour on the shortest day of the year (on December 21 for northern hemisphere). The minimum row distance is calculated from Equation 4-2, where h is the height differential between the top and the bottom of one row to the north and calculated from Equation 4-3.

$$d = \frac{H}{\tan \alpha_s} \times \cos \gamma_s \qquad (4\text{-}2)$$

$$H = L \times \sin \beta_\alpha \qquad (4\text{-}3)$$

The design calculations call for a shade-free solar window, which is obtainable between 9 am and 3 pm on the shortest day of the year in the winter solstice of the northern hemisphere. With that being said, the sun's altitude angle (α_s) is about 13° and the sun's azimuth (γ_s) is approximately 43° on December 21st for Tarragona climate (Latitude: 41.12° , longitude: 1.24°), while the sun's altitude angle is about 21° and the sun's azimuth (γ_s) is approximately 45° on December 21st for Cairo climate (Latitude: 30.1° , longitude: 31.3°). The sun path charts for the case buildings in Tarragona, Spain and

Cairo, Egypt are obtained by reference [4].

Most of the commercial PV modules as well as the LCPV/T system in the previous chapter (Chapter 3) have a length of 1.65 m. The minimum row distance is 3.35 m for Tarragona climate and 1.52 m for Cairo climate for a shade-free solar window from 9 am to 3 pm.

In the northern hemisphere, solar panels work best when they are facing the south direction. The average efficiency drop of a solar panel mounted away from the south in the northern Hemisphere is around 1.1% for every five degrees.

4.3.3 The building's orientation

For the case building A, the building's roof orientation is not completely facing the south, so the solar panels are mounted on the roof with an angle of 40° to directly face the south (see Figure 4-12).

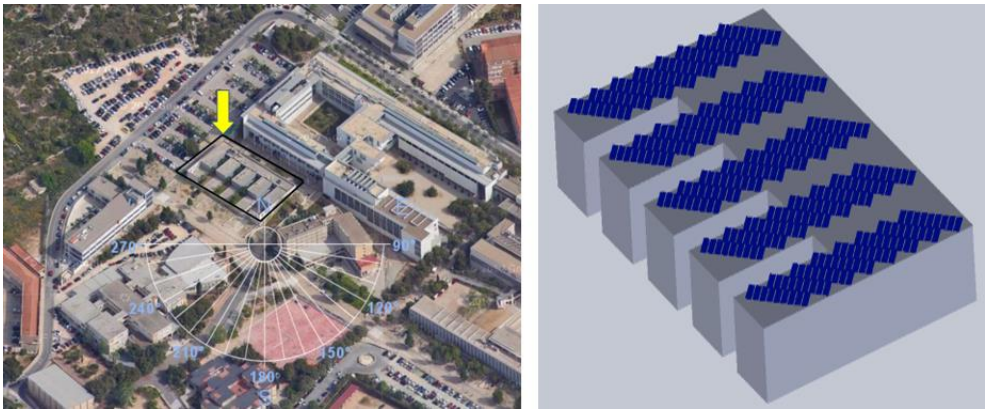

(a) (b)

Figure 4-12. a) Aerial view of the university campus where the reference building A is located. b) PV modules mounted on the building's roof.

For the case building B, the building's roof orientation is not completely facing the south, so the solar panels are mounted on the roof with an angle of 20° to directly face the south (see Figure 4-13).

Figure 4-13. Aerial view of the university campus where the reference building B is located.

4.3.4 Fulfilment of the total building's loads

Fulfilment of the total building's loads considering the integration of the selected reversible heat pump for cooling/heating the case building A and the existing air-cooled chiller integrated with the selected thermal chiller for cooling the case building B. As the total electricity demand for the case buildings including lighting, equipment, cooling or/and heating fluctuates monthly, a diversified

number of PV modules is required monthly to meet the total building demands.

The performance of different commercial PV technologies and the development of LCPV/T have been experimentally investigated and dynamically simulated in nine different climate conditions in Chapter 3. Based on the one-year simulation, the maximum power produced from this LCPV/T is 300 W in Tarragona and 390 W in Cairo while maximum power produced from the air-based PV/T (Ecomesh-265) is 243 W in Tarragona and 306 W in Cairo. The maximum power produced from the Eurener-235 polycrystalline PV module is 234 W in Tarragona and 301 in Cairo, while the maximum power produced from the JASOLAR-290 monocrystalline PV is 280 W in Tarragona and 358 W in Cairo. The maximum power produced from the selected four PV technologies are shown in Figure 4-14. Each one has a module length of 1.65 m, while the system area is 3.9 m^2 for the LCPV/T, 1.6 m^2 for the selected monocrystalline JASOLAR-290 module, Ecomesh-265 air-based collector and Eurener-235 polycrystalline panel.

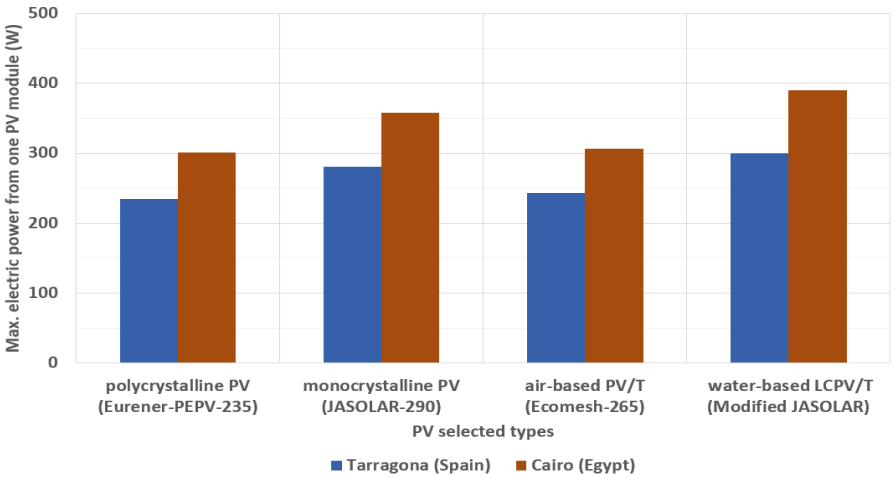

Figure 4-14. Maximum electric power generated from one selected PV system based on one-year dynamic simulation in Cairo, Egypt and Tarragona, Spain.

The maximum electric power demanded by the case buildings (air-conditioning system, lights and equipment) for one-year dynamic operating has been investigated. The maximum power demanded by the lights and equipment is 30 kW for case building A (medium-size) and 403 kW for case building B (large-size).

In order to reach the maximum electric power demanded by the building, the number of PV module varies according to the solar radiation availability and the building`s power demand. For case building A, the number of modules is 271 (448 m^2) when using the monocrystalline PV, 325 (537 m^2) when using the polycrystalline PV module, 313 (517 m^2) when using the air-based PV/T collector, and 253 (988 m^2) when using the developed commercial LCPV/T system. For case building B, the number of modules is 1757 (2,900 m^2) when using the monocrystalline PV, 2090 (3449 m^2) when using the polycrystalline PV module, 2056 (3,393 m^2) when using the air-based PV/T collector, and 1612 (6,289 m^2) when using the developed commercial water-based LCPV/T system.

4.3.5 The arranged PV systems for the case buildings

In agreement with the above design parameters and the grid-tie configuration, the maximum

number of PV modules is: 172 PV modules (284 m^2) or 73 LCPV/T systems (285 m^2) with a row distance of 3.5 m for the case building A; and 1,931 PV modules (3,187 m^2) or 817 LCPV/T systems (3,187 m^2) with a row distance of 1.6 m for the case building B.

The monocrystalline PV module with an area of 1.65 m^2 and peak power of 290 W at the standard test conditions (irradiance of 1000 W/m^2 and ambient temperature of 25 °C) has an average price of 280 €/module, while the polycrystalline PV module with the same area and peak power of 290 W has an average price of 260 €/module. The air-based PV/T with an area of 1.6 m^2 and peak power 265 W has an average price of 320 €/collector, while the developed low-cost LCPV/T collector with an area of 3.9 m^2 and peak power around 390 W has an average price of 490 €/collector. The average cost is obtained from refences: [5-8] for the Si modules, inverters, regulators, cables and brackets. The capital cost is calculated as 30,000 € for the air-to water heat pump and 38,000 € for the water-to water heat pump from [9]. The capital cost of the water system for the thermal integration of the LCPV/T into the water network (Pipes, Pressure vessels, pumps) is obtained from [10] and its calculated as 20,440 € for the case building A and 228,760 € for the case building B. The capital cost of the arranged PV systems with different commercial PV modules and the developed LCPV/T systems for the two case buildings are shown in Table 4-15. The electricity price was recorded as 0.06 €/kWh for commercial buildings in Egypt in 2019 [11] and an increase of 19% was reported in the second half of 2020 to exceed 0.07 €/kWh [12]. The study assumes that the chilled water energy is exported to the campus' water network at a price of 0.03 €/kWh, while the hot water temperature stream leaves the absorption chiller is exported to the hot water network at a price of 0.01 €/kWh.

The maximum useful thermal power and the solar thermal conversion efficiency of the air-collector (Ecomesh 265) is 254 W and 16% in Tarragona climate, 298 W and 19% in Cairo climate. Meanwhile, the maximum useful thermal power and the solar thermal conversion efficiency of the developed LCPV/T system is 1.4 kW_t and 40% in Tarragona climate and 1.6 kW_t and 48% in Cairo climate.

Table 4-15. Capital cost of the arranged PV systems with different types of commercial PV modules and the developed LCPV/T for the different case buildings

Case study	Technology	Max. power (kW)	PV modules (€)	Inverters and regulators (€)	Cables and brackets (€)	Total (€)
Building A						
	Monocrystalline PV	48	44,789	18,787	8,829	72,406
	Polycrystalline PV	40	41,590	15,224	8,829	65,643
	Air based PV/T	41	48,896	19,194	7,969	76,059
	Water based LCPV/T	21	33,266	10,723	4,585	48,574
Building B						
	Monocrystalline PV	697	502,200	210,921	97,694	810,814
	Polycrystalline PV	581	466,916	170,919	97,694	735,528
	Air based PV/T	626	537,920	211,224	98,047	847,191
	Water based LCPV/T	318	372,307	120,012	55,922	548,241

4.4 Energy matching with quantifying the environmental and financial benefits

For the case building A (2,672 m²), the yearly electricity consumption by the building is 386.5 MWh. For the case building A 16,109 m²), the yearly electricity consumption by the building is 1.7 GWh (see Table 4-16).

Table 4-16. Yearly electricity consumption by the two case buildings

Case building		Electricity consumption (MWh)		
Case	Building area (m²)	Lights and equipment	Electric HP	Electric chiller
A	2,672	125	217	-
B	16,109	1,100	-	600

The mean solar electric contribution percentage (SC_e) is defined as the ratio between total electricity produced from PV technologies and total electricity consumed by the case building (see Table 4-17).

Table 4-17. Yearly solar contribution and energy production from the PV systems

PV system types and modules	A_{PV}(m²)	Q_e (MWh)	Q_T (MWh)	SC_e(%)	SC_{total}(%)
Building A					
172 of the polycrystalline	285	71.8	-	19	19
172 of the monocrystalline	285	86.7	-	22	22
172 of the air-based PV/T	285	70.2	30.2	18	18
73 of the water-based LCPV/T	121	41.5	205	11	15
Building B					
1,931 of the polycrystalline	3,186	900	-	53	53
1,931 of the monocrystalline	3,186	1,100	-	64	64
1,931 of the air-based PV/T	3,186	800	389	47	47
817 of the water-based LCPV/T	1,347	590	1,878	35	49

The mean solar energy contribution percentage (SC_{total}) is defined as the ratio between total energy produced from PV technologies and total energy consumed by the case building. The A_{PV} refers to the PV surface area, Q_e refers to the total electricity produced from the PV systems, and $Q_T$refers to the useful energy produced from the PV/T and LCPV/T systems.

The monthly monetary saving of three exporting schemes are calculated for the two case buildings using the LCPV/T coupled with electric and thermal chillers for 9-month cooling for the case building B in Cairo climate, and the LCPV/T coupled with reversible water-to-water HP for 6-month cooling and 6-month heating for the case building A in Tarragona climate, considering the electricity price is 0.12 €/kWh and thermal energy (hot water) price is 0.04 €/kWh (see Figure 4-15). The three schemes are: i) bidirectional energy distribution systems (excess electricity produced is exported to the microgrid and excess useful thermal energy is exported to the chilled/hot water network); ii) bidirectional microgrid (only excess electricity produced is exported to the microgrid); and iii) bidirectional thermal district network (only excess useful thermal energy is exported to the thermal

water network). Figure 4-15.a shows the impact of applying the three schemes in the two case buildings. The maximum monetary saving for the case building A in Tarragona climate is on July. While the maximum monetary saving for the case building B in Cairo climate is on May (see Figure 4-15.b). Table 4-18 shows the maximum monetary saving of the LCPV/T coupled with electric and thermal chillers for 9-month cooling for the case building B in Cairo climate, and the LCPV/T coupled with reversible water-to-water HP for 6-month cooling and 6-month heating for the case building A in Tarragona climate. The maximum monthly monetary saving is 961€ for building A and 12,206€ for building B.

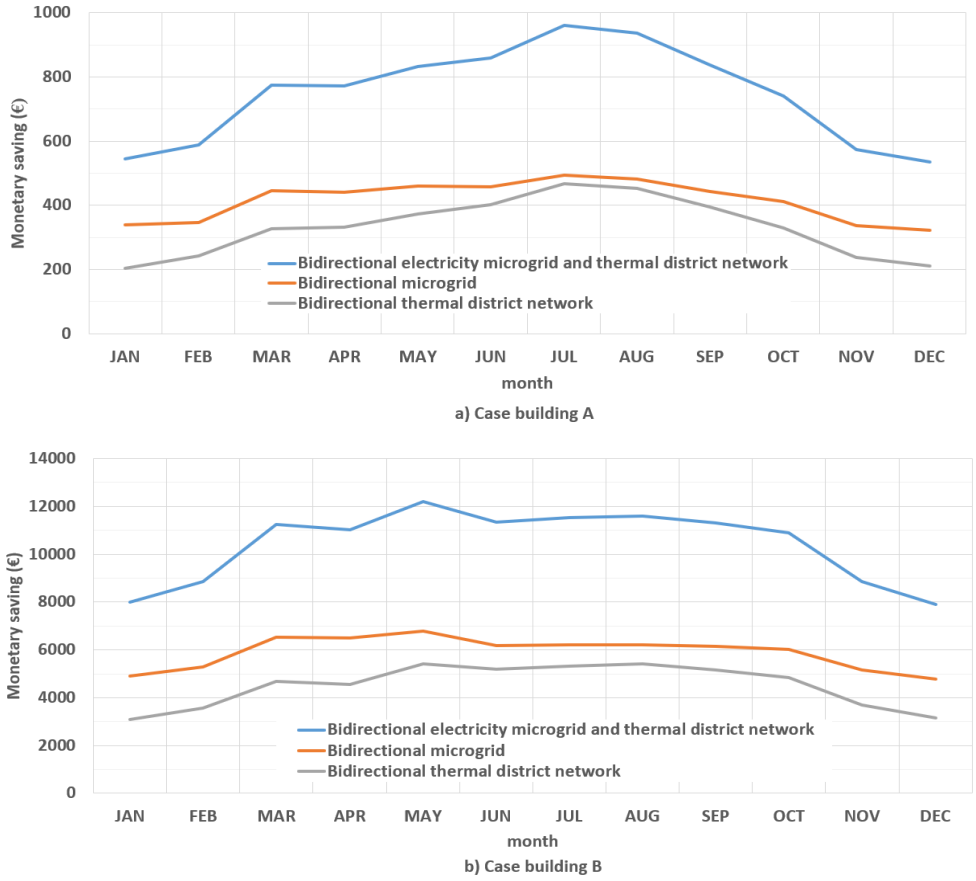

Figure 4-15. The effect of electricity and thermal energy exporting scheme on the payback period of the LCPV/T for cooling and heating different case buildings: a) in Tarragona; and b) in Cairo.

Table 4-18. Maximum monthly monetary saving of applying the three schemes:

Maximum monthly monetary saving (€)	building A	building B
Bidirectional electricity microgrid and thermal district network	961	12,206
Bidirectional microgrid	495	6,778
Bidirectional thermal district network	466	5,418

The payback period of the water based LCPV/T when its heat power is exported to the hot water network at a price of .04 €/kWh, converted and exported to the district cooling at a price of 0.07€/kWh, and its electric power is exported to the electricity grid at a price of 0.12€/kWh is less

than 5 years for case building A (configuration of LCPV/T with reversible HP) and less than 4 years for case building B (configuration of LCPV/T coupled with electric and thermal chillers. The payback period of the LCPV/T systems with exporting its electricity and without its thermal power is 8.8 year for the case building A and 7.1 years for the case building B. The payback period of the air-based collector is about 9 years for the two case buildings. The payback period of the designed monocrystalline and polycrystalline PV systems are 7 and 7.6 years, respectively for the case building A, 6.3 and 6.9 years, respectively for the case building B.

The maximum monthly bill is -2,591 € on July for the reference case building A. Integrating the LCPV/T and HP into the building reduces this July monthly bill to -1,397 € when only excess electricity is exported to the grid, -1,512 € when only hot water above 45 °C produced from the LCPV/T coupled with the HP is imported to the hot water network, and +301 € when applying the bidirectional configuration of the reversible water-to-water HP and the LCPV/T system with the microgrid and cooling/heating district network. Positive and negative signs are based on the difference between the consumption bill and the exported payment.

By implementing the four integration scenarios on integrating the designed PV systems in the case building B, the minimum payback is achieved by the LCPV/T for the four scenarios. The payback of the LCPV/T is 4.3 years for scenario 1 (when meeting the lights and equipment power demand), scenario 3 (when meeting the total building's power demand) and scenario 4 (when the electricity generated is exported to the grid), while its about 5.6 years for scenario 2 (when meeting the air-cooled chiller power demand). The hot water produced above 40 °C is exported to the hot water network for the four scenarios at a price of 0.04 €/kWh and the electricity imported price for scenario 4 is 0.12€/kWh. The highest payback period for all four scenarios is recorded in scenario 2, while the highest payback period for the PV systems is recorded in the air-based PV/T case because of its high capital cost and the fact that its heat produced is dissipated in summer (see Figure 4-16).

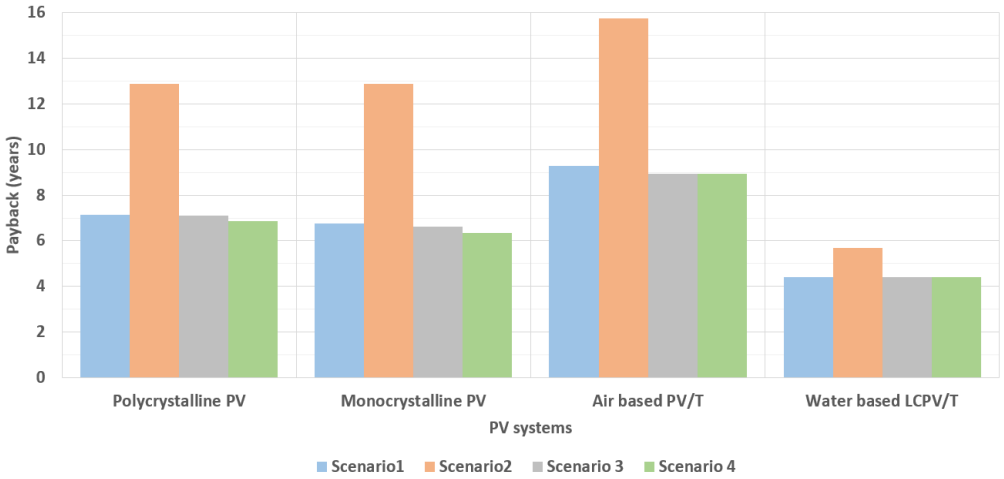

Figure 4-16. The impact of the four integration scenarios on the payback period of the different types of grid-tie PV systems for the case building B.

The designed PV systems for the two case buildings help to reduce the CO_2 emissions in one-year of operation by 505-682 tons CO_2 for the case building B, 45-56 tons CO_2 for the case building A,

considering the emission reduction is 0.64 kg of CO_2 for kWh electricity production and 0.26 kg of CO_2 for hot water production with a temperature above 45 °C.

The maximum CO_2 emissions reduction achieved by the monocrystalline PV system is 682.3 tons CO_2 for the case building B and 56 tons CO_2 for the case building A for one-year of operation. The CO_2 emissions reduction achieved by the water based LCPV/T is 658.3 tons CO_2 for the case building B and 47.2 tons CO_2 for the case building A for one-year of operation (see Figure 4-17).

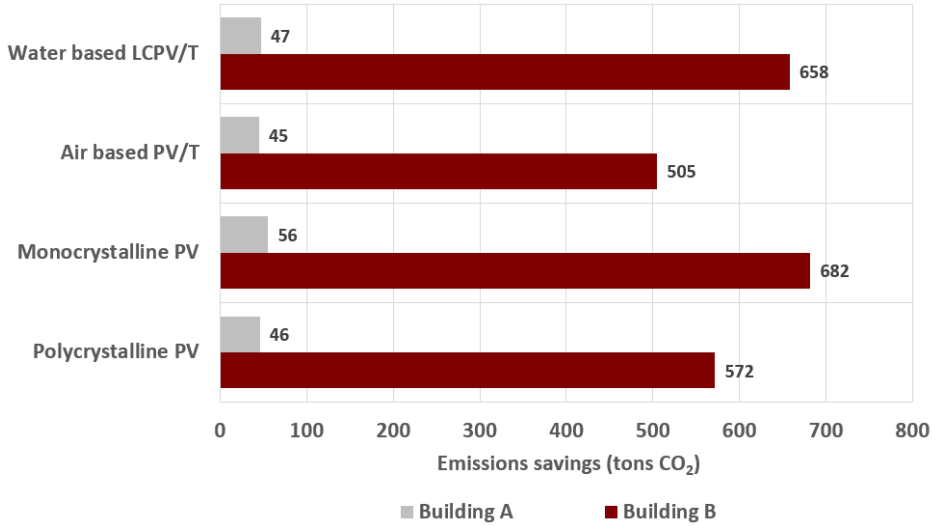

Figure 4-17. CO_2 emissions reduction achieved by the sized PV systems for one-year of operation in the case buildings.

The payback of the PV system coupled with air cooled compressor chiller/air-to-water HP to meet the building cooling is about 9 years (without importing to the grid) and 7 years (with importing to the grid). The payback of the air-based PV/T assists the air-to-water HP to meet the building heating demand is about 8 years (without importing to the grid) and 7 years (with importing to the grid). The payback of the LCPV/T system assisted the single stage heat recovery absorption chiller and powered the scroll chiller simultaneously to meet the building cooling demand in hot climate is about 7 years (without importing to the grid), 5 years (with importing to the grid) and less than 4 years (with importing to the grid and the chilled water network). The proposed configuration of integrating LCPV/T with absorption and compression chillers for cooling in hot climates reduces the payback of solar cooling technology by about 40%.

4.5 Conclusion

This chapter elaborated on investigating the use of on-site energy production from the validated models (PV, PV/T and the developed LCPV/T) along with the integration of efficient cooling and heating systems. Two case study buildings in hot and warm climate conditions have been selected. The two case study buildings have been dynamically operated to characterize the thermal demand of the buildings and match the energy demand and on-site energy generation. The design of the grid-tie photovoltaic system has been taken the available roof area, the distance between module rows, the building's orientation and the fulfilment of building's demands into consideration. The cooling

and heating systems are sized to meet the building's demands. The solar contribution index, monthly bill saving, CO_2 emissions reduction and the payback of the PV, PV/T and LCPV/T systems coupled with cooling and heating systems in the two case buildings have been evaluated. The size of the solar generation system was limited by the available roof area and the size of the cooling and heating systems was based on the building demands. In the case buildings, balancing supply and demand with the connection to the electricity microgrid and the hot/chilled water network minimizes the unmatched effect.

The payback is less than 5 years for case building A (configuration of LCPV/T with reversible HP) and less than 4 years for case building B (configuration of LCPV/T coupled with electric and thermal chillers. The designed LCPV/T systems for the two case buildings help to reduce the CO_2 emissions in one-year of operation by 505-682 tons CO_2 for the case building B and 45-56 tons CO_2 for the case building A, considering the emission reduction is 0.64 kg of CO_2 for kWh electricity production and 0.26 kg of CO_2 for hot water production with a temperature above 45 °C.

References

[1]- Menezes AC, Cripps A, Buswell RA, Wright J, Bouchlaghem D, 2014. Estimating the energy consumption and power demand of small power equipment in office buildings, Energy and Buildings, 75, pp. 199-209.
[2]- A. Aronescu, and J. Appelbaum, Design optimization of photovoltaic solar fields-insight and methodology, Renewable and Sustainable Energy Reviews, 2017, 76, pp. 882-893.
[3]- K. Brecl and M. Topič, Self-shading losses of fixed free-standing PV arrays, Renewable Energy, 2011, 36, pp. 3211-3216.
[4]- Sun path chart program. University of Oregon, solar radiation monitoring laboratory. Available from: (http://solardat.uoregon.edu/SunChartProgram.php).
[5]- IEA PVPS - Trends 2016 in photovoltaic applications. Photovoltaic power systems programme - international energy agency, (http://www.iea-pvps.org/); 2016 [Accessed 2020.03.01].
[6]- Ramos A, Chatzopoulou MA, Guarracino L, Freeman J, Markides CN. Hybrid photovoltaic-thermal solar systems for combined heating, cooling and power provision in the urban environment. Energy Conversion and Management 2017; 150: 838-850.
[7]- Ferreira A, Kunh SS, Fagnani KC, De Souza TA, Tonezer C, Dos Santos GR, Coimbra-Araújo CH. Economic overview of the use and production of photovoltaic solar energy in brazil. Renewable and Sustainable Energy Reviews 2018; 81: 181-191.
[8]- Fu R, Chung D, Lowder T, Feldman D, Ardani K, Margolis R. U.S. Solar photovoltaic system cost benchmark: Q1 2016. National renewable energy laboratory, (https://www.nrel.gov/docs/); 2016 [Accessed 2017.02.01].
[9]- Mohanraj M, Belyayev Y, Jayaraj S, Kaltayev A. Research and developments on solar assisted compression heat pump systems – A comprehensive review (Part-B: Applications). Renewable and Sustainable Energy Reviews 2018; 83: 124-155.
[10]- Ayompe LM. Solar thermal systems. In: Boemi SN, Irulegi O, Santamouris M, editors. Energy performance of buildings: Springer, Cham; 2015, p. 349-377.
[11]- Egypt electricity prices - September 2019, (https://www.globalpetrolprices.com/Egypt/electricity_prices/); 2019 [Accessed 2020.04.09].
[12]- Electricity prices – Egypt oil and gas newspaper, (https://egyptoil-gas.com/tag/electricity-prices/); 2020 [Accessed 2020.06.09].

Chapter 5. Conclusion and recommendations

5.1 Conclusion

The integration of grid-tie photovoltaic/thermal and efficient air conditioning systems into existing buildings allows the provision of heating, cooling and electricity with a reduction in greenhouse emissions. The results of this study emphasize that integrating: i) LCPV/T with compression and absorption chillers for cooling; ii) LCPV/T with water-to-water HP for cooling and heating; iii) PV/T with air-to-water HP for heating; iv) PV with air-cooled chiller for cooling; and v) PV with air-to-water HP for cooling and heating has a great potential in replacing the depleting fossil fuel resources and boosting the share of onsite PV-electricity and the recoverable thermal energy utilization.

By modifying the installed monocrystalline PV module to the LCPV/T system, the temperature of the outlet fluid stream from the LCPV/T systems can exceed 80 °C while the PV module is kept below 75 °C in summer (hot climates) and exceeds 55 °C in winter (cold climates). In comparison to the typical configuration of PV integrated compression chiller, the LCPV/T coupled with the compression-absorption system reduces the payback period by 10-40%. However, a drop in the yearly electric energy production from the LCPV/T system of 18% is noted when changing the water stream temperature entering the LCPV/T from 20 °C to 50 °C (when the temperature of PV module without cooling is above 50 °C). Nevertheless, Egypt climate features a high solar radiation intensity, the payback of the solar cooling system could be between 4-9 years. The reason for that is the electricity price in Egypt is so low compared to the other countries in the Mediterranean region. Substituting the connection to the bidirectional district water network with the use of reversible heat pump reduces the operating cost for cooling and heating in the case building A by 15%. The average payback period of the PV with heat pump system is less than 7 years. Exporting the chilled/hot water to campus' water network while the heat pump is operating in full capacity mode has a significant potential to reduce the payback period to less than 4 years.

The performance of the polycrystalline module, monocrystalline panel, air-based PV/T collector, and LCPV/T has been investigated for the two different size and activity buildings; the office building of 2,672 m^2 in Tarragona and the university building of 16,109 m^2 in Cairo. The minimum row distance is 3.35 m for Tarragona climate and 1.52 m for Cairo climate for a shade-free solar window from 9 am to 3 pm

The use of a PV-thermal evaporator helps maintain the PV panel at a favourable temperature level, as well as improve the COP of the HP in heating mode. The use of the evaporator outlet stream beneath the PV panels improves the electrical efficiency of the PV module by 4%. The COP is around 5-6 and 4-5 for heating in Tarragona and Cairo, respectively. The maximum temperature different between air leaving the PV/T and air entering the PV/T is 4.7 °C in Cairo and 3.9 °C in Tarragona. The temperature fluctuation by using the air-based PV/T is so high and sometimes when the irradiance and ambient temperature are low, the PV/T could be heated instead of being cooled as shown at 5 pm of the typical winter day in Cairo. Therefore, a precise control and a bypass HX with the ambient

could help to reduce the impact of these limitations of the air based PV/T assists air-to-water HP for heating in Winter.

This study highlights the potential of the bidirectional configurations with electricity microgrid and chilled/hot water network for space cooling and heating of buildings in different climate conditions. Different case study buildings are then chosen and dynamically operated to match the building energy supply and demand. Moreover, the effective control mechanism takes numerous decision-making techniques into account. The payback of the PV system coupled with air cooled compressor chiller/air-to-water HP to meet the building cooling is about 9 years (without importing to the grid) and 7 years (with importing to the grid). The payback of the air-based PV/T assists the air-to-water HP to meet the building heating demand is about 8 years (without importing to the grid) and 7 years (with importing to the grid). The payback of the LCPV/T system assisted the single stage heat recovery absorption chiller and powered the water-to-water HP simultaneously to meet the building cooling demand in hot climate is about 7 years (without importing to the grid), 5 years (with importing to the grid) and less than 4 years (with importing to the grid and the chilled water network) and less than 3 years (with importing to the grid and the bidirectional cooling and heating network).

5.2 Recommendations

Selecting the adequate solar system (PV, PV/T or LCPV/T) depends on the required application and the climate conditions. Cooling the PV panels is essentially for concentrating systems as the solar intensity is increased by the reflectors, the temperature of the PV panel is raised as well. Cooling the PV cells improves its efficiency, but the capital cost of the LCPV/T is higher than the cost of PV/T system and the cost of the PV/T is higher than the cost of PV systems. Therefore, the heat produced from cooling the PV cells should be used to reduce the payback period of the PV/T and LCPV/T systems. Moreover, boosting the cost-effectiveness of PV/T could be achieved by assisting thermally driven air-conditioning in summer when the domestic hot water applications are not demanded. The payback period of the CPV/T could be minimized when the useful fluid stream can be used to supply absorption chillers for hot climates at 75-90 °C, adsorption chillers at 50-70 °C, desiccant systems at 50-65 °C for high humidity climates, water heaters at 40-65 °C, and evaporator-heat pump at 30-45 °C. This process helps to reduce the cooling power load in summer and decrease the payback period of LCPV/T systems. The leading challenges faced upon accepting the PV self-consumption approach is that the hours of the day that experience the greatest production of solar power may occur when the consumption is at its lowest rate or vice versa, as well as the required high capital investment. In the case study buildings, balancing supply and demand with a connection to the electricity grid and the water network minimizes the effect of these problems reported.

UNIVERSITAT ROVIRA I VIRGILI
Modelling and Experimental Characterization of Photovoltaic/Thermal Systems for Cooling and Heating of Buildings in different climate conditions
Khaled Mohamed Ramadan

UNIVERSITAT
ROVIRA i VIRGILI